



Dipartimento di Medicina Molecolare e dello Sviluppo

Dottorato di Ricerca in Medicina Molecolare

CICLO XXXIII

COORDINATORE Prof. Vincenzo Sorrentino

**Bitter taste receptors: new players
in female and male fertility**

Settore Scientifico-Disciplinare: BIO/13, BIOLOGIA APPLICATA

DOTTORANDO

Dr.ssa Bianca Semplici

TUTOR

Prof.ssa Paola Piomboni

ANNO ACCADEMICO: 2019/2020

INTRODUCTION	3
1 TASTE RECEPTORS	3
1.1 THE TASTE SIGNAL TRANSDUCTION CASCADE	4
1.2 EXTRA-ORAL EXPRESSION OF TASTE RECEPTORS	5
2 OOGENESIS, FOLLICULOGENESIS AND FOLLICULAR MICROENVIRONMENT	8
2.1 OOGENESIS AND FOLLICULOGENESIS	8
2.2 FOLLICULAR MICROENVIRONMENT	10
2.2.1 <u>Granulosa cells</u>	11
2.2.2 <u>Cumulus cells</u>	13
3 MALE GONADS AND SPERMATOGENESIS	14
3.1 STRUCTURE OF TESTIS	14
3.2 SPERMATOGENESIS	15
3.3 SPERMATOZOA	17
3.4 CAPACITATION OF SPERM IN THE FEMALE GENITAL TRACT	19
RESEARCH STUDY PURPOSE	20
MATERIALS AND METHODS	21
1 SAMPLE COLLECTION	21
1.1 FOLLICULAR CELLS RECOVERY AND ISOLATION	21
1.1.1 <u>Granulosa cells isolation</u>	22
1.1.2 <u>Cumulus cells isolation</u>	23
1.2 HUMAN GRANULOSA CELL LINE (HGL5)	23
1.3 SPERM AND TESTICULAR TISSUE	23
2 GENE EXPRESSION ANALYSIS	25
2.1 RNA EXTRACTION	25
2.1.1 <u>Granulosa and cumulus cells</u>	25
2.1.2 <u>Human sperm</u>	25
2.1.3 <u>Testicular tissue</u>	25
2.2 RNA CONCENTRATION MEASURING	25
2.3 COMPLEMENTARY DNA PREPARATION	26
2.4 DROPLET DIGITAL PCR (ddPCR)	26
2.4.1 <u>ddPCR data analysis</u>	29

2.4.2	<i>ddPCR statistical analysis</i>	30
2.5	QUANTITATIVE REAL TIME-PCR	30
3	PROTEIN ANALYSIS	32
3.1	PROTEIN EXTRACTION	32
3.2	WESTERN BLOT	33
3.3	IMMUNOFLUORESCENCE	34
3.4	METACORE ANALYSIS	35
	RESULTS AND DISCUSSION	36
1	FOLLICULAR CELLS	36
1.1	<i>TAS2Rs</i> EXPRESSION ANALYSIS IN GRANULOSA AND CUMULUS CELL	37
1.2	PROTEIN QUANTIFICATION AND LOCALIZATION OF <i>TAS2Rs</i>	42
1.3	METACORE PROTEIN NETWORK ANALYSIS OF PROTEIN INVOLVED IN <i>TAS2Rs</i> SIGNALING	44
1.4	EXPRESSION PROFILE OF GENES INVOLVED IN THE SIGNAL TRANSDUCTION ELICITED BY <i>TAS2Rs</i>	46
1.4.1	<i>Correlation analysis</i>	54
1.5	PROTEIN QUANTIFICATION AND LOCALIZATION OF GUSTDUCIN AND TRANSDUCIN	55
2	HUMAN SPERM AND TESTIS	57
2.1	<i>TAS2Rs</i> EXPRESSION ANALYSIS IN HUMAN SPERM AND TESTIS TISSUE	57
2.2	METACORE PROTEOMIC ANALYSIS OF PROTEIN INVOLVED IN <i>TAS2Rs</i> SIGNALING	58
2.3	GENE EXPRESSION ANALYSIS OF GENES INVOLVED IN <i>TAS2Rs</i> SIGNALING	60
2.3.1	<i>Correlation analysis</i>	60
2.4	PROTEIN EXPRESSION AND LOCALIZATION	61
3	DISCUSSION	69
	REFERENCES	74

Introduction

1 Taste receptors

The mammalian taste sensation provides valuable information about the nature and quality of food. Usually, taste transduction involves the interaction of flavors with specific taste receptors expressed by cells of taste buds located on the papillae of the tongue; this interaction is responsible for the proper detection of bitter, sweet, sour, salty, and umami stimuli. The recognition of salty and sour tastes is directly mediated by ion channels, while sweet, umami and bitter flavors are detected by two families of G-protein-coupled receptors (GPCRs): Type 1 Taste Receptors (TAS1Rs) and Type 2 Taste Receptors (TAS2Rs). Three different TAS1Rs have been identified, coded by *TAS1R* genes: *TAS1R1*, *TAS1R2* and *TAS1R3* (Montmayeur & Matsunami, 2002, Nelson et al, 2002, Nelson et al, 2001, Sainz et al, 2001). The TAS1Rs were found to form functional receptors by specific pair-wise dimerization, with *TAS1R3* serving as an obligate partner. The heterodimer *TAS1R1*+*TAS1R3* is responsible for the perception of umami taste, defined as the taste of monosodium glutamate; instead, the heterodimer *TAS1R2*+*TAS1R3* mediates the sweet taste perception. The TAS2Rs, responsible for the bitter sensation, is a large family including about 25 different isoforms in humans and about 30 in rodents (Margolskee, 2002; Meyerhof et al, 2011) (Figure 1). In the human genome, there are 25 functional genes and 11 pseudogenes belonging to the TAS2Rs gene family.

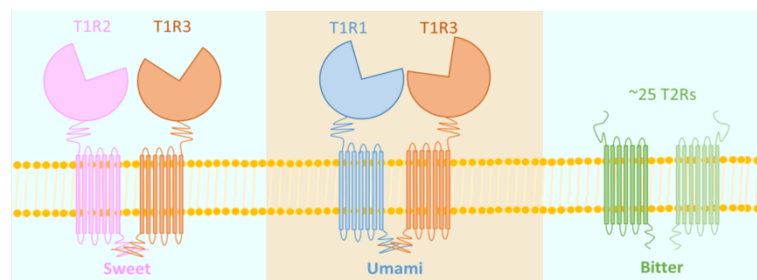


Figure 1: By heterodimerization, the three members of the TAS1Rs family detect either sweet (*TAS1R2*+*TAS1R3*) or umami (*TAS1R1*+*TAS1R3*) tastes. Bitter receptors (*TAS2R*) are composed of a large family including about 25 different isoforms in humans. Image from Wu et al, 2017.

1.1 THE TASTE SIGNAL TRANSDUCTION CASCADE

The binding of tastant molecules to TAS1Rs and TAS2Rs induces the activation of same intracellular transduction pathways, mediated by the heterotrimeric G-protein, which consists of the α -gustducin and the β_3/γ_{13} subunits (Scott, 2004).

This interaction leads to the release of the G β/γ subunits (Huang et al, 1999; Zhang et al, 2003), that in turn activates phospholipase C β_2 (PLC β_2), an enzyme able to catalyze the hydrolysis of phosphatidylinositol 4,5-bisphosphate to the second messenger inositol 1,4,5-trisphosphate (IP $_3$) and diacylglycerol (DAG) (Finger & Kinnamon, 2011; Kinnamon, 2012; Rossler et al, 1998). IP $_3$ opens IP $_3$ receptor type 3 (IP $_3$ R3) ion channels on the ER, releasing Ca $^{2+}$ into the cytosol of receptor cells. The increased intracellular Ca $^{2+}$ levels subsequently activate the cation channel Transient Receptor Potential Cation Channel Subfamily M Member 5 (TRPM5) (Hofmann et al, 2003; Liu & Liman, 2003). The consequent influx of Na $^+$ and the increased Ca $^{2+}$ concentrations depolarize the cell membrane, leading to a release of the neurotransmitter ATP through pannexin 1 and Calcium Homeostasis Modulator 1 (CALHM1) (Huang et al, 2007; Taruno et al, 2013). ATP finally transmits the signal to P2X2 and P2X3 receptors on gustatory afferent fibers (Huang et al, 2011). At the same time, G-protein α -gustducin activates a phosphodiesterase (PDE) that hydrolyses the second messenger cyclic adenosine monophosphate (cAMP) to adenosine monophosphate (AMP), thus decreasing the intracellular levels of cAMP (Figure 2).

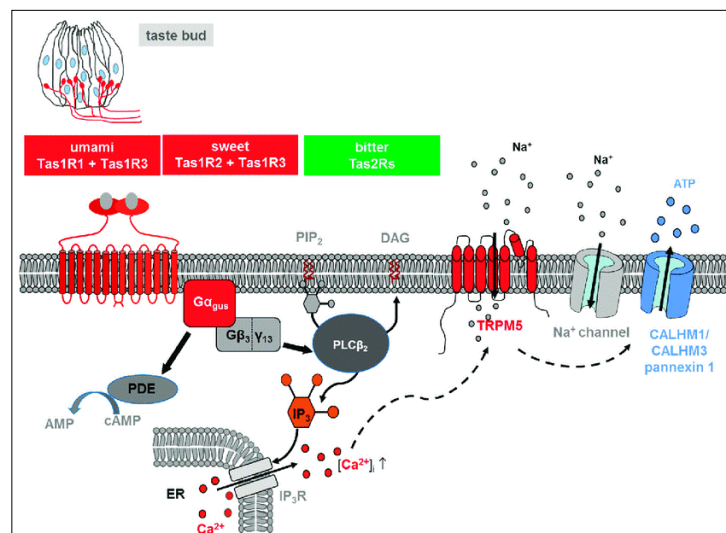


Figure 2: The binding of the ligand to the receptor induces the activation of an intracellular signal cascade. The heterotrimeric G-protein dissociates and the β/γ subunit activates PLC β_2 , which consequently catalyzes hydrolyzes PIP $_2$ into DAG and IP $_3$. The second messenger IP $_3$ causes the release of Ca $^{2+}$ from the ER, leading to the increase of intracellular Ca $^{2+}$ concentration that opens TRPM5 ion channels. Na $^+$ ions enter the cell and depolarize the cell. Image from Luddi et al, 2019.

1.2 EXTRA-ORAL EXPRESSION OF TASTE RECEPTORS

Taste receptors were first found in the taste buds of the oral cavity (Hoon et al, 1999). However, extra-oral taste receptor expression has been described in several recent reports, for example in the respiratory air ways (Freund et al, 2018), the gastrointestinal tract (Rozengurt, 2006), the brain (Dehkordi et al, 2012), the pancreas and the liver (Taniguchi, 2004), in reproductive organs, such as testes (Figure 3) (Fehr et al, 2007; Li & Zhou, 2012; Meyer et al, 2012; Li, 2013; Luddi et al, 2019).

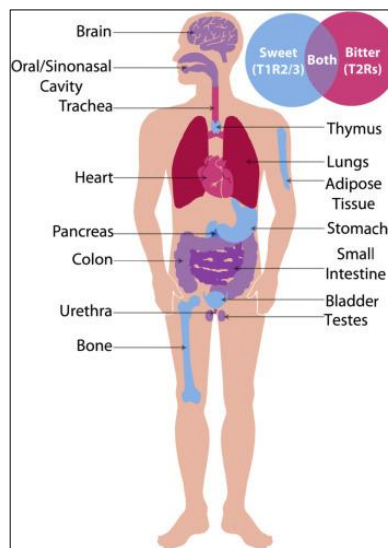


Figure 3: “Extra-oral” expression of G-protein-coupled receptors (GPCRs) involved in bitter, sweet, and umami taste. Despite their originally identified role on the tongue, taste receptors have been found in multiple organs and tissues outside of the oral cavity, where they play largely unknown roles. Red and blue colors indicate organs/tissues where bitter and sweet taste receptors, respectively, have been identified. Purple color indicates organs where both types of receptors have been identified. Image from Freund et al, 2018.

Even if extraoral functions of TASRs are not well understood yet, these receptors have been suggested to play specific roles in different tissues; for example, TAS1R2 and TAS1R3 regulate the insulin release in the brain mouse (Ren et al, 2009), while in the urothelium they control bladder contraction induced by artificial sweeteners (Elliott et al, 2011). A possible involvement of TASRs in osteogenesis and bone marrow adipogenesis has been also reported (Simon et al, 2014).

Several studies report the expression of taste receptors in both testis and sperm (Meyer et al, 2012; Li et al, 2013; Gentiluomo et al, 2017; Luddi et al, 2019). Data from mice suggest that their silencing or reduced expression may have a massive impact on sperm production and fertility, but their physiological function in spermatogenesis remains unclear (Fehr et al, 2007; Li & Zhou, 2012; Meyer et al, 2012; Voigt et al, 2012). It was found that the dimer of umami taste receptor (TAS1R2/TAS1R3) is expressed in mouse and human spermatozoa (Meyer et al, 2012).

Furthermore, the G-protein α -subunit gustducin, first identified in taste cells of the tongue (McLaughlin et al, 1992), was also found to be expressed in mammalian spermatozoa (Fehr et al, 2007), suggesting that taste receptors may act as molecular sensors during the sperm passage through the female reproductive tract. The expression of TASRs in human sperm was reported by analyzing the signal transduction cascade during chemotactic activation and various member of the TAS1Rs and the TAS2Rs receptor family was detected in ejaculated human sperm (Luddi et al, 2019). The evidence of the presence of taste receptors and their signaling transduction cascade in mammalian testis and sperm, suggests a possible functional role for these molecules in sperm development and maturation, where they could be responsible for the signal transduction controlling sperm chemotaxis or for the process of sperm motility activation (Fehr et al, 2007), but little is known about their regulatory function. In a recent report, the expression of members of the bitter TAS2Rs family was demonstrated in ejaculated human sperm and in testicular tissue (Governini et al, 2020). Moreover, it also provided evidence that molecules involved in taste signal transduction cascade, whereby α -subtypes gustducin and transducin as well as the enzymes phosphodiesterase 4A, cAMP-specific (PDE4A), PLC β 2, and TRPM5, were detected in testicular tissue and ejaculated spermatozoa. The association of taste receptors activity with male infertility is realistic, because, to reach and fertilize the mature oocyte, mammalian sperm must undertake a long journey toward their destination in the upper region of the female genital tract. During their journeys through the female genital tract, mammalian sperm are exposed to a wide range of compounds of different origins and chemical properties (Figure 4). From the anterior vagina towards the mature oocyte, located in the ampulla of the fallopian tube, ejaculated sperm have to sense slight variations in the composition of different environmental chemical stimuli in the different regions of the female genital tract, like changes in the carbohydrate concentrations (Leese et al, 1981), in the levels of single amino acids (Harris et al, 2005; Jozwik et al, 2006), or variations in the ion composition and pH (Suarez et al, 2006; De Blas et al, 2009).

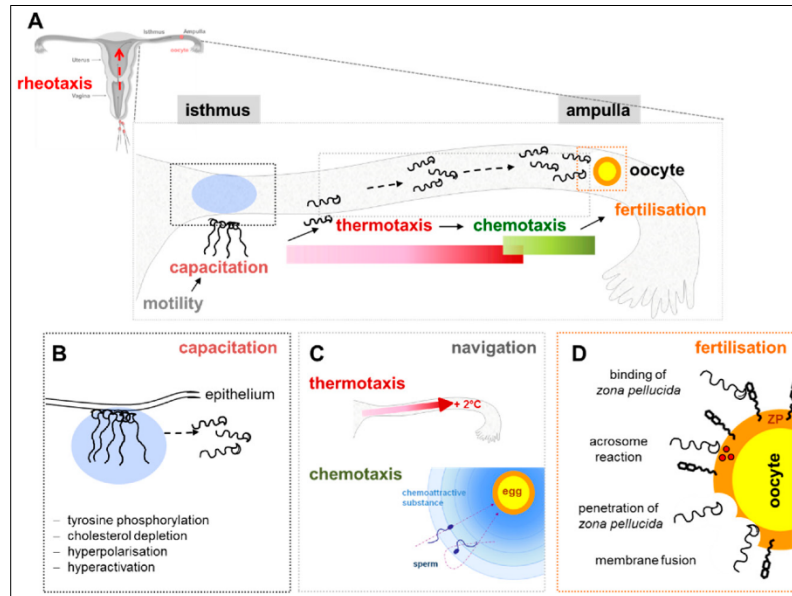


Figure 4: The journey of sperm through the female genital tract includes: rheotaxis, thermotaxis and chemotaxis, that allow sperm migration through the female reproductive tract, capacitation, a biochemical and morphological sperm change, and the fertilization (A). The mammalian sperm must undergo a series of modifications to be able to fertilize the oocyte, process called “capacitation” (B). The movement of sperm into the ampulla is due to the chemotaxis that allow to locate the oocyte (C). The fertilization takes place after specific steps: binding of zona pellucida, acrosome reaction, penetration of zona pellucida and final membrane fusion (D). Image from Luddi et al, 2019.

For the proper chemical communication with the oocyte’s environment, as well as with the oocyte itself, sperm are functionally reprogrammed in consequence of the capacitation process within the female’s genital tract (Austin, 1951; Chang, 1951; Florman et al, 2010). During their journeys through the female genital tract, sperm cells are exposed to different concentration of hormonal stimuli such as pH, amino acids and carbohydrates. All these factors seem to actively regulate the sperm maturation, motility and the chemoattraction.

However, despite the fundamental importance of detecting diverse chemical ligands for correct sperm function, our current knowledge about the molecular identity of chemosensory receptors on the sperm surface is still rudimentary. This notion holds true for promising zona pellucida-receptor candidates (Asano et al, 1997; Nixon et al, 2001), but also for receptor proteins that are able to detect chemical compounds in the different fluids of the female reproductive tract or chemoattractive cues responsible to successfully guide sperm towards the egg.

2 Oogenesis, folliculogenesis and follicular microenvironment

2.1 OOOGENESIS AND FOLLICULOGENESIS

The follicular development is a highly coordinated series of events that take place in the ovary, a multicompartamental organ with two key functions: the production of a competent oocyte and the secretion of steroid hormones, such as estrogen and progesterone, are required for the preparation of the endometrium to establish and to support a pregnancy (Oktem & Oktay, 2008). Follicles are the functional units of the ovary and they provide for and influence maturation and competence acquiring of the oocyte; it is composed by highly differentiated cells that grown in a follicular niche and develop cyclically after puberty (Gosden & Lee, 2010).

The Primordial Germ Cells (PGCs) are the primordial undifferentiated diploid sex cells, initially located outside the gonad. Oogenesis begins during embryonic development, between the sixth and eighth week of gestation, when PGCs migrate to the gonadal ridge from the yolk sac of the endoderm, the region that will form the future female gonad. During this period, the PGCs undergo to a great number of mitotic divisions that peak around 20 weeks of gestation to a total of about 7 million oogonia, unipotent stem cells (Ezzati & Zosmer, 2007). At the fifth month of embryonic life, the oogonia differentiate into primary oocytes that starts meiosis, but it stops at the diplotene stage of the prophase I. In this phase, folliculogenesis starts and each oocyte has to be provided with a single layer of cells, called granulosa cells to form a primordial follicle. The primordial follicle develops into a primary follicle characterized by the presence of one or more cuboidal granulosa cells. At the puberty, the number of primordial follicles is about 400,000, but only 400-450 of these will complete their maturation cycle (Baum et al, 2005). In fact, these primordial follicles remain in a quiescent state until, periodically, they are selected through a process called "initial recruitment". Those are selected continue their growth and thus enter a part of the pool of developing follicles (McGee & Hsueh, 2000) (Figure 5). During primary follicle development, a molecular and biological internship between granulosa cells and oocyte starts. Granulosa cells form gap junctions with the oocyte cell membrane, or oolemma, that are important channels for the diffusion of ions, metabolites, and other signaling molecules such as cAMP and calcium. This communication between granulosa cells and oocyte remains throughout folliculogenesis and it is responsible for the synchronous expression of important activities.

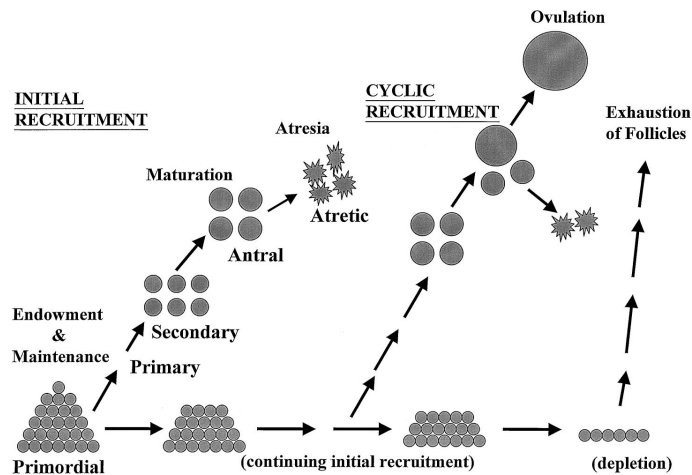


Figure 5: A fixed number of primordial follicles are determined during early life, and most of them are maintained in a quiescent state. Growth of some of these dormant follicles is initiated before and throughout reproductive life (Initial recruitment). Follicles develop through primordial, primary, and secondary stages before acquiring an antral cavity. At the antral stage most follicles undergo atresia; however, under optimal gonadotropin stimulation that occurs after puberty, a few of them are recruited to reach the preovulatory stage (Cyclic recruitment).
Image from McGee & Hsueh, 2000

During the recruitment, cuboidal granulosa cells undergo mitotic divisions and begin to express follicle stimulating hormone receptors (FSHR). The oocyte grows and differentiates. At this stage, the oocyte begins to synthesize a glycoprotein envelope, that encapsulates the egg, and which is called zona pellucida. The importance of the zona pellucida is emphasized by the ZP-3 protein, the species-specific sperm-binding molecule, responsible for initiating the acrosome reaction in capacitated sperm.

At the puberty, the hypothalamus secretes the gonadotropin releasing hormone (GnRH) which stimulates the pituitary gland to release follicle stimulating hormone (FSH) and luteinizing hormone (LH) in the bloods. FSH acts at the follicle level, in particular on the monolayer of granulosa cells, inducing their proliferation and forming the secondary follicle, characterized by somatic cells arranged in a multi-layered. At the same time, FSH stimulates the follicular cells to secrete a fluid, the follicular fluid, that is located inside of this structure creating a cavity called “antrum”, forming the tertiary follicle. After that, the follicle develops in the Graafian follicle, characterized by the enlargement of the antrum, with the FF pushing the oocyte close to the wall of the follicle itself (Hennet et al, 2012). The mature Graafian follicle is a big follicle of about 19-24 mm of diameter. At the antral stage, most follicles undergo atretic degeneration, whereas a few of them, under the cyclic gonadotropin stimulation that occurs after puberty, reach the preovulatory stage (McGee et al, 2000).

Simultaneously, also FSH and LH acts at the oocyte level and they stimulate the completion of the first meiotic division, that consists in an asymmetric division of the primary oocyte with the

formation of the secondary oocyte and a polar body. The secondary oocyte undergoes the second meiotic division, which stops in metaphase II; instead the polar body degenerates. The oocyte, blocked in metaphase II, is expelled from the ovary, by a process called ovulation, and it can be fertilized (Hyttel et al, 1997). Only with fertilization, the second meiotic division is completed with the release of the second polar body, while in the absence of fertilization the oocyte degenerates.

During the ovulation, the wall of the follicle becomes very thin and presents the stigma that is the point at which there will be the rupture of the follicle. In response to a peak of LH, the follicle breaks out and opens at the level of the stigma projecting outside the FF and the entire cumulus-oocyte complex. At the time of ovulation, the follicle empties most of its content and the cavity is filled with a blood clot, turning into a yellow, expanded structure, which is called the *corpus luteum* (Fausser & Van Heusden, 1997). If fertilization doesn't occur the corpus luteum remains active for twelve days and is called the corpus luteum albicans; if pregnancy begin, the corpus luteum increases in size and remains active for 3-4 months, and it becomes the *corpus luteum gravidarum*.

2.2 FOLLICULAR MICROENVIRONMENT

The ovarian follicle is a highly specialized microenvironment that provides for and influences the quality of the oocyte within. The antral stage is characterized by the appearance of a fluid-filled cavity, the antrum, which begins to form when follicles reach a critical size and a critical number of granulosa cells (Boland et al, 1994).

The follicular fluid, derived from the blood and from the secretion of the cells that delimits the follicle itself, provides a very important microenvironment and contains regulatory molecules, such as proteins, hormones, steroids and electrolytes, that are important for the maturation and quality of the oocytes (Revelli et al, 2009). The appearance of the antral cavity establishes the morphological and functional separation of granulosa cells into mural granulosa cells, which line the follicle wall, and the cumulus cells, which surround the oocyte (Hennet et al, 2012) (Figure 6). Cumulus cells have highly specialized cytoplasmic projections which penetrate through the zona pellucida and form gap junctions at their tips with the oocyte, forming an elaborate structure called the cumulus-oocyte complex (COC) (Albertini et al, 2001).

Each follicle is enveloped by a basal lamina, a specialized sheet of extracellular matrix that separates the internal follicle from the third somatic follicular cell type, the theca cells.

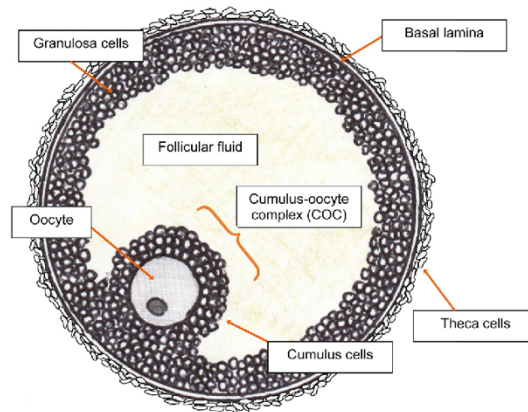


Figure 6: Schematic representation of an antral follicle. Image from Hennet et al, 2012.

The oocyte competence is defined as the mature oocyte's ability to resist steps of development, from fertilization to embryo implantation into the uterus. Each component of the antral follicle contributes to the formation of an essential microenvironment for oocyte maturation, differentiation and additional protection to the oocyte. The correct communication between the oocyte and surrounding somatic cells, namely granulosa and cumulus cells, play a key role in the acquisition of oocyte competence (Hussein et al, 2006). The close connection between the somatic cells and the oocyte itself, depending structurally and metabolically one each other, suggests that the healthy status state of these cells is closely correlated with the quality of the oocyte (Assidi et al, 2011). These coordinated interactions are crucial to develop a follicular microenvironment that controls primordial follicle growth, within a cohort of growing follicles, from which one antral follicle is selected to ovulate a mature oocyte. *In vitro* studies have shown that granulosa-oocyte communication is essential for the normal oocyte growth; in fact, immature oocytes separated from granulosa cells do not grow (McGee et al, 2000).

2.2.1 Granulosa cells

As the follicles mature, the granulosa cells multiply to form many layers around the oocyte, becoming the most abundant somatic follicular cells. Granulosa cells form a barrier around developing oocyte follicles and participate, through their steroidogenic activity, in the regulation of the oocyte development inside the follicle. Before ovulation, the granulosa cells produce estrogen that is then secreted into the bloodstream. After ovulation, these cells produce progesterone and they become granulosa lutein cells. The progesterone keeps the endometrium ready for the implantation of the embryo, and supports a pregnancy if fertilization occurs.

During folliculogenesis, granulosa cells differentiate into two distinct populations and they acquire different functional competencies depending on their location: mural granulosa cells and cumulus cells (Figure 7). While these populations are similar in many aspects, their migration to the outer or to the inner surface of the follicle is triggered by differences in both transcripts and proteins (Latham et al, 1999). In fact, mural granulosa cells support the oocyte via endocrine and paracrine pathways while cumulus cells are specialized in nutritional support and trafficking of macromolecules (Andrei et al, 2019).

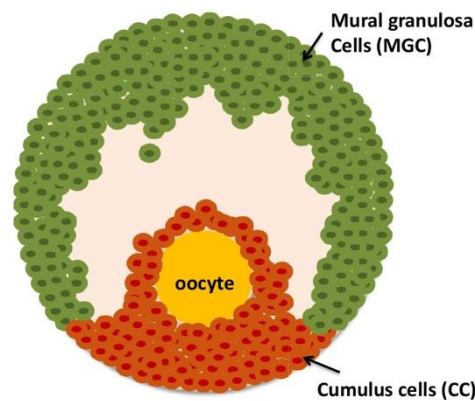


Figure 7: Mural Granulosa Cells (MGC) and Cumulus Cells (CC) are two specialized cell types that differentiate from a common progenitor during folliculogenesis. Image from Andrei et al, 2019.

The granulosa cells contact and communicate with the oocyte by prolongations forming gap junctions (TZP, Trans-Zonal Projections) (Simon et al, 1997). This communication is bi-directional and essential for the development of both granulosa cells and oocytes (Eppig et al, 1997). Paracrine communication also plays a key role in ovarian follicle homeostasis: there are many molecules, secreted by both oocyte and granulosa cells, which play a fundamental role in leading growth and differentiation of follicles.

2.2.2 *Cumulus cells*

Cumulus cells originate from relatively undifferentiated granulosa cells and form a multilayered structure surrounding the oocyte, generating the cumulus-oocyte complex (COC). Cumulus cells have highly specialized cytoplasmic projections that penetrate through the zona pellucida and form tight junctions with the oolemma (Albertini et al, 2001) (Figure 8).

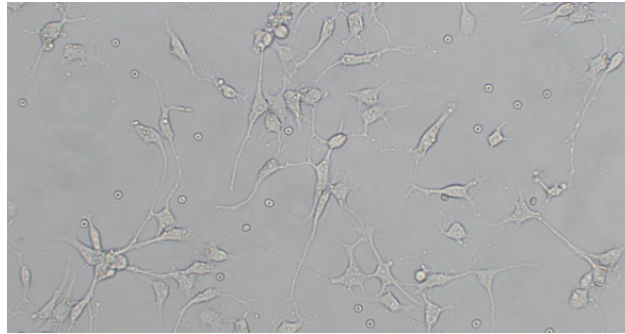


Figure 8: Representative image of cumulus cells in culture.

This close association allows cumulus cells to play key roles, supporting oocyte maturation and transmitting endocrine and environmental signals, such as ions, metabolites, amino acids and low molecular weight molecules involved in the signal transduction, hence providing the basis for a metabolic cooperation between oocytes and follicular cells (Gilchrist et al, 2008). The oocyte itself has a relatively poor capacity to utilize glucose for many essential metabolic processes. It has been demonstrated that mouse oocytes cultured in a medium with glucose, are not able to use it when isolated from cumulus cells; instead, when the oocytes are surrounded by cumulus cells, in the same conditions, glucose is converted into pyruvate by cumulus cells and transferred to the oocyte via the gap junctions, allowing a regular meiotic maturation (Biggers et al, 1967). It has also been shown that cumulus cells removal before complete maturation of the oocyte, determines a nuclear alteration and an alteration of the distribution of the cortical granules, which undergo early exocytosis, and this causes a hardening of the zona pellucida and a reduced penetrability of oocytes by sperm (Ge et al, 2008).

3 Male gonads and spermatogenesis

3.1 STRUCTURE OF TESTIS

Testis is covered by a dense protein envelop which creates a partition extending into the forming lobules. Inside each lobule, from 1 to 4 seminiferous tubules are located; they are convoluted tubules with spermatogenic epithelium inside (Figure 9). It is there that spermatogenesis occurs. The spermatogenic epithelium extends from the basal membrane, and it is organized in several layers, each of which, is a separate “generation” of germ cells. Between the germ cells, Sertoli cells are located, supporting and supplying nutrients and oxygen during division, growth and maturation of germ cells. In addition, they indirectly regulate spermatogenesis, producing androgen binding protein (ABP), which binds specifically to testosterone (T), dihydrotestosterone (DHT), and 17-beta-estradiol.

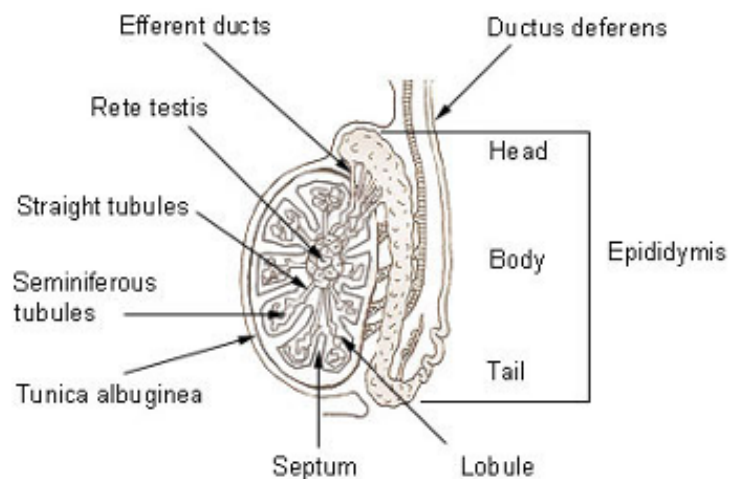


Figure 9: The male gonads, testis, is covered by seminiferous tubules containing germ cells and Sertoli cells. Spermatogenesis takes place in the tubules in concentric layers starting from the outer basal epithelium.

Tight junctions among Sertoli cells form the hemato-testicular barrier around developing male gametes, protecting them from immunological attacks. Sertoli cells produce inhibin, that inhibits the secretion of gonadotrophins from the hypophysis decreasing the proliferation rate of spermatogonia and enhances the synthesis of testosterone and the maturation of spermatozoa from spermatogonia (Rato et al, 2012). Sertoli cells also produces activins, anti-Müllerian hormone, ABP, estradiol, glial cell line-derived neurotrophic factor. The involvement of Sertoli cells in sperm’s DNA repairing has been also suggested (Ahmed et al, 2009).

In the interstitial spaces, between the seminiferous tubules, Leydig cells are located: they produce testosterone and other androgenic compounds.

Around the seminiferous tubules, peritubular myoid cells are involved in the sperm transport and in maintaining the structural integrity of the tubules. Moreover, peritubular myoid cells affect Sertoli cells function through the secretion of growth factors and components of the extracellular matrix (Maekawa et al, 1996; Johnson et al, 2007).

3.2 SPERMATOGENESIS

The spermatogenesis is a dynamic developmental process of proliferation and differentiation during which spermatogonial stem cells (SSCs) become fully differentiated spermatozoa. The process begins at puberty, when a complex system of hormonal regulation is activated and promotes the formation of spermatozoa and seminal plasma. Spermatogenesis takes place in the testes and proceeds inside the seminiferous tubules, whose epithelium consists of different cell types: somatic cells, called Sertoli cells and Leydig cells. The germ cells are organized in concentric layers, at different stages of development, from the basement membrane to the lumen of seminiferous tubules (Luddi et al, 2019) (Figure 10). Spermatogenesis is supported by the spermatogonial stem cells, which are defined as possessing the ability to self-renew and to differentiate into spermatozoa. The dual capacity of these cells ensures the long-lasting ability of the testes to produce spermatozoa. The process of spermatogenesis occurs in mitotic, meiotic and postmeiotic phases.

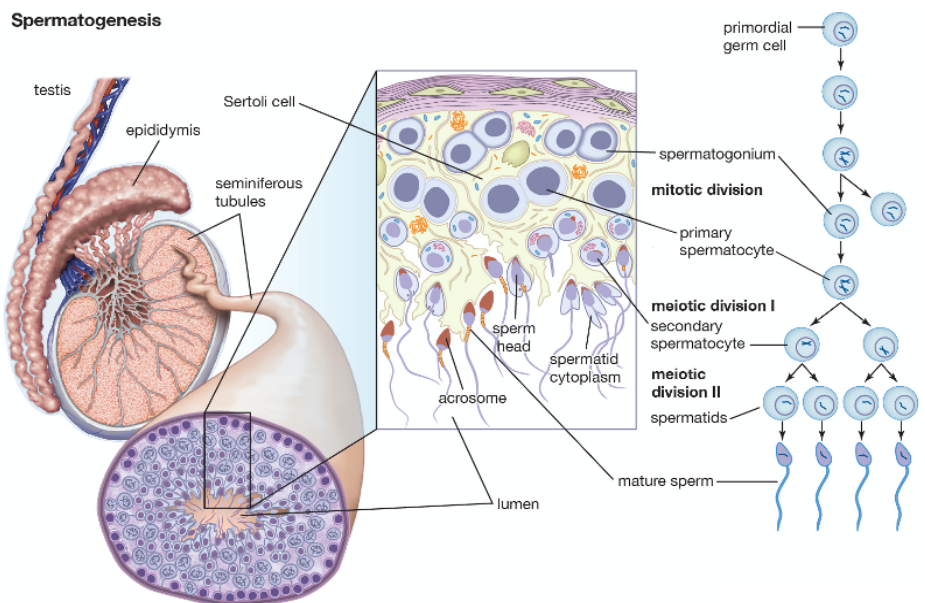


Figure 10: Structure and cellular organization of the mammalian testis: 1 Testicle; 2 Cross section of a seminiferous tubule; 3 Enlargement of the tubule region; 4 Main events of division and differentiation taking place during the spermatogenesis cycle.

In the mitotic phase, called also proliferative phase, the diploid spermatogonial cells (spermatogonia), located on the basal membrane of the seminiferous tubule (De Rooij, 1998), undergo multiple mitotic divisions. During this phase two types of spermatogonia are generated: type A spermatogonia (distinguishable in A dark (Ad) spermatogonia, reserve stem cells, and A pale (Ap) spermatogonia), and type B spermatogonia, derived from Ap, to form primary spermatocytes. Primary spermatocytes are located in the adluminal compartment, and they enter in the second phase of spermatogenesis (De Jonge & Barratt, 2006). The meiotic phase begins when the primary spermatocytes undergo the first meiotic division generating the secondary spermatocytes which, undergo the second meiotic division forming, for each secondary spermatocyte, two haploid spermatids. The following process of maturation is called spermiogenesis, during which spermatids undergo deep morphological and cytological changes. At morphological level, spermatids develop a distinct head, midpiece and tail region. At cytological level, they undergo chromatin remodeling, develop an acrosome and lose almost all of the cytoplasm. Mature spermatozoa are released into the lumen of the seminiferous tubules and they are pushed by the contractile myoid cells of the tubular wall towards the epididymis, where they complete their maturation becoming mobile.

The entire process is under strict hormonal control and the differentiated germ cells are supported physically and metabolically by Sertoli cells, which by establishing occlusive junctions, create the blood-testicular barrier necessary for the protection of developing gametes (Luddi et al, 2019)

(Figure 11). Sertoli cells, that are in the basal lamina of the seminiferous tubules, are stimulated by FSH to secrete ABP, protein that by binding to testosterone it is able to regulate its concentration to a level that supports spermatogenesis. Testosterone is released from Leydig cells located between the seminiferous tubules of the testis following stimulation by LH. The pituitary secretion of FSH and LH is regulated by the releasing factor produced by the hypothalamus, specifically the GnRH.

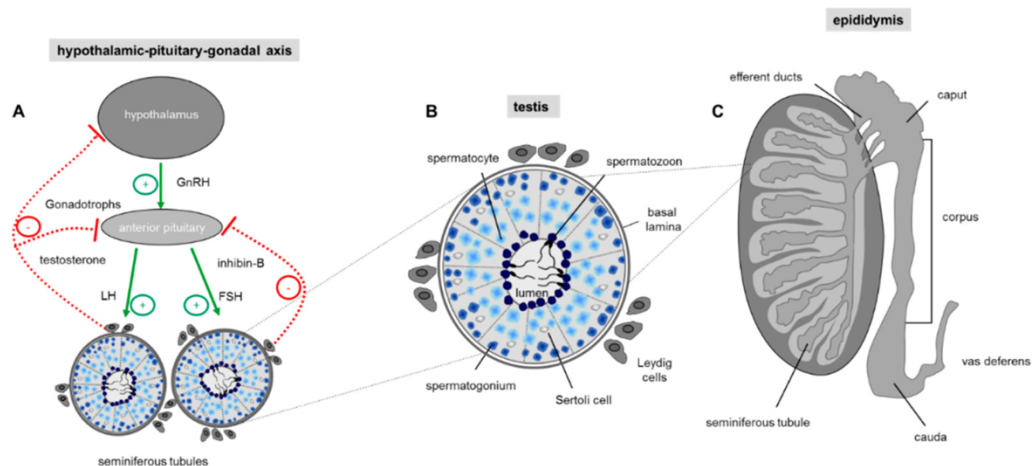


Figure 11: Regulation of sperm production. (A) Hormonal control of spermatogenesis in the testis. (B) Schematic drawing of a single seminiferous tubule with different stages of developing germ cells during spermatogenesis. (C) Schematic drawing showing a sagittal section through a whole testis and the overlying epididymis. Image from Luddi et al, 2019.

3.3 SPERMATOZOA

During the spermiogenesis process, spermatids become spermatozoa due to a series of important morphological modifications. It is in fact during this phase that the acrosome and a long flagellum are formed and the typically round cells assume a hydrodynamic shape thanks to the removal of the cytoplasm, worked by the Sertoli cells, and to the replacement of nuclear histones with basic proteins called protamine, which guarantee maximum chromatin compaction (Champroux et al, 2016). The spermatozoa are specialized cells whose functions are strictly dependent on the morphology, that allows it to move and fertilize the egg cell. A mature sperm is 60 μm long and consists of the head, a connection region called the neck and a flagellum (about 55 μm) made up of the intermediate, main and terminal segments (Figure 12).

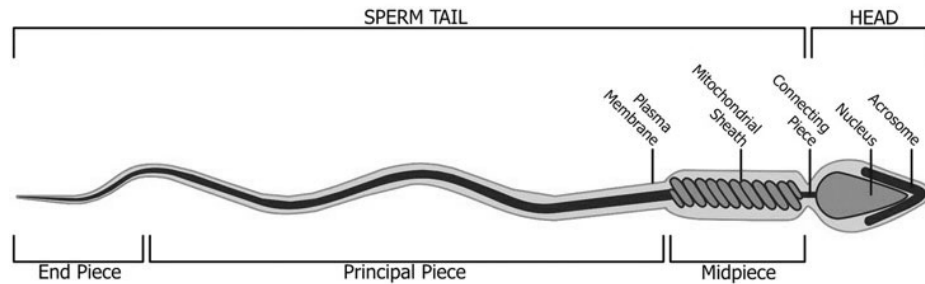


Figure 12: Representation of a mature sperm and its main parts

The head of sperm contains the nucleus, which includes the genetic material and the acrosome. With spermatogenesis, spermatozoa of two types are formed: carriers of the X chromosome and carriers of the Y chromosome. Sperm nucleus is much smaller than the nuclei of other cells, approximately 5% of the nuclear volume of a somatic cell; this is mainly due to the high degree of sperm chromatin condensation (Ward et al, 1991) that makes sperm transcriptionally and translationally silent. The DNA in mammalian sperm is about 6 times denser than that of mitotic chromosomes and shows a "DNA loop domains" organization (Balhorn, 1982). The acrosome, which partly covers the head, is a large lysosome that originates from the Golgi apparatus and contains enzymes (including acid hydrolases, hyaluronidase, acrosin, beta-galactosidase, neuroaminidase) essential for the sperm to penetrate the envelopes covering the oocyte. During the acrosomal reaction, these enzymes are released when the outer acrosomal membrane and the plasma membrane fuse and vesiculate, allowing the sperm to penetrate the oocyte through the zona pellucida (Zanetti & Mayorga, 2009).

Between the head and the flagellum there is a thin section of conjunction, called neck which contains the proximal centriole, a variable amount of cytoplasm and a basal plate of dense material where the axoneme is anchored, composed of 9 outer doublet tubules surrounding circumferentially two central microtubules (9+2 complex), which originates from the proximal centriole present right in the neck.

The flagellum or tail, starting from the neck, contains the energy sources and apparatus to produce the motility necessary for the movement of the sperm to fertilize the oocyte. The central component of the flagellum is the axoneme. The flagellum consists of different segments: the middle piece, the principal piece and the end piece. The middle-piece segment is characterized by the presence of a tight helix of mitochondria around the outer dense fibers of the sperm tail, which are important for energy supply during the flagellar movement. The principal piece constitutes most of the tail and provides flexibility for the spermatozoa. It contains a sheath of ring fibers that are attached to the outer wall of the doublet microtubules of the axial filament. The sudden ending of the fibrous sheath marks the region of transition between the principal and the end piece. The end piece is the

narrowest part of the sperm, consisting of a central pair of axial fibrils and ring of nine doublet fibers, which are surrounded by the plasma membrane. The 9+2 pattern of axial filament complex extends also in the end piece, but the arrangement of the fibers in the tip of the end piece contains a smaller number of fibers.

3.4 CAPACITATION OF SPERM IN THE FEMALE GENITAL TRACT

After ejaculation, although motility has acquired, sperm are still not fertile. In order to become able to fertilize the oocyte, a series of modifications are necessary which take place along the female genital tract (Chang, 1951). During the journey through the genital female tract, the sperm cells undergo a series of biochemical and physiological modifications (De Jonge, 2006); for example, the plasma membrane of the spermatozoa are deeply remodeled with the removal of glycerophospholipids and cholesterol, acquired by the spermatozoa during their stay in the epididymis (Feki et al, 2004). Cholesterol is the main inhibiting factor of capacitation (Cross, 1998) and its removal is important for increasing the influx of Ca^{2+} and terminating HCO_3^- ions and for altering the permeability and fluidity of the sperm plasma membrane. A subsequent cascade of signaling events activates the adenylyl cyclase, thus stimulating an increase of the level of cAMP and activation of protein kinase A (PKA), leading a phosphorylation of various target proteins (Chen et al, 2000; Ickowicz et al, 2012). In addition, CatSper, a specific cation channel receptor (Strünker et al, 2011), is activated by progesterone during capacitation, in a hyperactivation of sperm, thereby increasing sperm motility (Ren et al, 2001).

Once in the oviduct, sperm cells find an environment completely different in terms of chemical and hormonal composition and they are guided toward oocyte by different mechanism: thermotaxis (De Toni et al, 2016), chemotaxis (Sugiyama & Chandler, 2014) and rheotaxis (Miki & Clapham, 2013). When the spermatozoa come into close contact with the oocyte in the ampulla of the fallopian tube and approach the zona pellucida, acrosomal reaction initiates. The acrosomal reaction is an exocytotic process, allowing the spermatozoa to penetrate through the corona radiata and the zona pellucida and join with the plasma membrane of the oocyte. This process determines the release via exocytosis of hydrolytic enzymes from the acrosome that destabilizes the zona pellucida, making the oocyte accessible for fusion with the spermatozoa (Clark & Dell, 2006).

In conclusion, it is possible to affirm that a complete maturation and capacitation of the spermatozoa confers on it the ability to cross the female genital tract, to undergo acrosomal reaction and to fertilize the oocyte (Yanagimachi, 2005).

Research study purpose

Infertility is defined by the World Health Organization (WHO) as a reproductive system disease; it results in the inability to conceive after one year of unprotected intercourse and it affects an estimated 15% of couples in reproductive age. About 40% of cases of infertility are due to a problem in the male, about 40% to a problem in the woman, and the remaining 20% of cases of infertility are due to combined problems in both partners and, in part, they still remain unexplained. A central point in the fertilization process is represented by the attraction and recognition between sperm and oocyte: chemoattractants are released from both cumulus cells and oocyte. Several molecules are involved in this crosstalk, among these, progesterone released from cumulus cells plays a pivotal role. The complete process is not fully understood yet and the identity of all the involved molecules as well as their matching receptors remains unknown. The expression of taste receptors in the human sperm seems to suggest their possible involvement in sperm maturation as well as in sperm behavior, chemotaxis and fertilization.

The purpose of this thesis was to shed light on the role of taste receptors in the process of sperm-oocyte attraction and recognition, and their potential function in the female and male reproductive system. To this end, we investigated the expression and localization of taste receptors in follicular somatic cells, granulosa and cumulus cell, obtained from women undergoing assisted reproduction techniques. In order to deeply investigate the functional role of these receptors in human gametes, we also analyzed their expression in testis and ejaculated sperm. Finally, the components of signal transduction cascade involved in the pathway of taste receptors were evaluated in all investigated cells.

Materials and Methods

1 Sample collection

Female subjects.

For this study, we have collected granulosa and cumulus cells from women, diagnosed with a male infertility factor, who underwent *in vitro* fertilization at the UOSA of Assisted Reproductive Technique (ART), Siena University Hospital. Ethical approval for the study was obtained from the Siena University Hospital local ethical Committee. All women have signed a written informed consent. Exclusion criteria from the study were the presence of severe bacterial or viral infections. The immortalized human granulosa cell line hGL5 was kindly provided by Prof. Livio Casarini (Unit of Endocrinology, Department of Biomedical, Metabolic and Neural Sciences, University of Modena and Reggio Emilia). In this work of thesis, hGL5 are used as control in the western blot analysis.

Male subjects.

This study was conducted in male undergoing fertility evaluation at the UOSA of Assisted Reproductive Technique, Siena University Hospital. A comprehensive clinical history of patients was obtained and possible causes of male infertility such as varicocele, cryptorchidism, genetic or endocrine disorders were excluded. All participants have signed a written informed consent and the study protocol was approved by the ethic Committee of the Siena University Hospital.

1.1 FOLLICULAR CELLS RECOVERY AND ISOLATION

Follicular cells were collected from women undergoing ART. To this end, hormonal controlled ovarian hyperstimulation was performed in order to stimulate a multifollicular growth, according to a protocol that provides treatment with GnRH antagonists, for hypophysis down-regulation, followed by administration of recombinant FSH (rFSH). The dose and the time of gonadotropin treatment was modified according to the individual response of the patient, by monitoring estradiol serum concentrations and size and number of follicles, using ultrasound. When at least two or three follicles had reached 18-20 mm in diameter, ovulation was induced with 10,000 IU of recombinant HCG. Oocyte retrieval was scheduled 34-36 h after HCG administration.

1.1.1 Granulosa cells isolation

After oocyte retrieval (pick-up), follicular fluid sample was immediately processed to collect granulosa cells by centrifugation at 500 rcf for 10 minutes. The obtained pellet, containing cellular fraction (granulosa cells but also endothelial cells, red blood cells, white blood cells and macrophages), was processed in order to isolate granulosa cells. The cell pellet was resuspended in 2 mL of Hanks Balanced Salt Solution (HANKS) (Sigma-Aldrich), layered on 4 mL of 45% Percoll and centrifuged at 2195 rcf for 20 minutes in a centrifuge without brake. After centrifugation, the red blood cells were at the bottom of the tube and the granulosa and endothelial cells were layered forming a clearly visible ring that was collected in HANKS and centrifuged at 500 rcf for 10 minutes. The cell pellet was resuspended in complete culture medium containing: DMEM (Dulbecco's Modified Eagle Medium) (Sigma-Aldrich), 10% fetal bovine serum, 1% essential amino acids (Sigma-Aldrich), 100 mM L-glutamine (Sigma-Aldrich), 5000 IU/ml of penicillin and 5 mg/ml of streptomycin (Sigma-Aldrich) and transferred into a Petri dish. After incubation for 10 minutes at 37 °C and 5% of CO₂, which allows selective adhesion of endothelial cells and macrophages, the medium containing purified granulosa cells was definitively plated in a new Petri dish and placed in an incubator (Figure 13). After 24 hours of culture, the granulosa cells were washed with HANKS and then collected with 350 µl Buffer RLT (Qiagen) and stored at -80°C until RNA extraction.

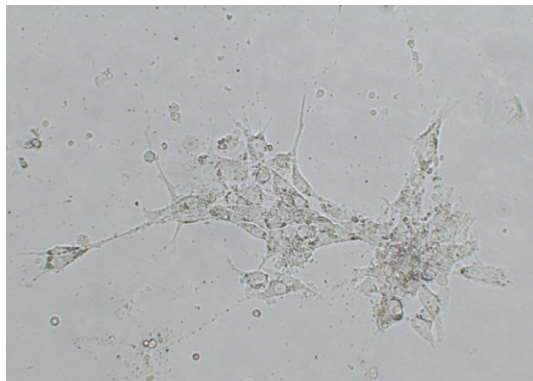


Figure 13: Representative image of granulosa cells in culture.

1.1.2 *Cumulus cells isolation*

Oocytes were decumulated by the action of 80 IU hyaluronidase enzyme (Irvine Scientific) and then by a mechanical action through the use of a denudation pipettes (170 and 140 µm of diameter). The cumulus cells were centrifuged at 500 ref for 10 minutes; then the supernatant was removed, and the cell pellet was washed with HANKS and resuspended with 350 µl of Buffer RLT (Qiagen) and stored at -80°C until RNA extraction.

1.2 HUMAN GRANULOSA CELL LINE (hGL5)

The immortalized human granulosa cell line hGL5 was previously characterized (Rainey et al, 1994; Casarini et al, 2016). The cell line hGL5 was permanently transfected by electroporation with LHCGR wild type (Casarini et al, 2012). hGL5/LHCGR cells were cultured in DMEM/F12 supplemented with 10% FBS, 2% Ultrosor G, 2 mM L-glutamine, 100 U/ml penicillin and 100 µg/ml streptomycin. The cell line was maintained in an incubator at 37°C and with 5% CO₂. In this work of thesis hGL5 are used as control in the western blot analysis.

1.3 SPERM AND TESTICULAR TISSUE

Semen sample were obtained by masturbation after 3-5 days of sexual abstinence. Standard semen analysis was performed according to WHO (2010) protocol and study subjects were characterized for main sperm parameters, namely concentration, morphology, progressive and total motility. The main sperm parameters are reported in the Table 1.

Table 1: Lower Reference Limit (Human Semen)

Parameter	Lower Reference Limit (Confidence interval)
Semen volume (ml)	1.5 (1.4-1.7)
Total sperm number (10 ⁶ per ejaculate)	39 (33 – 46)
Sperm concentration (10 ⁶ per ml)	15 (12 – 16)
Total motility (PR+NP, %)	40 (38 – 42)
Progressive motility (PR, %)	32 (31 – 34)
Vitality (live spermatozoa, %)	58 (55 – 63)
Sperm morphology (normal forms, %)	4.0 (3.0 – 4.0)

After semen analysis, spermatozoa were isolated from seminal fluid. For this purpose, the seminal fluid of each patient was stratified on a 2 ml gradient formed by 80% and 40% Percoll and centrifuged at 400 rcf for 20 minutes. The sperm pellet thus obtained was resuspended in 2 ml of HANKS and centrifuged at 500 rcf for 10 minutes and then resuspend in Trizol (TRI Reagent® Sigma) and stored at -80°C until RNA extraction. Small fragment of testicular tissue, obtained during testicular surgery from patients undergoing diagnostic testicular biopsy for obstructive azoospermia, were washed in a Petri dish containing Sperm Washing Medium (Irvine Scientific) and fragmented into small pieces. The presence of spermatozoa is confirmed by observation under an optical microscope. The fragments of testicular tissue were immediately immersed in 600 μl of Buffer RLT (Qiagen) and stored at -80°C until RNA extraction.

2 Gene expression analysis

2.1 RNA EXTRACTION

2.1.1 Granulosa and cumulus cells

RNA was extracted by using the Qiacube (Qiagen) automatic extractor following the manufacturer protocol of RNeasy Mini kit (Qiagen). At the end of the protocol, the RNA extracted from each sample was eluted in a final volume of 30µl of water.

2.1.2 Human sperm

The sperm samples collected in Trizol were thawed and then RNA was extracted. After homogenization by TissueLyzer (Qiagen), 200 µl of chloroform were added to each sample and centrifuged at 13,000 rcf for 15 minutes at 4°C, allowing the separation of an organic phase and an aqueous phase. The organic phase was isolated and stored for subsequent extraction of the proteins, while the aqueous phase, containing the RNA, was transferred to a new vial with 500µl of isopropanol at 4°C. The samples were incubated at -20°C for about 24h. The following day the samples were centrifuged at 13,000 rcf for 15 minutes at 4°C. The supernatant was discarded, and the pellets washed twice with 250 µl of 70% ethanol and centrifuged at 13,000 rcf for 5 minutes at 4°C. The pellets were dried and then resuspended in 20 µl of H₂O nuclease free.

2.1.3 Testicular tissue

Frozen tissue samples were homogenized with TissueLyzer (Qiagen) and RNA was extracted by using the RNeasy Mini kit (Qiagen) according to the manufacturer's instructions.

2.2 RNA CONCENTRATION MEASURING

RNA purity and concentration of each sample was evaluated using an ND-1000 Nanodrop Spectrometer (Thermo Fisher Scientific, Wilmington, Delaware). Moreover, the quality of the extracted RNA was estimated in terms of purity, by evaluating the ratios A260/A280 and A260/A230 that are the index of protein contamination and the index of presence of other contaminants, respectively.

2.3 COMPLEMENTARY DNA PREPARATION

Extracted mRNA was reverse transcribed into cDNA using the iScript gDNA Clear™ cDNA Synthesis Kit (Bio-Rad Laboratories, Hercules, CA, USA); in the first step it includes a treatment with the reaction master mix of DNase to eliminate any contaminating genomic DNA. The digestion protocol requires that the mix is prepared in a volume of 8 µL for each sample; 500 ng of RNA are reverse transcribed for each sample.

iScript DNase Buffer	0,75 µl
iScript DNase	0,25 µl
RNA template (500 ng)	6,5 µl
H ₂ O	0,5 µl
Total	8 µl

Using a thermal cycler, the samples were incubated for 5 min at 25°C and then for 5 min at 75°C, in order to inactivate the DNase and stop the reaction. After the first step, we added 2 µl of iScript Reverse Transcription Supermix in each sample, then they are incubated in the thermal cycler.

Step	Temperature	Time
Primer pairing	25°C	5 min
Reverse transcription	46°C	20 min
Inactivation	95°C	1 min

2.4 DROPLET DIGITAL PCR (DDPCR)

The ddPCR is a method that uses an emulsion PCR technology, providing a series of steps that lead to generate tens of thousands, even millions, of single water-in-oil droplets. The droplets serve as sample dispersion carriers for digital PCR and the fluorescence signal within each droplet is detected at the end of the PCR reaction. The droplets in which the amplification reaction of the target gene took place were defined as positive and are fluorescent, a characteristic that their reading through a fluorescence detector; droplets that do not contain the target gene were defined as negative and they were not fluorescent. The primer assays used in this study are shown in Table 2.

The ddPCR method was applied using the QX200™ Droplet Digital™ PCR System (Bio-Rad Laboratories, Hercules, CA, USA). The samples were prepared, in a 96-well PCR plate, using a reaction mix shown in the following tables.

ddPCR Supermix for Probes (No dUTP)

2x ddPCR Supermix for Probes (No dUTP)	11µl
20x target probe (FAM)	1.1µl
20x target probe (HEX)	1.1µl
RNase-free sterile water	6.3µl
cDNA	2.5µl
Total	22µl

QX200 ddPCR EvaGreen Supermix

2x QX200 ddPCR EvaGreen Supermix	11µl
PrimePCR EvaGreen Assays	0.6µl
RNase-free sterile water	8µl
cDNA	2.5µl
Total	22µl

Each 20 µl ddPCR reaction was loaded into an 8-channel droplet generation cartridge (Bio-Rad Laboratories, Hercules, CA, USA); 70 µL of QX200 Droplet generation oil (Bio-Rad Laboratories, Hercules, CA, USA) were added into the appropriate wells and the cartridge was loaded in the QX200™ Droplet Generator (Bio-Rad Laboratories, Hercules, CA, USA) to generate the emulsion. The system generates until 20000 droplets in the superior row of the strip, that are transferred in a 96-well plate (Bio-Rad Laboratories, Hercules, CA, USA) plate that is sealed with a PX1 PCR plate sealer at 175°C and amplified by standard PCR using T100™ Thermal cycler (Bio-Rad Laboratories, Hercules, CA, USA).

ddPCR Supermix for Probes (No dUTP)

Cycling step	Temperature	Time	Ramp rate	Number of cycles
Enzyme activation	95°C	5 min	2°C/sec	1
Denaturation	95°C	30 sec		40
Annealing	58°C	1 min		40
Signal Stabilization	4°C	5 min		1
	90°C	5 min		1
Stabilization	4°C	30 min		1
Hold	4°C	Infinite		1

QX200 ddPCR EvaGreen Supermix

Cycling step	Temperature	Time	Ramp rate	Number of cycles
Enzyme activation	95°C	5 min	2°C/sec	1
Denaturation	96°C	30 sec		40
Annealing	58°C	1 min		40
Signal Stabilization	4°C	5 min		1
	90°C	5 min		1
Stabilization	4°C	30 min		1
Hold	4°C	Infinite		1

After the PCR reaction, the plate is stored at 4°C for 24h in order to stabilize the droplets. After other 30 min at room temperature, the plates were loaded into QX200™ Droplet Reader (Bio-Rad Laboratories, Hercules, CA, USA) for detection, whereby the strument aspirates the droplets with a needle, separates and aligns each droplet, that is analyzes by two lasers to detect fluorescence. In the final step, the analysis of the data is represented in graphs as EvaGreen® fluorescence relative to each droplet (Event Number). The software is used for data acquisition to calculate the absolute concentration of target DNA in copies/μl of reaction using Poisson distribution analyses. Primers used in this thesis are Bio-Rad validated primers.

Table 2: PrimePCR ddPCR Gene Expression Probe Assays, specific for ddPCR

Target Genes	Acronym	ID assay Probe	ID assay Primer
<i>Taste receptor, type 2, member 3</i>	TAS2R3	dHsaCPE5028212	dHsaEG5003946
<i>Taste receptor, type 2, member 4</i>	TAS2R4	dHsaCPE5028214	dHsaEG5003947
<i>Taste receptor, type 2, member 14</i>	TAS2R14	dHsaCPE5043852	dHsaEG5003736
<i>Taste receptor, type 2, member 19</i>	TAS2R19	dHsaCPE5027704	dHsaEG5003736
<i>Taste receptor, type 2, member 43</i>	TAS2R43	dHsaCPE5192389	dHsaEG5004567
<i>G-protein subunit alpha transducin 1</i>	GNAT1	dHsaCPE5025595	dHsaEG5000400
<i>G-protein subunit alpha transducin 3</i>	GNAT3	dHsaCPE5043953	dHsaEG5024588
<i>Phosphodiesterase 4A, cAMP-specific</i>	PDE4A	dHsaCPE5046851	dHsaEG5014540
<i>Phospholipase C, beta 2</i>	PLCB2	dHsaCPE5047389	dHsaEG5015173
<i>Transient receptor potential channel, subfamily M, member 5</i>	TRPM5	dHsaCPE5032805	dHsaEG5001934
Reference Genes	Acronym	ID assay Probe	ID assay Primer
<i>Hypoxanthine-Guanine Phosphoribosyl Transferase 1</i>	HPRT1	dHsaCPE5192871	-
<i>Tata Binding Protein</i>	TBP	dHsaCPE5058363	-
<i>Peptidylprolyl isomerase B (cyclophilin B)</i>	PPIB	dHsaCPE5055049	dHsaEG5022088
<i>Glyceraldehyde-3-phosphate dehydrogenase</i>	GAPDH	dHsaCPE5031596	dHsaEG5006642
<i>Actin, beta</i>	ACT-B	-	dHsaEG5188254
<i>Beta-2-microglobulin</i>	B2M	-	dHsaEG5020739

2.4.1 ddPCR data analysis

The software QuantaSoft (Bio-Rad Laboratories, Hercules, CA, USA), provided with the ddPCR system, was used for data analysis; according to international guidelines, only reactions having more than 10,000 droplet events were analyzed. Discrimination between droplets that did not contain target (negatives) and those that did (positives), is achieved by applying a global fluorescence amplitude threshold in the QuantaSoft. The data from the ddPCR are given in target copies/ μ l reaction. Template copies/ μ l present in the initial sample are then calculated using Poisson statistics.

$$\lambda = -\ln(1 - p)$$

In this equation, λ represents the average number of target DNA molecules per replicate reaction and p represents the fraction of positive end-point reactions. From λ , together with the volume of each replicate PCR and the total number of replicates analyzed, an estimate of the absolute target cDNA concentration is calculated. QuantaSoft uses a proprietary signal processing algorithm to

automatically perform droplet gating within each run. The threshold was set as the midpoint between the average fluorescence amplitude of positives and negative droplet clusters. In digital PCR an increase of number of replicates produces approximately an increase of dynamic range. Increasing the number of partitions also improves the precision and for this reason it enables resolution of small concentration differences between nucleic acid sequences in a sample.

2.4.2 ddPCR statistical analysis

All the data have been normalized using the geometric means of reference genes, and the relative gene expression has been shown as Normalized Sample Amount (NSA). As evaluation of ddPCR gene expression data has been applied to a t-test and differences with p-value ≤ 0.05 were considered statistically significant.

2.5 QUANTITATIVE REAL TIME-PCR

The quantitative real-time PCR allows real-time measure of the concentration of a target sequence in a biological sample. If combined with the reverse transcription (qRT-PCR), this procedure is used to quantify the expression of genes of interest relating to that of the control genes, named housekeeping genes. In this way it is possible to know the level of expression of one or more genes within different tissues or cell types. The qRT-PCR primers were ordered from Integrated DNA Technologies (IDT). Conditions for reaction (annealing time and number of cycles) have been developed in an appropriate manner for each single pair of primers. The primer assays used in this study are shown in Table 3.

Table 3: Primers for qRT-PCR analysis

Target Genes	Acronym	Primers forward (5'→3')	Primers reverse (5'→3')
<i>Androgen Receptor</i>	AR	TTGTCCATCTTGTCGTCTTCG	ACCAAGTTTCTTCAGCTTCCG
<i>c-myc</i>	MYC	TCCTCGGATTCTCTGCTCTC	TCTTCCTCATCTTCTTGTTCCTC
<i>Signal Transducer and Activator of Transcription 5A</i>	STAT5A	AACAGAGGCTGGTCCGA	CTGGTTGATCTGAAGGTGCT
<i>Signal Transducer and Activator of Transcription 5B</i>	STAT5B	CAGTGTGGGTGGAAATGAGC	AAGCATTGTCCCAGAGAACAG
<i>Peroxisome Proliferator-Activated Receptor Gamma</i>	PPARG	GTTTCAGAAATGCCTTGCACT	GGATTCAGCTGGTCGATATCAC
<i>GA-Binding Protein Alpha</i>	GABPA	TGGAACAGAGAAAGCAGAGTG	TGTAGTCTTGTTCTAGCAGTTTC
Reference Genes	Acronym	Primers forward (5'→3')	Primers reverse (5'→3')
<i>Hypoxanthine-Guanine Phosphoribosyl Transferase 1</i>	HPRT1	TTGTTGTAGGATATGCCCTTGA	GCGATGTCAATAGGACTCCAG

The mRNA levels were measured in triplicate on 1:5 dilutions of each cDNA in a reaction mix using SsoAdvanced Universal SYBR Green Supermix (Bio-Rad Laboratories, Hercules, CA, USA) shown in the following table.

SsoAdvanced Universal SYBR Green Supermix

SsoAdvanced Universal SYBR Green Supermix	6µl
PrimeTime qPCR Primers	1.2µl
RNase-free sterile water	3.3µl
cDNA	2.5µl
Total	12µl

The sample are amplified by standard PCR on CFX Connect Bio-Rad Laboratories, Hercules, CA, USA). For each run, melting curve analysis was used to confirm the specificity of the amplified products. Final results were expressed as fold differences in gene expression relative to the normalized calibrator, calculated by $\Delta\Delta C_t$ method. Finally, through the formula $2^{-\Delta\Delta C_t}$, it is possible to calculate the number of times of expression (Expression Fold).

3 Protein analysis

3.1 PROTEIN EXTRACTION

Granulosa and cumulus cells and hGL5 cell line were resuspended in RIPA +++ buffer (containing 0.05 M Tris; 0.15 M NaCl; 1% Triton X; 0.1% sodium deoxycholate; 0.1% Sodium Dodecil Sulphate, SDS; addition of 0.1M sodium orthovanadate, 0.01M phenylmethylsulfonyl fluoride, PMSF and protease inhibitor) for Sodium Dodecil Sulphate-polyacrylamide gel electrophoresis (SDS-PAGE). Samples were sonicated three times, each 10 seconds, and then centrifuged at 13000 g for 10 minutes.

For protein extraction from sperm, the organic phase previously obtained by the RNA extraction procedure was processed. After adding 300 µl of ethanol, the samples were agitated and then centrifuged at 12,000 rcf for 5 min at 4°C. The supernatant was transferred into new tubes containing 1,5 mL of isopropanol, vortexed and then centrifuged at 12,000 rcf for 10 min at 4°C. The protein pellet obtained was washed three times, for 20 min, in a solution of 0.3M guanidine in 95% ethanol. The protein pellet was washed for the last time with 100% ethanol for 20 min and then ethanol was removed. The pellet was finally dried and resuspended in an appropriate volume of H₂O.

The protein concentration of each sample was evaluated by the Bradford assay, a colorimetric method based primarily on the use of a dye, the Coomassie Brilliant blue, which binds to proteins at residues of arginine, tryptophan, tyrosine, phenylalanine and histidine (Bradford, 1976). This stain exists in two forms, a cationic one which has a maximum absorption at 470 nm (red color) and an anionic form, able to bind to proteins, which has a maximum absorption at 590 nm (blue color). Discrete volumes of samples to be measured were reacted with Bradford's dye and, by determining their absorbance at 590 nm, it was possible to extrapolate the protein concentration of the samples based on a standard curve constructed by relating known concentrations of bovine serum albumin (BSA; Sigma-Aldrich), and their respective absorbance.

3.2 WESTERN BLOT

SDS-PAGE and Immunoblotting

In the western blot technique, proteins are resolved by electrophoresis on a polyacrylamide gel and transferred, for electro-capillarity (blotting), on a nitrocellulose membrane. The proteins to be identified are then visualized by filter hybridization with specific antibodies. The electrophoresis on polyacrylamide gel was carried out in the presence of sodium dodecyl sulphate (SDS), an anionic detergent that binds proteins by causing denaturation. In this way, the separation of denatured polypeptide chains coated with the detergent (which gives them a negative charge) will be due exclusively to the size of proteins, which have the same charge/mass ratio. Each spot resulting from the separation by SDS-PAGE corresponds to a single protein species in the sample. About 50µg of each sample were resuspended in a 5X sample loading buffer, loaded on the polyacrylamide gel at 12% and, together with a marker of molecular weights, were subjected to electrophoresis. They were boiled for 10 minutes to promote the denaturing action of the SDS and loaded on polyacrylamide gel and, together with a molecular weight marker, were subjected to electrophoretic stroke. Proteins separated by SDS-PAGE were electroblotted from polyacrylamide gels to nitrocellulose (Bio-Rad Laboratories) using a Mini TransBlot System (BioRad Microsciences) overnight at 50mA. Membranes were blocked by incubation with 3% wt/vol nonfat dry milk in 10 mMTris-HCl (pH: 7.5), 0.15 M NaCl, and then incubated with primary antibodies (Table 3) overnight at 4 °C. After three washes in TTBS, nitrocellulose membranes were incubated for 1 hour with a secondary (Table 4). After incubation, membranes were further washed in TTBS, and Immuno Star Chemiluminescent HRP kit (BioRad) was used to detect the antigen-antibody reaction. The detected proteins were observed through the Bio-Rad Chemi-Doc system and then analyzed with the program PDQuest analysis software (Bio-Rad).

Table 4: Primary and secondary antibodies and their dilutions for western blot (WB) analysis.

Antigen	Donor species	Dilution WB	Manufacturer
Primary Antibodies			
TAS2R3	Rabbit	1:500	Thermo Fisher Scientific
TASR4	Rabbit	1:500	Thermo Fisher Scientific
TAS2R14	Rabbit	1:500	NovusBio Laboratories
TAS2R19	Rabbit	1:1000	Thermo Fisher Scientific
TAS2R43	Rabbit	1:500	Thermo Fisher Scientific
B-ACTIN	Mouse	1:2000	Bio-Rad Laboratories
Secondary Antibodies			
Anti-Rabbit IgG HRP	Goat	1:8000	Bio-Rad Laboratories
Anti-Mouse IgG HRP	Goat	1:8000	Bio-Rad Laboratories

3.3 IMMUNOFLUORESCENCE

For immunofluorescence analysis, granulosa and cumulus cells were grown on coverslips, washed with PBS, and fixed for 10 min in 4% paraformaldehyde (Sigma-Aldrich) at room temperature; sperm in basal condition and *in vitro* capacitated sperm were fixed on glass slides. The samples were washed 3 times with PBS for 5 min and then permeabilized with 0.5% Triton X-100 in PBS for 10 min. After repeating the three washes with PBS and blocking with 5% BSA in PBS for 30 min at room temperature, cells were incubated for 1h at 25°C with a primary antibody (Table 4). After the three washes with PBS, the cells were incubated for 1h at room temperature with the secondary antibody (Table 5). Finally, after washing three times with PBS, the cell nuclei were stained with 4',6-Diamidine-2'-phenylindole dihydrochloride (DAPI) in mounting medium (Santa Cruz Biotechnology) for 10 min at room temperature, and then the slides were mounted with antifade solution and observed with a Leica DMB 6000 microscope. Images were captured with an CFTR6500 digital camera (Leica).

Table 5: Primary and secondary antibodies and their dilutions for immunofluorescence (ICC) analysis.

Antigen	Donor species	Dilution ICC	Manufacturer
Primary Antibodies			
TAS2R3	Rabbit	1:100	Thermo Fisher Scientific
TAS2R4	Rabbit	1:100	Thermo Fisher Scientific
TAS2R14	Rabbit	1:100	NovusBio Laboratories
TAS2R19	Rabbit	1:100	Thermo Fisher Scientific
TAS2R43	Rabbit	1:100	Thermo Fisher Scientific
Secondary antibodies			
Anti-rabbit IgG FITC	Goat	1:100	Sigma Life Science

3.4 METACORE ANALYSIS

The gene names of the identified proteins were submitted to MetaCore network building tool (Thomson Reuters, New York City, USA) software to find their functional activity and the functional correlation existing among them. The MetaCore included a manually annotated database of protein interactions and metabolic reactions obtained by scientific literature. Gene names of the all identified proteins were imported into MetaCore and processed using the shortest path algorithm; consequently, only those proteins known to be closely related were included in the resulting path. Hypothetical networks were built among the experimental proteins and the MetaCore proteins database. The relevant pathway maps were then prioritized according to their statistical significance ($p \leq 0.001$) and networks were graphically visualized as nodes (proteins) and edges (the relationship between proteins). This analysis suggested the biochemical context in which the proteins of interest act, and how their aberrant expression may alter cellular and/or tissue biology in the disease status.

Results and discussion

1 Follicular cells

For this thesis work, we collected granulosa cells (GC) and cumulus cells (CC) from about 30 women undergoing IVF cycles because of male factor infertility problems at the UOSA of Assisted Reproductive techniques, at University Hospital in Siena.

In all samples, we analyzed both the gene expression and the protein localization of five members of *TAS2R* family, namely: *TAS2R3*, *TAS2R4*, *TAS2R14*, *TAS2R19* and *TAS2R43*. Proteins extracted from both GCs and CCs were analyzed by SDS-PAGE and western blot to confirm gene expression data, while protein localization was assessed through immunofluorescence.

A protein network analysis, performed by MetaCore software, provided the functional information about the investigated proteins and their possible functional associations. Based on this MetaCore protein analysis, we also analyzed the expression of the gene coding for the α -subunit of transducin (*GNAT1*), and the gene encoding for the α -subunit of gustducin (*GNAT3*). Moreover, we analyzed the expression of other enzymes and membrane channel known to be fundamentals in the signal transduction cascade elicited by bitter taste receptors: the gene encoding for phosphodiesterase 4A (*PDE4A*), the gene responsible for *TRPM5* and the gene encoding for *PLCB2*, all genes known to play a key role in TASRs signaling pathway. It's interesting how connections with bitter taste receptors are associated also with nuclear factors, such as androgen receptor (*AR*), a ligand-dependent nuclear transcription factor activated by binding any of the androgenic hormones, c-myc (*MYC*), that is a member of transcription factors family that regulate growth and cell cycle entry by their ability to induce expression of genes required for these processes, signal transducer and activator of transcription 5A and 5B (*STAT5A* and *STAT5B*), the nuclear receptor peroxisome proliferator-activated receptor gamma (*PPARG*) and GA-binding protein alpha (*GABPA*).

1.1 *TAS2Rs* EXPRESSION ANALYSIS IN GRANULOSA AND CUMULUS CELL

QuantaSoft® software (Bio-Rad Laboratories), provided us the absolute concentration of investigated genes, with the relative interval of confidence, in both GCs and CCs. The normalized sample amount (NSA) was obtained by normalizing the absolute concentration as respect to the concentration of selected reference genes (*HPRT*, *TBP* and *PPIB*) (for more details, see Luddi et al, 2018).

Figure 14 shows the distribution of NSA values in GCs (panel A) and in CCs (panel B), that appears to be significantly modulated, with *TAS2R14* being the most expressed in both GCs (mean NSA=0.05958) and in CCs (mean NSA=0.01970) ($p<0.001$).

An inter-individual variability for single *TAS2Rs* must be disclosed: while the expression of *TAS2R4* and *TAS2R14* was detected in 100% of samples, *TAS2R19* and *TAS2R43* were detected in about 96% of samples, and *TAS2R3* in 85% of GCs samples. Analogously, in CCs only *TAS2R14* was expressed in 100% of tested samples, while *TAS2R4*, *TAS2R19* and *TAS2R43* in about 89% and *TAS2R3* in 79% of tested CCs samples.

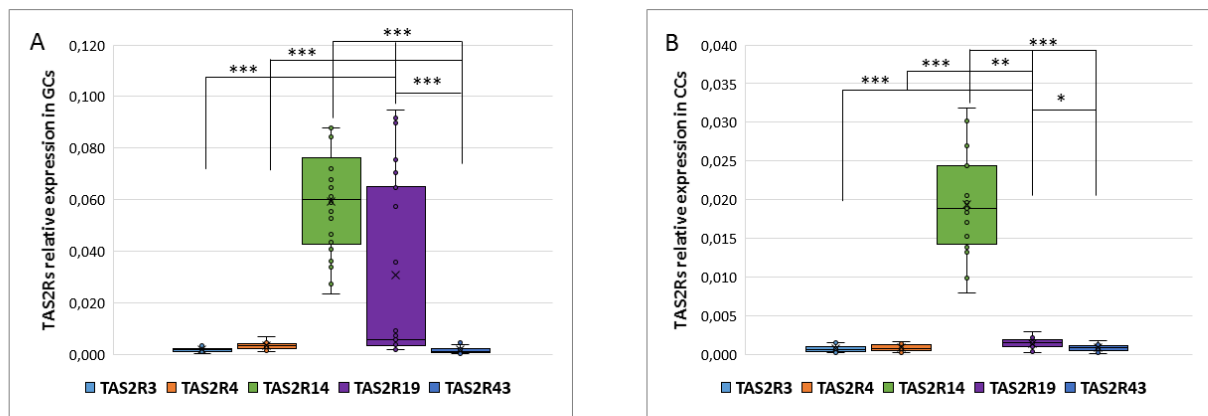


Figure 14: Relative quantity expression of *TAS2Rs* in GCs (panel A) and in CCs (panel B). Graphical diagrams are plotted as box-whisker plots, where boxes show the interquartile range with median and mean values, and whiskers represent min and max confidence intervals. Statistically significant differences in NSA levels were tested by *t* test. * $p<0.05$, ** $p<0.01$, *** $p<0.001$

The comparison between the expression level of each gene between GCs and CCs, shown in Figure 15, confirmed a different expression profile of *TAS2Rs* genes in these cell types, suggesting that this may be depending on the specific cell differentiation.

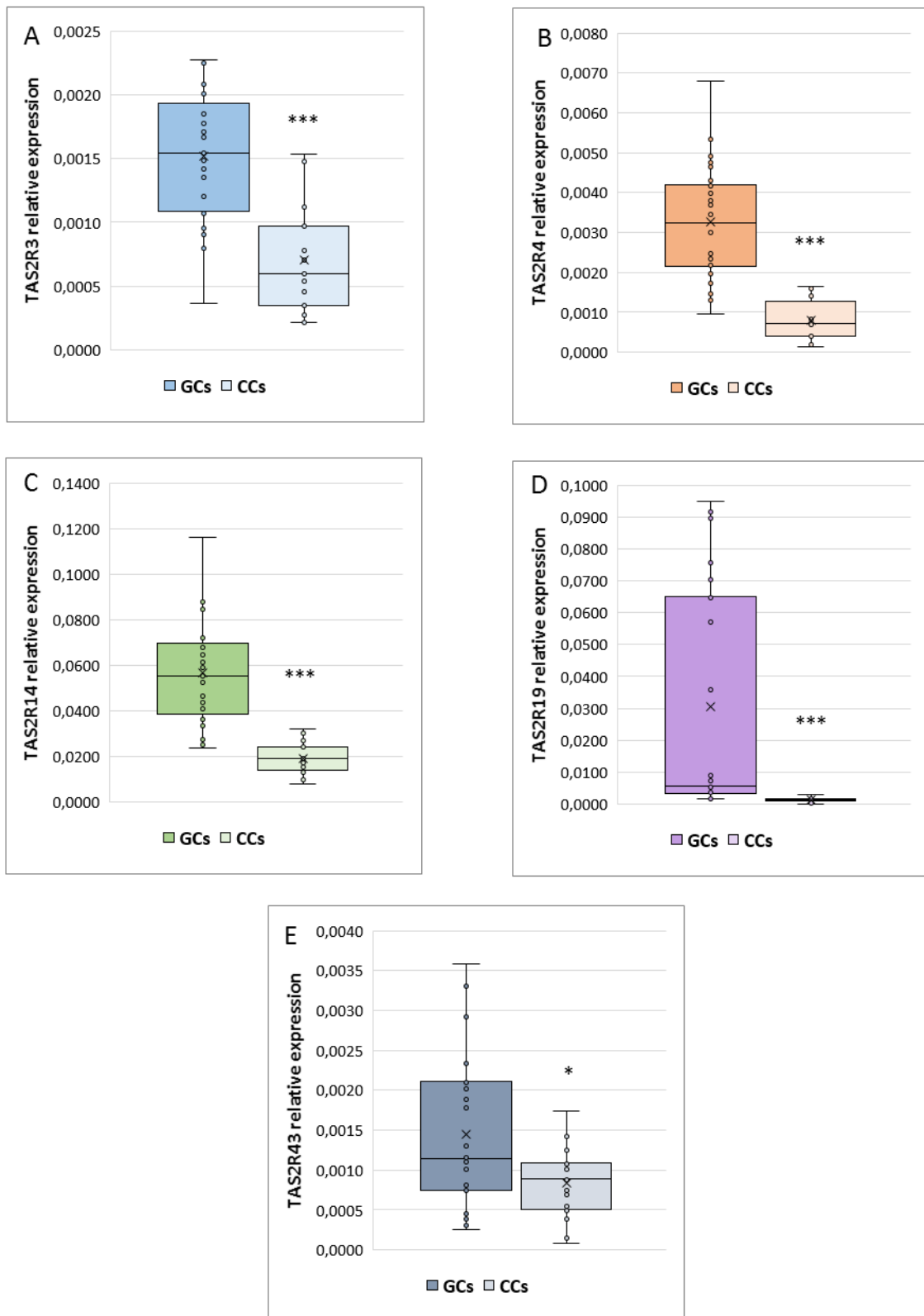


Figure 15: Relative NSA levels in GCs and CCs for TAS2R3 (panel A), TAS2R4 (panel B), TAS2R14 (panel C), TAS2R19 (panel D) and TAS2R43 (panel E). Graphical diagrams are plotted as box-whisker plots, where boxes show the interquartile range with median and mean values, and whiskers represent min and max confidence intervals. Statistically significant differences in mRNA levels were tested by t test. * $p < 0.05$, ** $p < 0.01$, *** $p < 0.001$

As shown in Figure 15, the expression of *TAS2R3* was significantly higher in GCs than in CCs ($p < 0.001$). Also, *TAS2R4* and *TAS2R14* were significantly up regulated in GCs compared with CCs ($p < 0.001$), and the same behaviour was observed for *TAS2R19*, which appeared nearly undetectable in cumulus cells ($p < 0.001$). Finally, we found a slightly significant difference in *TAS2R43* expression between GCs and CCs ($p \leq 0.05$).

These data were also analyzed according to specific parameters potentially affecting IVF outcome, such as the patient age (young women ≤ 33 years vs old women ≥ 36 years) and number of retrieved oocytes (poor responders ≤ 5 vs high responders ≥ 6). According to the patients age, no significant correlations were detected in both GCs and CCs, except for *TAS2R14* and *TAS2R43* that were slightly increased in GCs from young women ($p < 0.05$) (Figure 16). This result may be interesting, because of *TAS2R14* has the highest expression compared with all the other receptors in GCs, suggesting a prevalent role for this receptor.

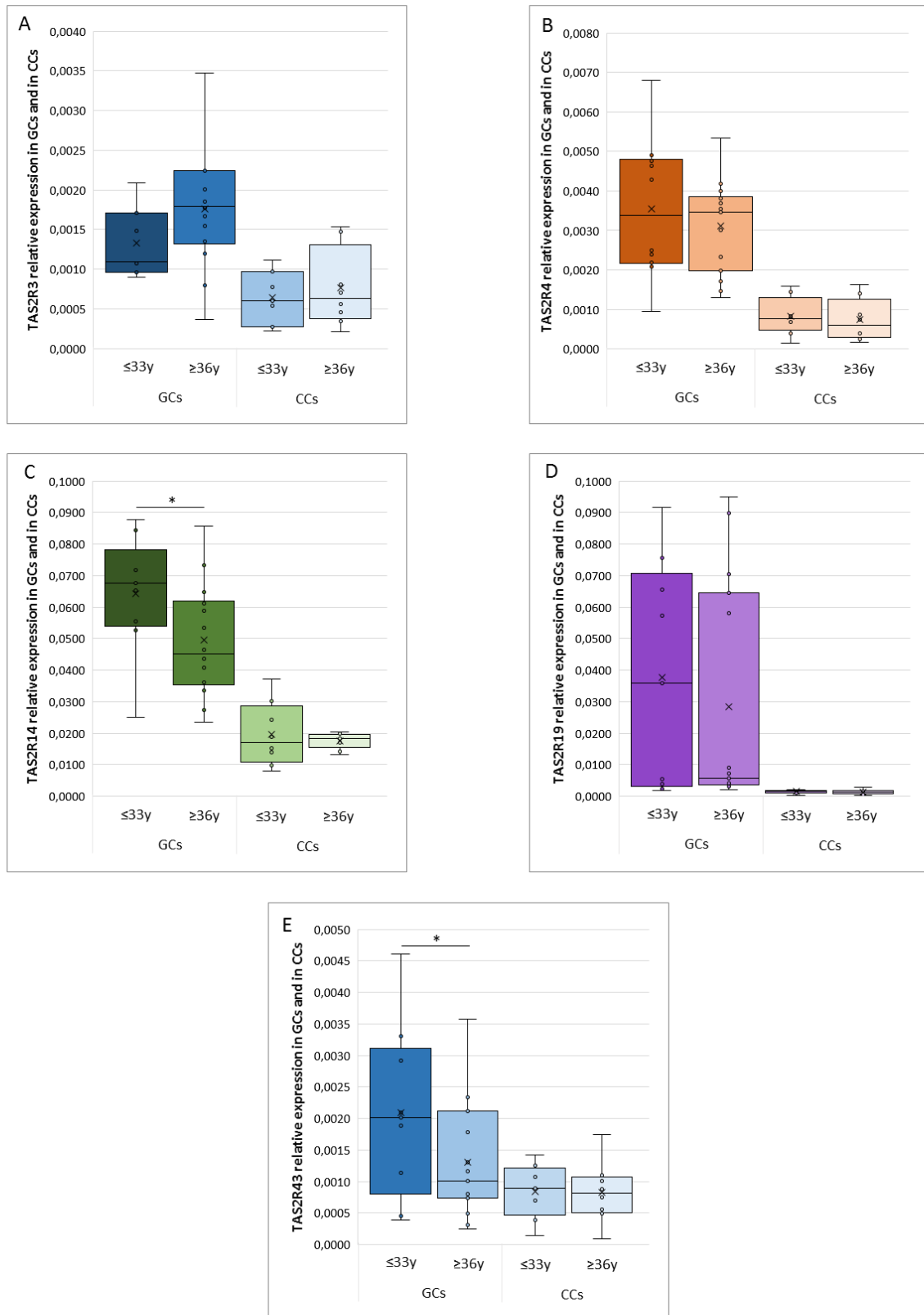


Figure 16: Relative NSA levels in young women (≤ 33 years) and in old women (≥ 36 years) in GCs and CCs for TAS2R3 (panel A), TAS2R4 (panel B), TAS2R14 (panel C), TAS2R19 (panel D) and TAS2R43 (panel E). Graphical diagrams are plotted as box-whisker plots, where boxes show the interquartile range with median and mean values, and whiskers represent min and max confidence intervals. Statistically significant differences in mRNA levels were tested by *t* test. * $p < 0.05$, ** $p < 0.01$, *** $p < 0.001$

When we evaluated the obtained results according to the number of recovered oocytes, as shown in Figure 17, *TAS2R14* was up regulated in GCs from patients with a low number of recovered oocytes at the pickup ($p < 0.05$); the same behavior was observed for *TAS2R43* in CCs ($p < 0.05$).

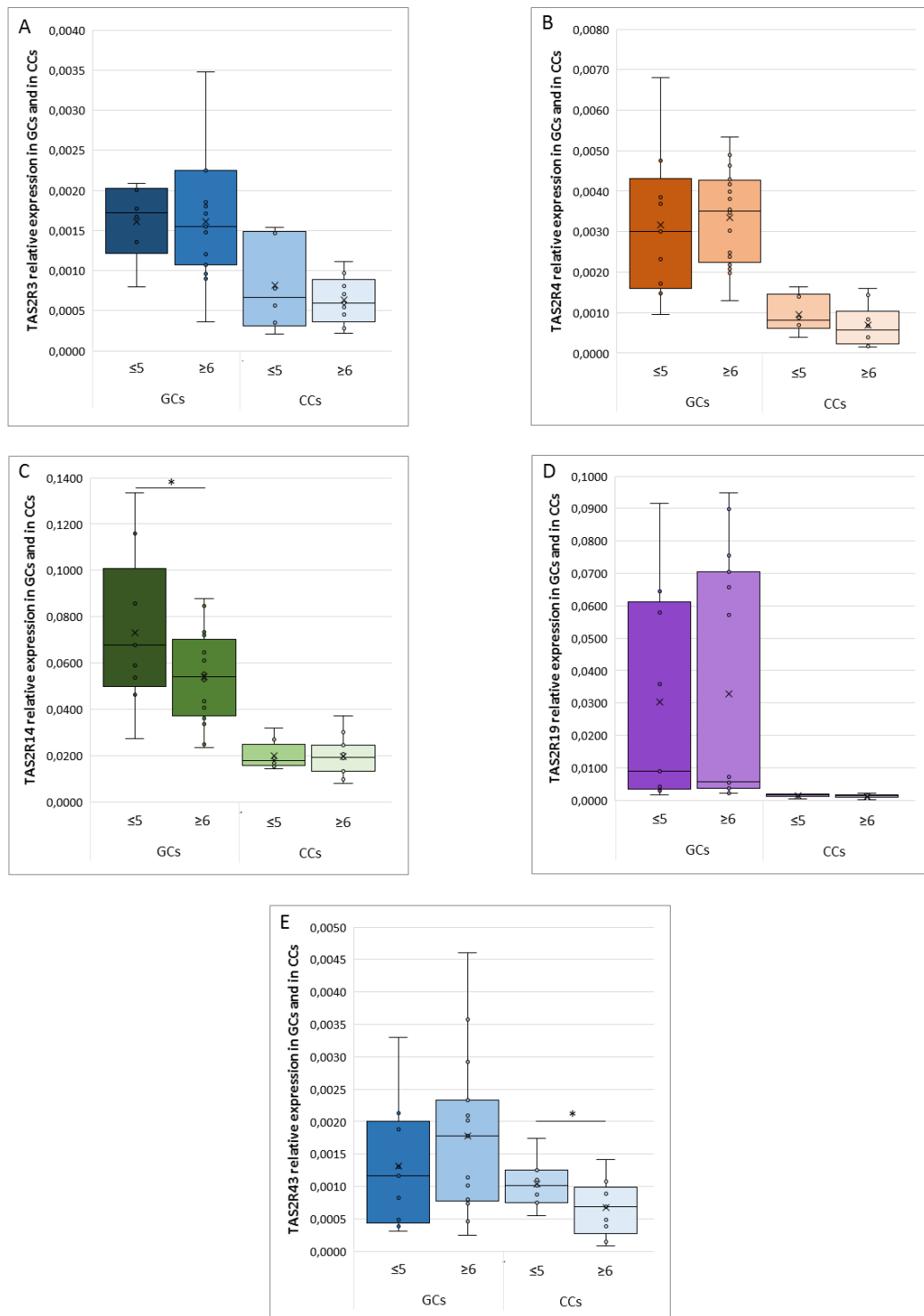


Figure 17: Relative NSA levels in poor responders (≤ 5 retrieved oocytes) and in high responders (≥ 6 retrieved oocytes) in GCs and CCs for *TAS2R3* (panel A), *TAS2R4* (panel B), *TAS2R14* (panel C), *TAS2R19* (panel D) and *TAS2R43* (panel E). Graphical diagrams are plotted as box–whisker plots, where boxes show the interquartile range with median and mean values, and whiskers represent min and max confidence intervals. Statistically significant differences in mRNA levels were tested by *t* test. * $p < 0.05$, ** $p < 0.01$, *** $p < 0.001$

1.2 PROTEIN QUANTIFICATION AND LOCALIZATION OF TAS2RS

In order to confirm the data obtained from the expression analyses of selected TAS2Rs, we evaluated by western blot the protein extracts prepared from GCs, obtained by pooling these cells from the same patients we used for gene expression analysis. Unfortunately, we were not able to perform western blot analysis in CCs because of the low protein amounts we collected from each patient and, at the same time, because of the low gene expression level of these receptors in CCs. To improve the reliability of our results, in this experiment we used the human immortalized granulosa cell line hGL5 as an internal control. The results confirmed the gene expression data obtained in GCs: both TAS2R14 and TAS2R19 show a single intense band with the predicted molecular weight of about 36kDa; by contrast, TAS2R43 confirmed to be the less expressed receptor, with a near detectable band at the predicted molecular weight of about 34kDa (Figure 18).

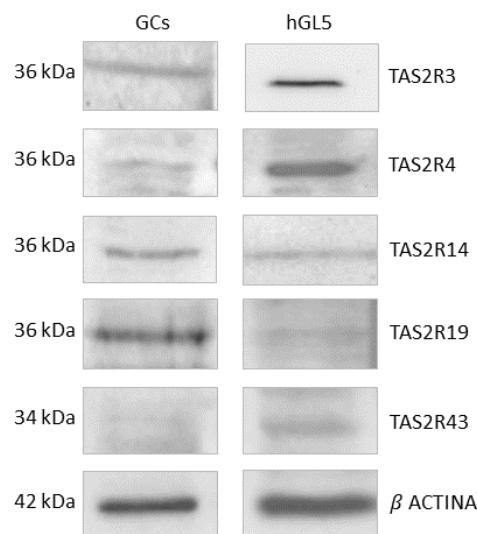


Figure 18: Representative image of western blot of TAS2R3, TAS2R4, TAS2R14, TAS2R19 and TAS2R43. β -actin was used as loading control.

Cellular localization of selected TAS2Rs was evaluated in both GCs and CCs. The localization of TAS2R3, evaluated through immunofluorescence, shows in GCs a faded signal distributed throughout the cytoplasm (Figure 19A), while in CCs a faint staining localized around the nucleus can be highlighted (Figure 19B). TAS2R4 protein showed an intense and dispersed signal with some sparse fluorescent granules in GCs (Figure 19C), while in CCs, a faint stain was present (Figure 19D). Regarding TAS2R14, immunofluorescence staining was concentrated around the nuclear envelope in both GCs and CCs (Figure 19, E and F). The analysis of TAS2R19 showed a

sparse and intense signal around the nuclei in both cell types, with the presence of some fluorescent granules, suggesting an accumulation of this protein inside the vesicles (Figure 19, G and H). Immunostaining of TAS2R43 in GCs points out a weak and distributed staining inside the cytoplasm. There is a great accumulation of fluorescent granules, especially in the cortical region of CCs, therefore suggesting a possible involvement of the protein in membrane trafficking (Figure 19, I and J).

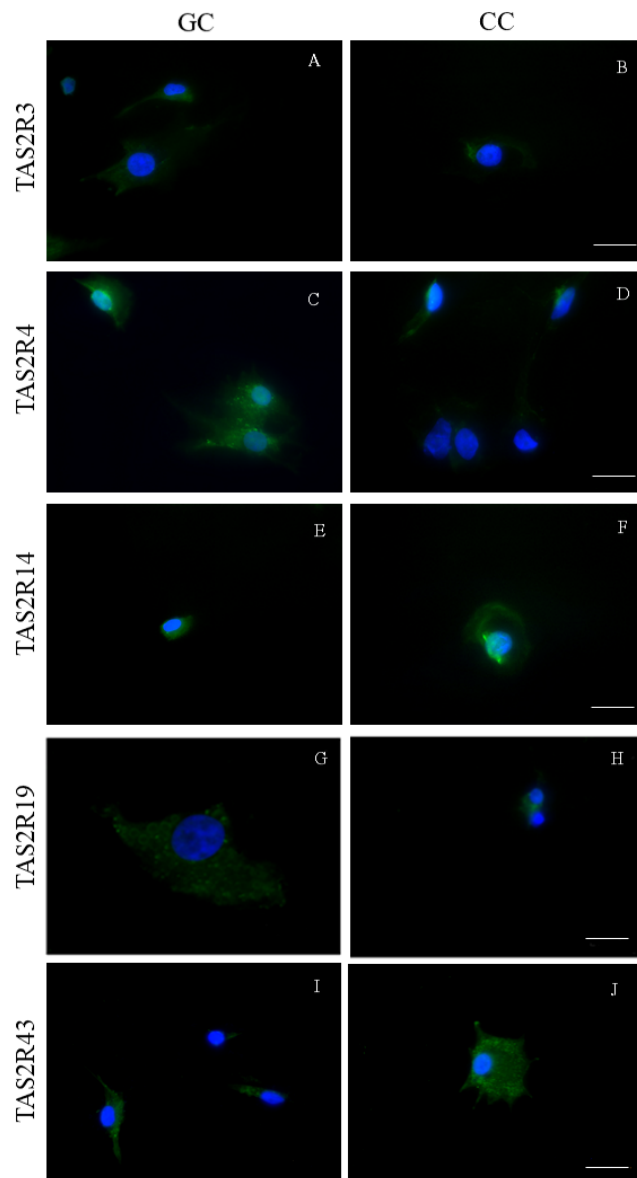


Figure 19: Immunofluorescence localization of (A, B) TAS2R3, (C, D) TAS2R4, (E, F) TAS2R14, (G, H) TAS2R19, and (I, J) TAS2R43 in (A, C, E, G, I) granulosa and (B, D, F, H, J) cumulus cells. TAS2Rs are stained in green. Nuclei were counterstained with DAPI (blue). Scale bar = 15 μ m.

1.3 METACORE PROTEIN NETWORK ANALYSIS OF PROTEIN INVOLVED IN TAS2RS SIGNALING

In order to elaborate an enrichment analysis to summarize functional information about the investigated proteins and to predict possible associations among them, a protein network analysis was performed by the MetaCore software (Clarivate analytics). Proteins were uploaded on MetaCore (<http://portal.genego.com>) that includes a manually annotated database of protein interactions and metabolic reactions obtained from the scientific literature. Thanks to the shortest-path algorithm, it was possible to connect “nodes” representing proteins, through “arches”, representing protein interactions. The shortest-path algorithm links two uploaded experimental proteins through at maximum, two single nodes. Graphical representation reports proteins distributed in their subcellular localization. For this analysis we used as input proteins, not only the investigated taste receptors, but also some of those factors known to play a key role in their signal transduction.

Selected proteins (TAS2R3, TAS2R4, TAS2R14, TAS2R19, TAS2R43, GNAT1, GNAT3, PDE4A, TRPM5, PLCB2) were analyzed and PDE4A, PLCB2, GNAT1, GNAT3 and T2R14 are considered central functional hubs, i.e. seeds with the greatest number of functional interconnections. MetaCore protein analysis suggests that bitter taste receptors are connected also with nuclear factors: *AR*, *MYC*, *STAT5A*, *STAT5B*, *PPARG* and *GABPA* (Figure 20).

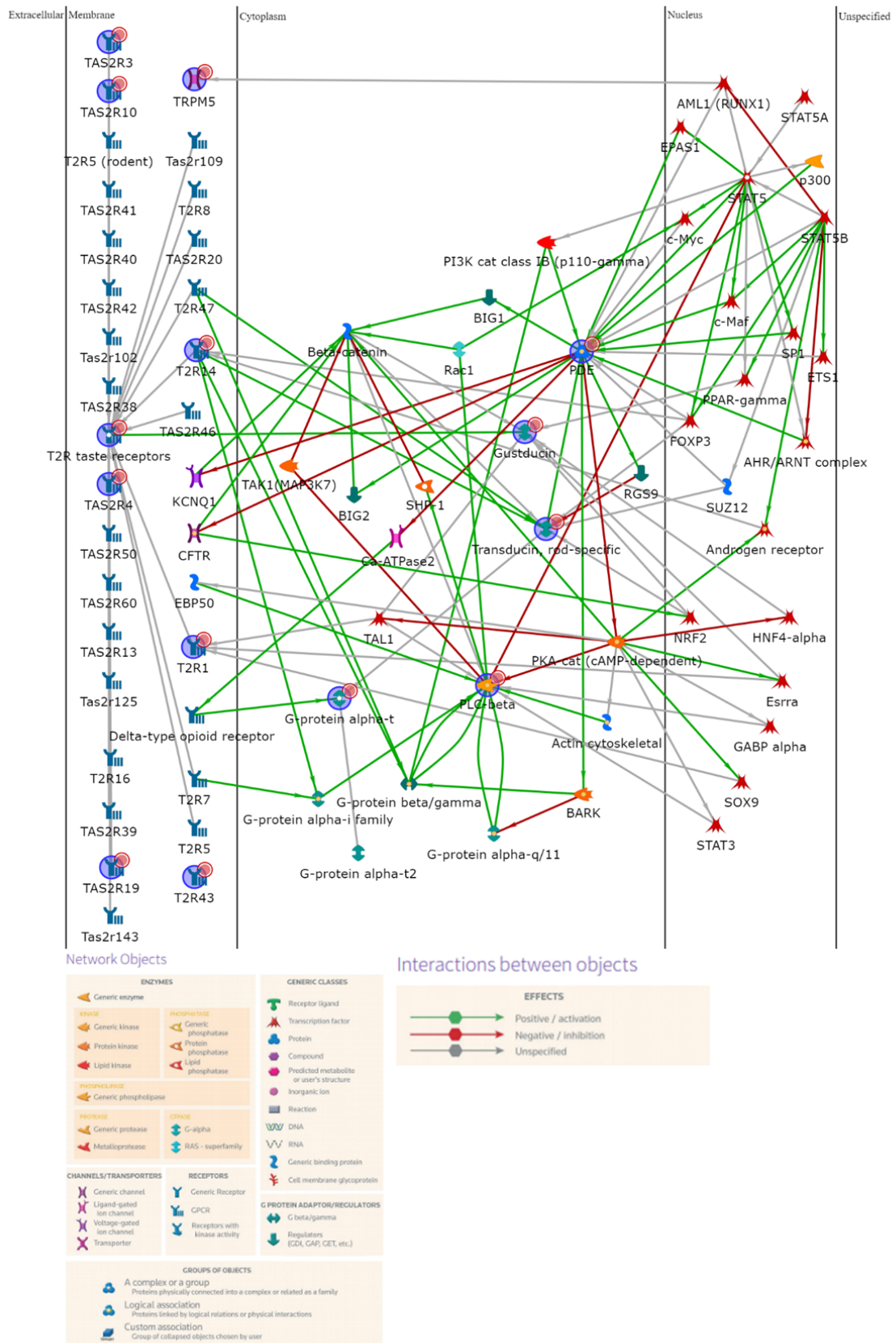


Figure 20: Protein network analysis of all the factors involved in this study, made using MetaCore software. PDE4A, PLCB2, GNAT1, GNAT3 and T2R14 were central functional hubs of the net built by shortest path algorithm. Only closely related proteins were included in the resulting path prioritized according to their statistical significance ($p \leq 0.001$).

1.4 EXPRESSION PROFILE OF GENES INVOLVED IN THE SIGNAL TRANSDUCTION ELICITED BY TAS2RS

Based on the data obtained by the MetaCore analysis, as well as on the data from the literature, we focused our attention on the expression of several genes involved in the signal transduction cascade elicited by TASRs receptors: *GNAT1*, *GNAT3*, *PDE4A*, *TRPM5* and *PLCB2*. We also evaluated the gene expression of nuclear factors connected with bitter taste receptors (*AR*, *MYC*, *STAT5A*, *STAT5B*, *PPARG* and *GABPA*).

As shown in Figure 21, the distribution of NSA values in both GCs and CCs has a significant modulation; indeed, *PDE4A* is the highest expressed gene in GCs (mean NSA=0.00466), while *GNAT3* is the highest expressed gene in CCs (mean NSA=0.00154). Moreover, a high inter-individual variability must be disclosed in both cell types: in GCs we detected the expression of *GNAT3*, *PDE4A* and *PLCB2* in 100% of tested samples, while *GNAT1* and *TRPM5* were detected in 62% and in 46% of samples, respectively. By contrast, in CCs we found *GNAT3* and *PDE4A* expressed in about 80% of samples, *GNAT1* and *PLC2B* in about 50% and *TRPM5* in 63% of analyzed CCs.

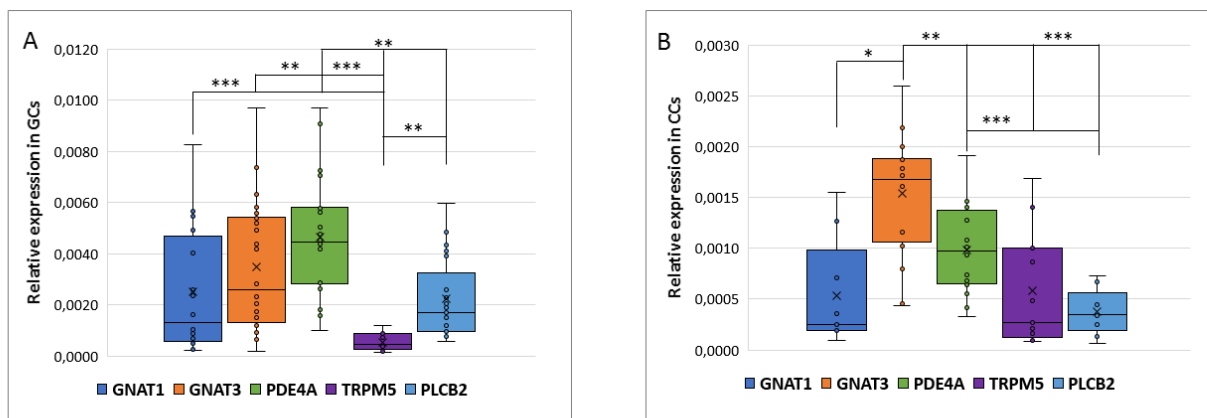


Figure 21: Relative quantity expression of genes involved in transduction cascade in GCs (panel A) and in CCs (panel B). Graphical diagrams are plotted as box-whisker plots, where boxes show the interquartile range with median and mean values, and whiskers represent min and max confidence intervals. Statistically significant differences in NSA levels were tested by t test. * $p < 0.05$, ** $p < 0.01$, *** $p < 0.001$

The direct comparison between the expression of each gene involved in the signal transduction cascade in GCs and CCs, shown in Figure 22, confirms the trend already reported for the expression of taste receptors in these cells. Indeed, *GNAT1*, *GNAT3*, *PDE4A* and *PLCB2* have significantly higher expression in GCs than in CCs ($p < 0.05$ or $p < 0.001$), whereas we didn't find any significant difference for *TRPM5* between GCs and CCs, which appeared nearly undetectable in both two cell types.

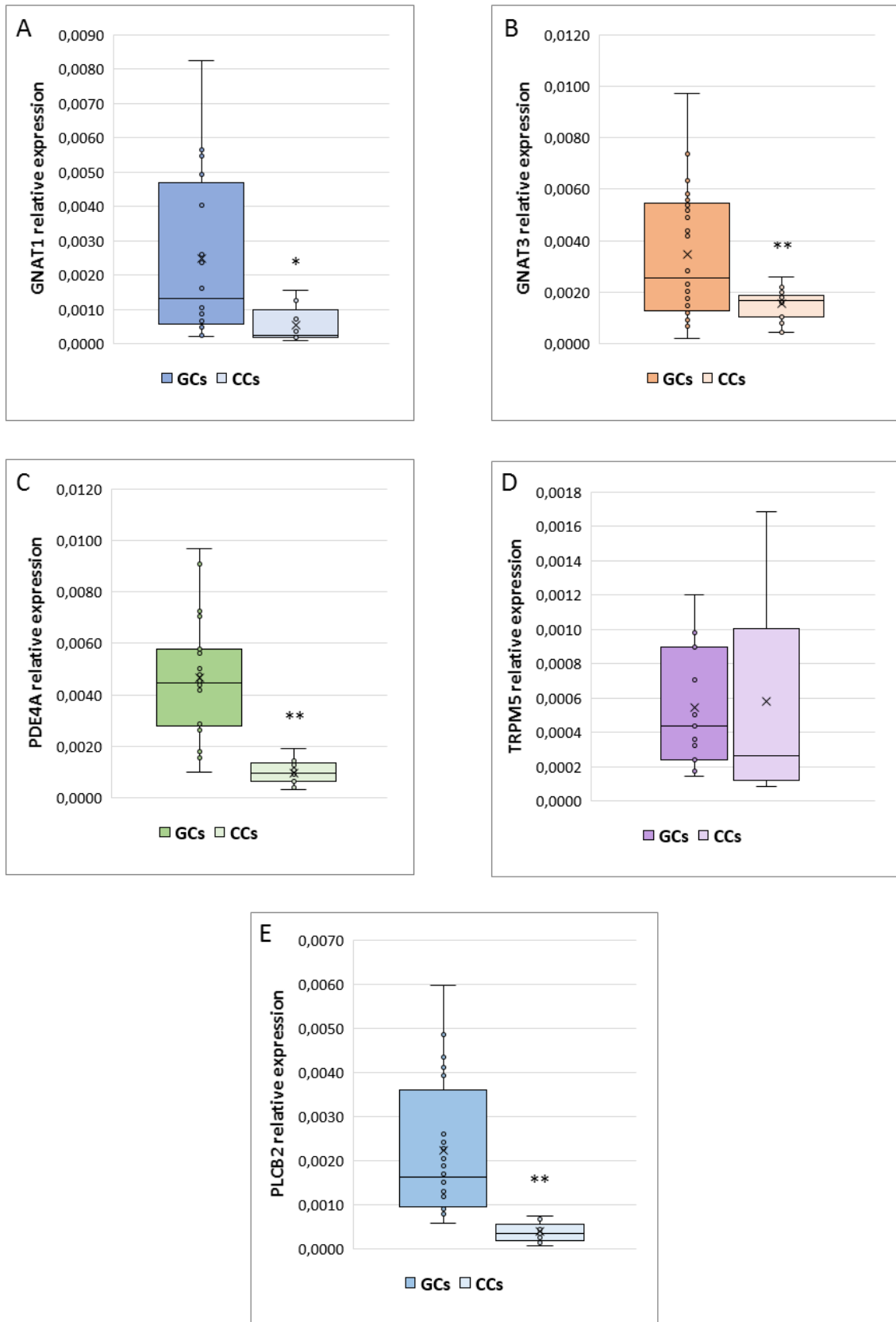


Figure 22: Relative NSA levels in GCs and CCs for GNAT1 (panel A), GNAT3 (panel B), PDE4A (panel C), TRPM5 (panel D) and PLCB2 (panel E). Graphical diagrams are plotted as box-whisker plots, where boxes show the interquartile range with median and mean values, and whiskers represent min and max confidence intervals. Statistically significant differences in mRNA levels were tested by *t* test. * $p < 0.05$, ** $p < 0.01$, *** $p < 0.001$

These data were also analyzed according to specific parameters potentially affecting IVF outcome, such as patient age (young ≤ 33 vs old ≥ 36) and number of retrieved oocytes (poor responders, ≤ 5 vs high responder, ≥ 6). As regard the patient age, we only found a slightly significant increase for *PLCB2* in CCs from older women ($p < 0.05$) (Figure 23).

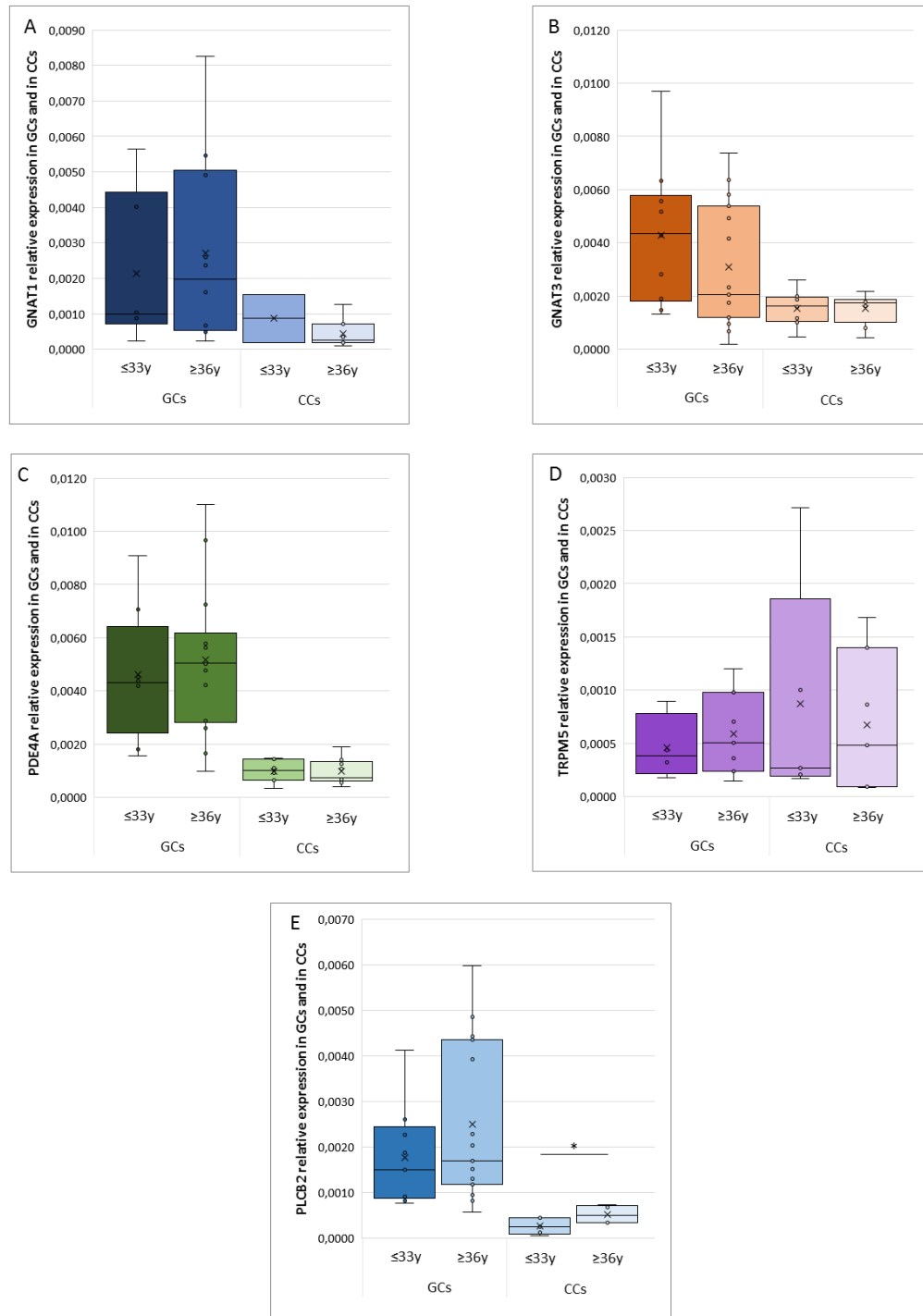


Figure 23: Relative NSA levels in young women (≤ 33 years) and in old women (≥ 36 years) in GCs and CCs for *GNAT1* (panel A), *GNAT3* (panel B), *PDE4A* (panel C), *TRPM5* (panel D) and *PLCB2* (panel E). Graphical diagrams are plotted as box-whisker plots, where boxes show the interquartile range with median and mean values, and whiskers represent min and max confidence intervals. Statistically significant differences in mRNA levels were tested by *t* test. * $p < 0.05$, ** $p < 0.01$, *** $p < 0.001$

According to the number of recovered oocytes, the Figure 24 shows that no significant results were obtained in both GCs and CCs.

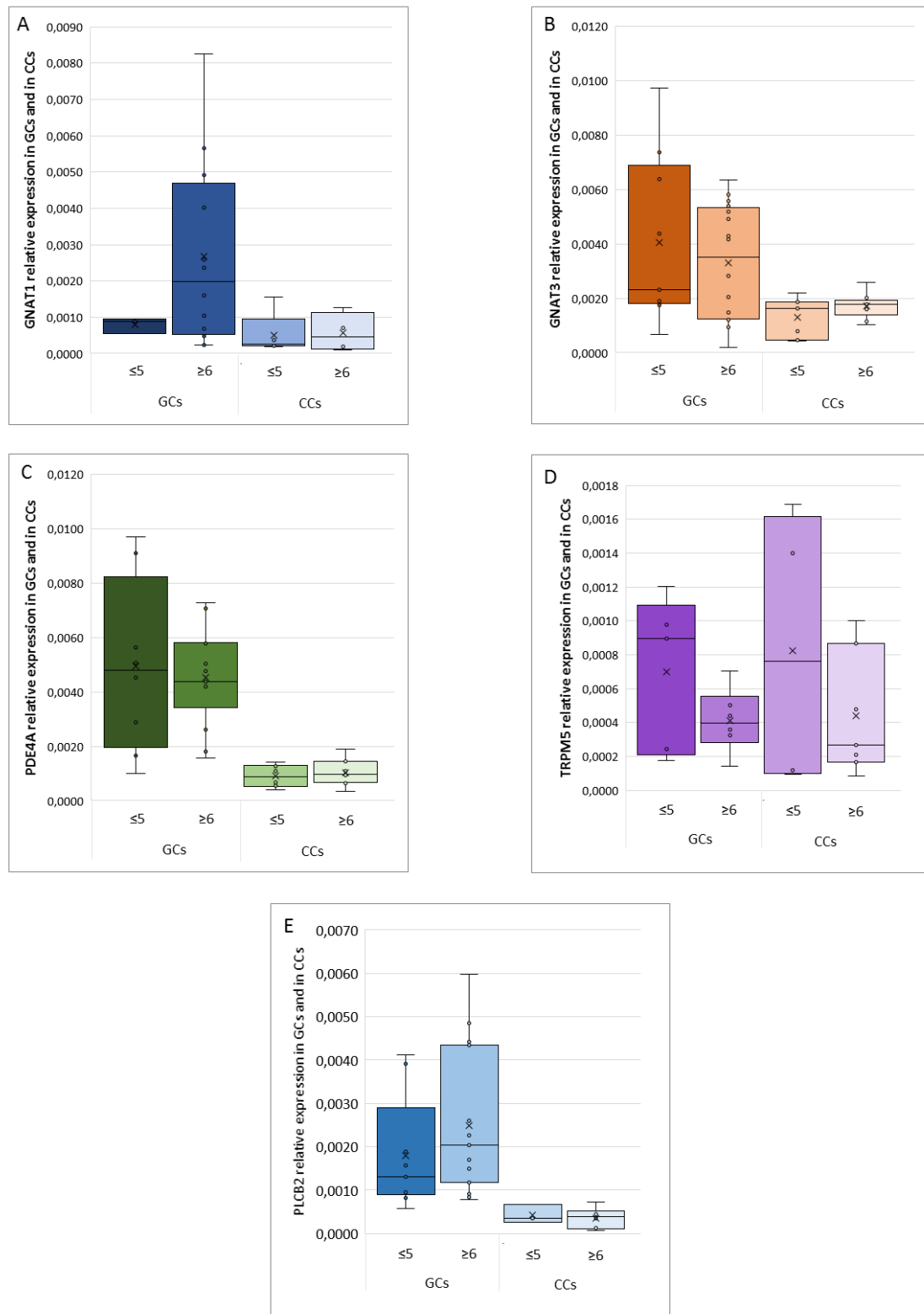


Figure 24: Relative NSA levels in poor responders (≤ 5 retrieved oocytes) and in high responders (≥ 6 retrieved oocytes) in GCs and CCs for GNAT1 (panel A), GNAT3 (panel B), PDE4A (panel C), TRPM5 (panel D) and PLCB2 (panel E). Graphical diagrams are plotted as box–whisker plots, where boxes show the interquartile range with median and mean values, and whiskers represent min and max confidence intervals.

Regarding nuclear factors, Figure 25 shows the distribution of values in GCs (panel A) and in CCs (panel B), that appears to be significantly modulated, with *PPARG* being the most expressed in both GCs (mean= 0.4023) and in CCs (mean= 0.1306).

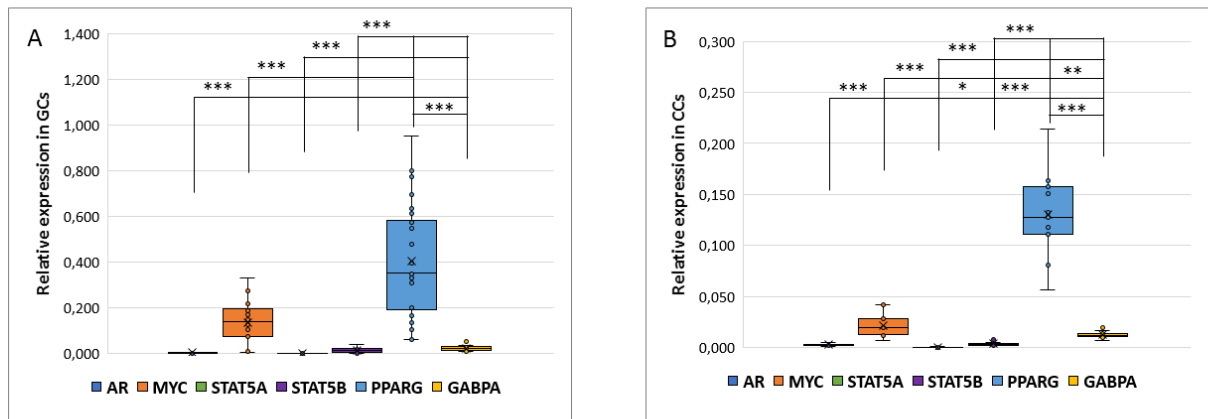


Figure 25: Relative quantity expression of nuclear factors involved in transduction cascade in GCs (panel A) and in CCs (panel B). Graphical diagrams are plotted as box-whisker plots, where boxes show the interquartile range with median and mean values, and whiskers represent min and max confidence intervals. Statistically significant differences in mRNA levels were tested by *t* test. * $p < 0.05$, ** $p < 0.01$, *** $p < 0.001$

As regarding the direct comparison between the expression of each gene involved in the signal transduction cascade in GCs and CCs, confirmed a different expression profile of this genes in these cell types. Indeed, *MYC*, *STAT5B*, *PPARG* have significantly higher expression in GCs than in CCs ($p < 0.01$ or $p < 0.001$), whereas we didn't find any significant difference for *AR* and *STAT5A* between GCs and CCs (Figure 26).

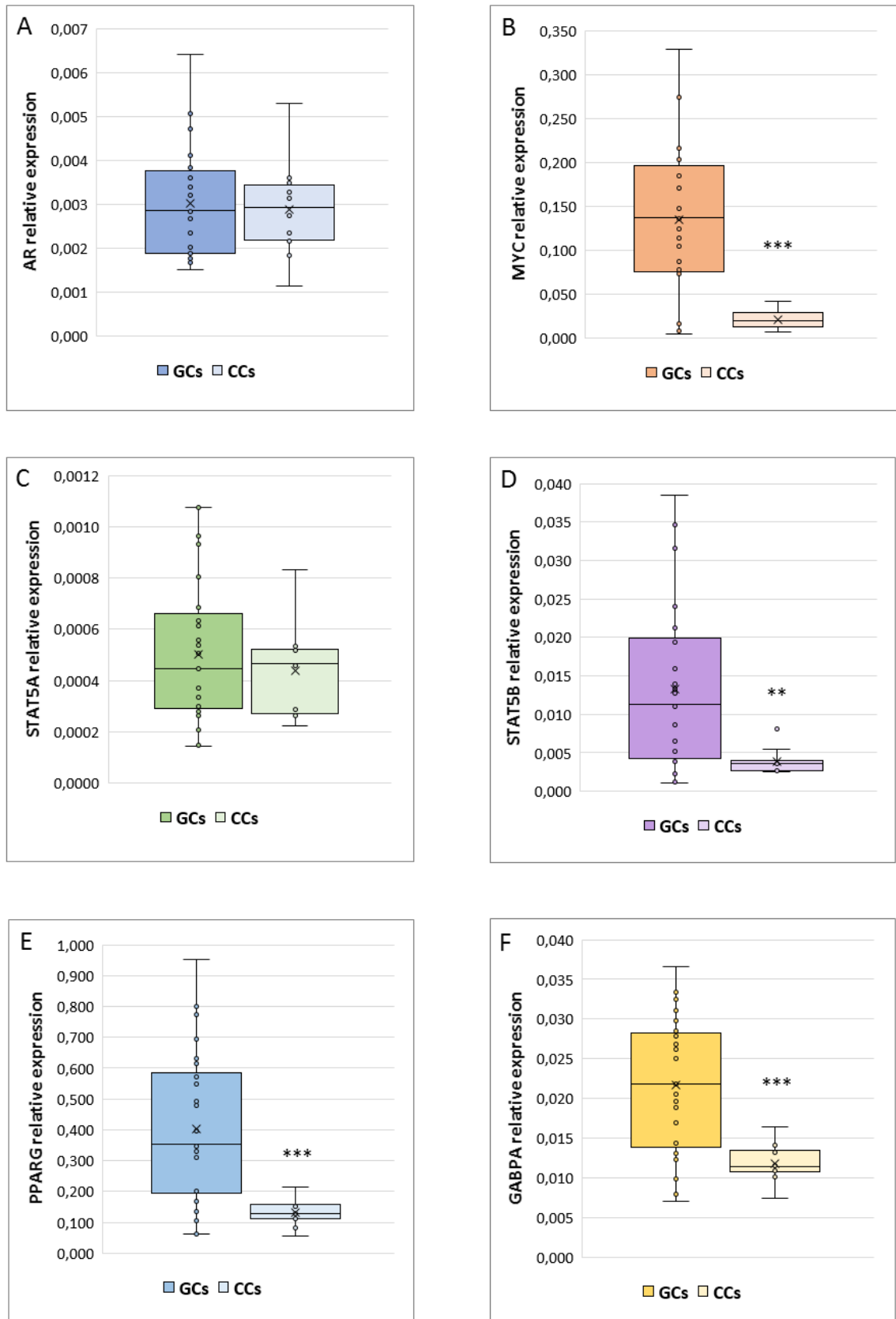


Figure 26: Relative mRNA levels in GCs and CCs for AR (panel A), MYC (panel B), STAT5A (panel C), STAT5B (panel D), PPARG (panel E) and GABPA (panel F). Graphical diagrams are plotted as box-whisker plots, where boxes show the interquartile range with median and mean values, and whiskers represent min and max confidence intervals. Statistically significant differences in mRNA levels were tested by t test. * $p < 0.05$, ** $p < 0.01$, *** $p < 0.001$

These data were also analyzed according to specific parameters potentially affecting IVF outcome, such as patient age (young ≤ 33 vs old ≥ 36) and number of retrieved oocytes (poor responders, ≤ 5 vs high responder, ≥ 6). As regard the patient age, we only found a slightly significant increase for *AR* in GCs and for *MYC* in CCs ($p < 0.05$) from older women (Figure 27).

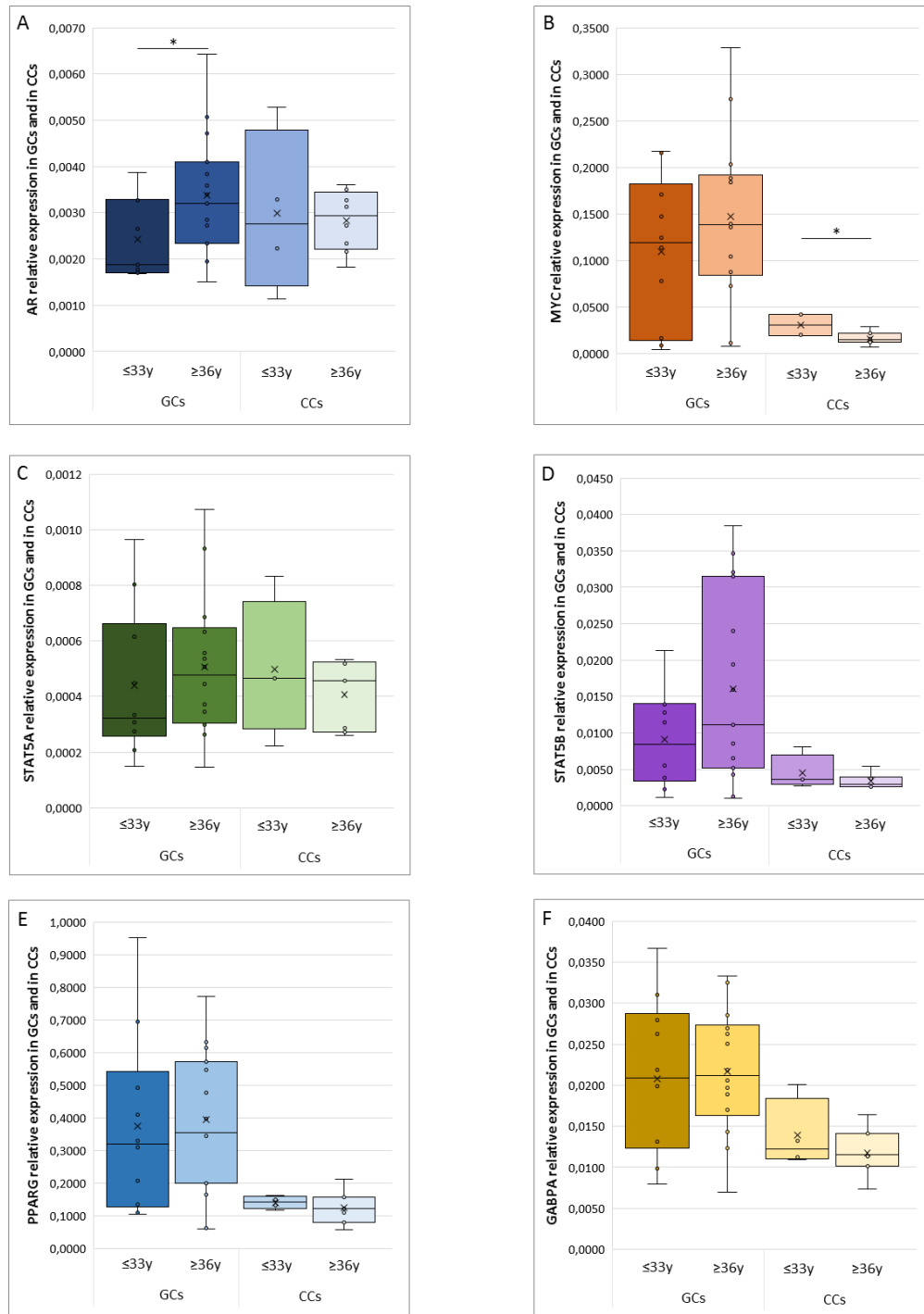


Figure 27: Relative mRNA levels in young women (≤ 33 years) and in old women (≥ 36 years) in GCs and CCs for *AR* (panel A), *MYC* (panel B), *STAT5A* (panel C), *STAT5B* (panel D), *PPARG* (panel E) and *GABPA* (panel F). Graphical diagrams are plotted as box-whisker plots, where boxes show the interquartile range with median and mean values, and whiskers represent min and max confidence intervals. Statistically significant differences in mRNA levels were tested by *t* test. * $p < 0.05$, ** $p < 0.01$, *** $p < 0.001$

When we evaluated the obtained results according to the number of recovered oocytes, as shown in Figure 28, *AR* was up regulated in GCs from patients with a low number of recovered oocytes at the pickup ($p < 0.05$); the same behavior was observed for *PPARG* in CCs ($p < 0.05$).

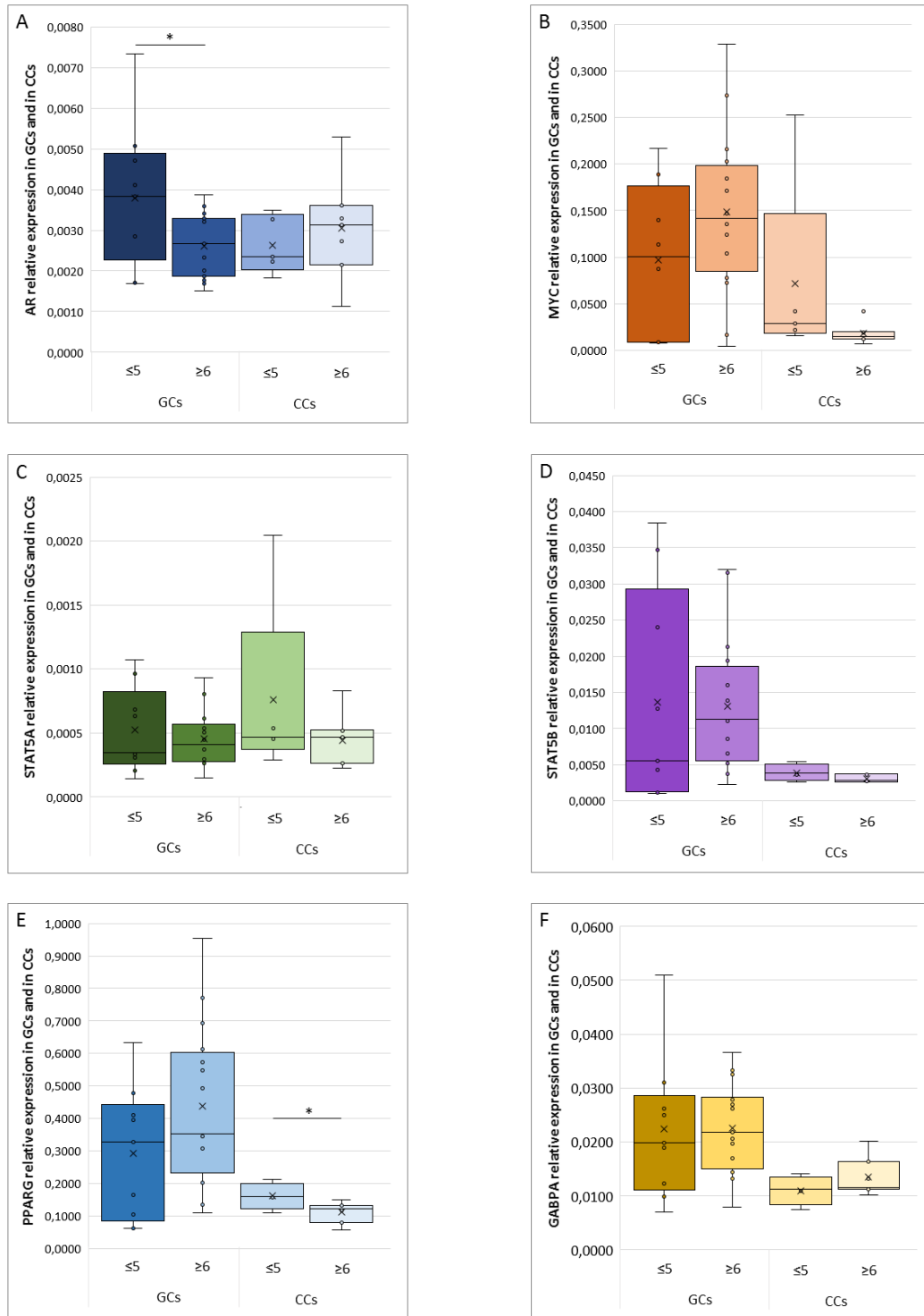


Figure 28: Relative mRNA levels in poor responders (≤ 5 retrieved oocytes) and in high responders (≥ 6 retrieved oocytes) in GCs and CCs for *AR*, *MYC*, *STAT5A*, *STAT5B*, *PPARG* and *GABPA*. Graphical diagrams are plotted as box-whisker plots, where boxes show the interquartile range with median and mean values, and whiskers represent min and max confidence intervals. Statistically significant differences in mRNA levels were tested by *t* test. * $p < 0.05$, ** $p < 0.01$, *** $p < 0.001$

1.4.1 Correlation analysis

In order to evaluate any possible correlation of *TAS2Rs* expression with the genes involved in their signaling pathway, the mean expression level of *TAS2Rs* was calculated for each sample, and then compared with the *GNAT1*, *GNAT3*, *PDE4A*, *TRPM5* and *PLCB2* expression, in both GCs and CCs. Regarding GCs, it was observed a positive correlation between *TAS2Rs* expression and *GNAT3* expression ($r= 0.68$; $p<0.001$) (Figure 29A). Each *TAS2Rs* single subset was then correlated with the genes involved in the signalling pathway, and interestingly the expression of *TAS2R14* resulted to be highly correlated with *GNAT3* expression ($r= 0.30$; $p<0.001$) (Figure 29B).

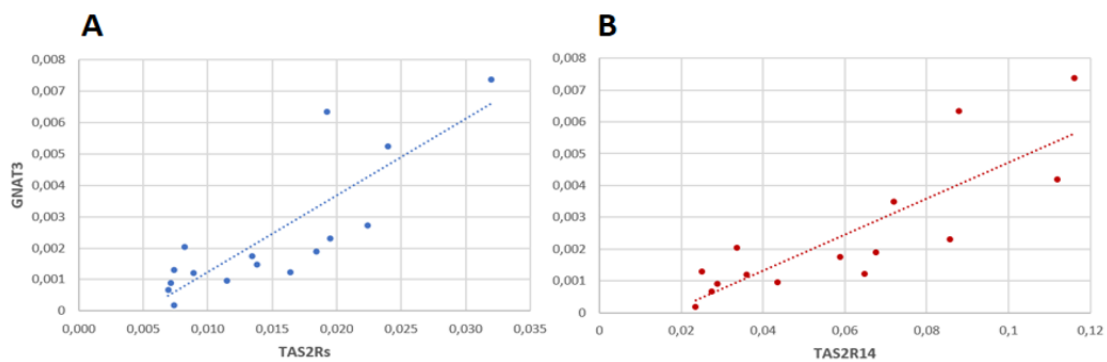


Figure 29: Representation of dispersion graphic with trendline done between *TAS2Rs* mean and *PDE4A* (Panel A) and *TAS2R4* versus *PDE4A* (Panel B).

As concerns CCs, the comparison between *TAS2Rs* NSA mean and signaling genes expression levels highlighted a correlation with *PDE4A* ($r= 0.30$; $p < 0.05$) (Figure 30A). In addition, each *TAS2R* single subset was correlated with the genes involved in the signaling pathway, and *TAS2R4* showed the highest correlation with the *PDE4A* gene expression ($r= 0.55$; $p<0.001$) (Figure 30B).

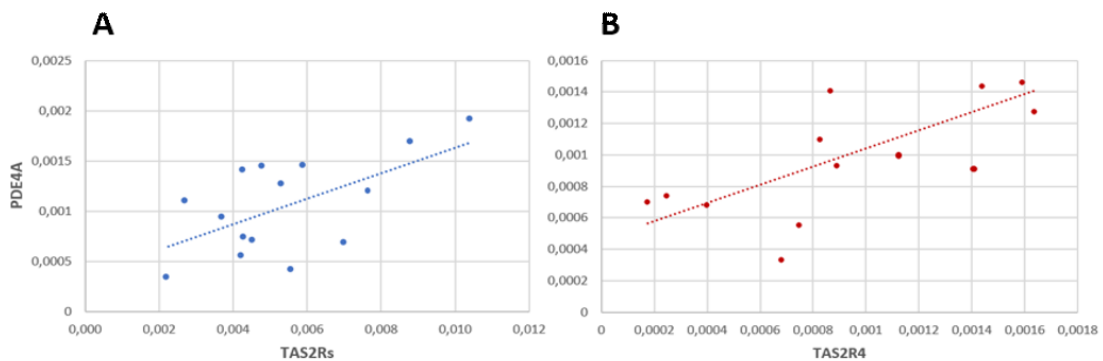


Figure 30: Representation of dispersion graphic with trendline done between *TAS2Rs* mean and *PDE4A* (Panel A), and *TAS2R4* versus *PDE4A* (Panel B).

1.5 PROTEIN QUANTIFICATION AND LOCALIZATION OF GUSTDUCIN AND TRANSDUCIN

In order to confirm, at the protein level, the presence of two of the most important G-proteins coupled to bitter taste receptors, namely α -transducin and α -gustducin, we analyzed by western blot the protein extracts prepared from GCs and CCs, obtained by pooling these cells from the same patients we used for gene expression analysis. The results partially confirmed the data obtained by gene expression.

As regard to the α -gustducin, a single band of the predicted molecular weight of about 36kDa was present in CCs, whereas in GCs we detected two more isoforms, in addition to the presumed band corresponding to the α -gustducin: one band at about 60 kDa, which recently has been described in taste tissue preparations, to represent α -gustducin within insoluble complexes (Von Buchholtz et al, 2004), and the other, less intense, at about 25 kDa. As regards the α -transducin, a strong band of the expected molecular size (approximately 50 kDa) is present in CCs, but not in GCs extracts (Figure 31).

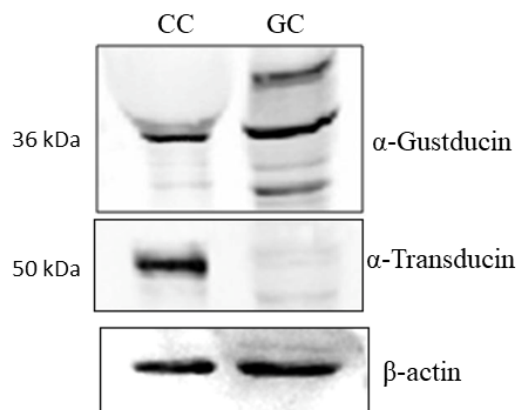


Figure 31: The upper panel shows the detection of α -gustducin by western blot with an anti- α -gustducin antibody, in CCs and GCs protein extracts. The central panel shows the detection of α -transducin by western blot with an anti- α -transducin antibody in GCs and CCs protein extracts. β -actin was used as loading control.

The cellular localization of α -transducin and α -gustducin G-proteins has been evaluated both in GCs and CCs. Immunofluorescence staining revealed a diffuse cytoplasmic signal for α -gustducin, confirming the western blot data, highlighting a strong expression of the protein. The α -gustducin showed a strong scattered signal at the cell periphery, consistent with a sub-membrane localization in CCs; in GCs α -transducin revealed a very faint signal, confirming the weak expression detected by western blot (Figure 32).

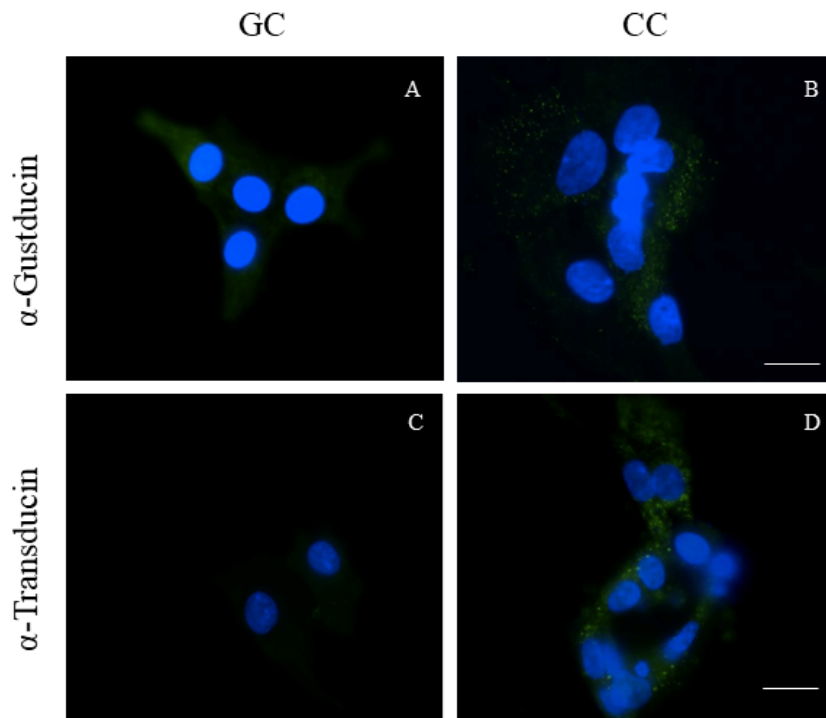


Figure 32: Immunofluorescence localization of (A, B) α -gustducin, (C, D) α -transducin, in (A, C) granulosa and (B, D) cumulus cells. α -gustducin and α -transducin are stained in green. Nuclei were counterstained with DAPI (blue). Scale bar = 15 μ m.

2 Human sperm and testis

In this thesis work, we collected spermatozoa from 15 normozoospermic men undergoing semen evaluation at the UOSA of Assisted Reproductive techniques, at University Hospital in Siena. Semen evaluation was performed according to the WHO guidelines (WHO, 2010). A comprehensive clinical history of patients was obtained, and possible causes of male infertility such as varicocele, cryptorchidism, or endocrine disorders were excluded. The median age of the patients was 33 years (22–42).

Testis samples were obtained from six patients undergoing diagnostic testicular biopsy for obstructive azoospermia. None of these patients received chemotherapy, radiotherapy, or hormonal treatment.

In all samples, the expression of *TAS2R3*, *TAS2R4*, *TAS2R14*, *TAS2R19* and *TA2R43* was measured and normalized to four reference genes (*PPIB*, *GAPDH*, *ACT-B* and *B2M*). In addition, we also analyzed the expression *GNAT1*, *GNAT3*, *PDE4A*, *TRPM5* and *PLCB2*, all genes known to play a key role in TASRs signaling pathway.

2.1 *TAS2Rs* EXPRESSION ANALYSIS IN HUMAN SPERM AND TESTIS TISSUE

ddPCR along with the QuantaSoft® (Bio-Rad Laboratories, Hercules, CA, USA) were carried out to determine the gene expression of five selected taste receptors belonging to the *TAS2R* family. *TAS2Rs* showed the same expression profile both in ejaculated sperm and testicular tissue, although the NSA was found to be significantly higher in ejaculated sperm (Figure 33A). Moreover, an inter-individual variation could be seen for each *TAS2R* subtypes; in fact, we detected the expression of *TAS2R3*, *TAS2R4*, *TAS2R19*, and *TAS2R43* in about 73% of semen samples, whereas *TAS2R14* was detectable in 80% of the probes. *TAS2R14* was found to be expressed at the highest level (mean NSA=0.0043), even if this doesn't reach the statistical significance. Figure 33B shows the expression of all selected *TAS2R* genes in human testis, although different levels were detectable.

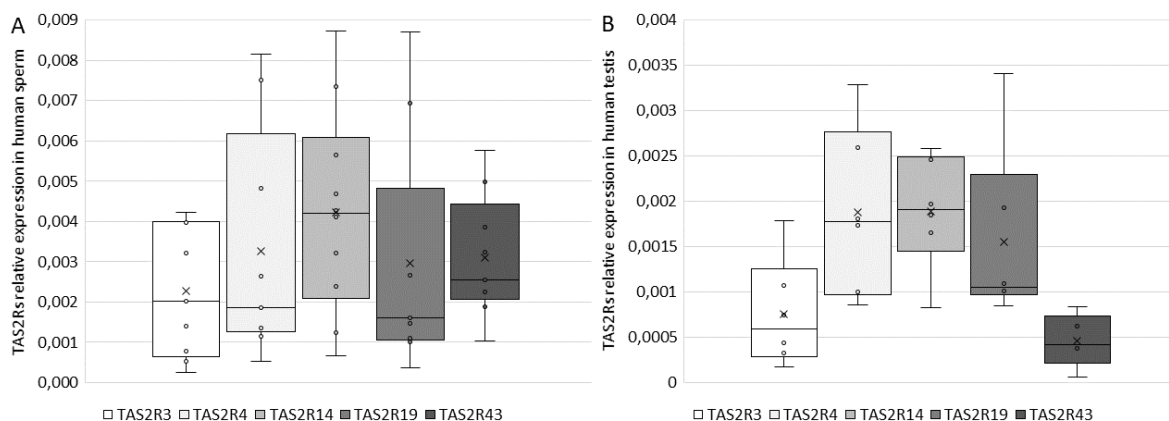


Figure 33: Expression of *TAS2Rs* in human sperm and in ejaculated testis. (A) *TAS2Rs* normalized sample amount in human sperm. (B) *TAS2Rs* normalized sample amount in human testis. Graphical diagrams are plotted as box-whisker plots, where boxes show the interquartile range with median and mean values, and whiskers represent min and max confidence intervals.

2.2 METACORE PROTEOMIC ANALYSIS OF PROTEIN INVOLVED IN *TAS2RS* SIGNALING

Based on these results showing for the first time the expression of several members of the *TAS2Rs* family in human sperm, we decided to perform an enrichment analysis, in order to better investigate the possible role of these receptors in male gametes. To this end, we used the MetaCore software (Clarivate analytics), that represents an *in silico* analysis usually performed to elaborate a protein network, summarizing functional information and interactions of the investigated proteins. This *in silico* analysis establishes networks that consist of nodes representing proteins, while edges represent the predicted mode of action among proteins (Figure 34). By this approach, we obtained a general idea of all the factors that have a role in a specific pathway.

For this analysis we used as input proteins not only the investigated taste receptors, but also some of those factors known to play a key role in their signal transduction and in the sperm capacitation and attraction to the oocyte (TAS2R3, TAS2R4, TAS2R14, TAS2R19, TAS2R43, GNAT1, GNAT3, PDE4A, PLCB2, TRPM5, CATSPER, RHO).

Shortest path algorithm was used in order to connect our protein species with a maximum of three more interactors obtaining a protein network were PLCB2, PDE4A, ARCGAP22 (RHO), GNAT1, CATSPER were central functional hubs. In this network it is possible to observe the *TAS2Rs* are directly connected with the predicted functional partners such as, between others, gustducin, G-protein α -t, G-protein β/γ , G-protein α -i family. All these proteins are reported to play an essential role in better, sweet and in umami taste transduction as well as in other transmembrane signalling system.

2.3 GENE EXPRESSION ANALYSIS OF GENES INVOLVED IN TAS2RS SIGNALING

In order to shed light in this complex net, we decided to confirm, at molecular level, the data obtained by the MetaCore analysis. To this end, we tested, by ddPCR, the expression of those molecules having, the highest numbers of interactions and/or occupying a key position in the net, namely: *GNAT1*, *GNAT3*, *PLCB2*, *TRPM5* and *PDE4A*.

The same genes investigated in GCs and CCs were analyzed in ejaculate sperm too. The five analyzed genes of downstream components of TAS2Rs signaling pathways were expressed in mature sperm, as showed in Figure 35. The NSA level of *PDE4A* was the highest (mean NSA=0.163), whereas *GNAT3* showed the lowest expression (mean NSA=0.010). Interestingly, our study demonstrated for the first time that transducin is expressed at a higher level than gustducin.

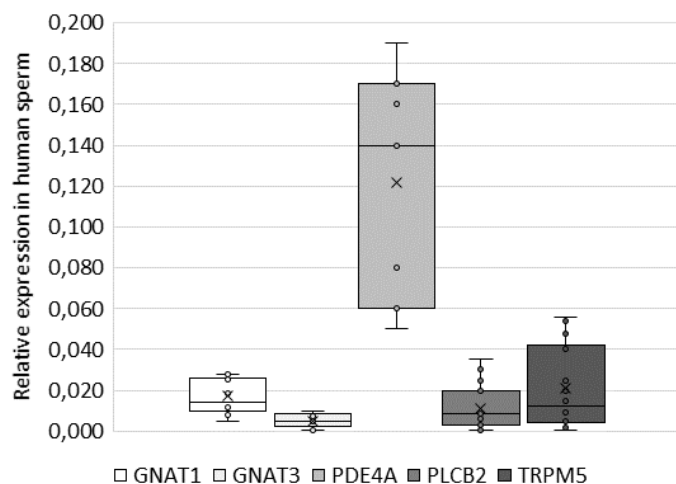


Figure 35: Relative quantity expression of genes involved in transduction cascade in human sperm. Graphical diagrams are plotted as box-whisker plots, where boxes show the interquartile range with median and mean values, and whiskers represent min and max confidence intervals.

2.3.1 Correlation analysis

In order to evaluate any possible correlation of *TAS2Rs* expression with the genes involved in their signaling pathway, the mean of *TAS2Rs* NSA was calculated for each sperm sample, and then compared with the NSA of *GNAT1*, *GNAT3*, *PLCB2*, *TRPM5* and *PDE4A* expression. Interestingly, by using Spearman's correlation analysis, it was observed a positive global correlation between *TAS2Rs* and *TRPM5* expression ($r=0.87$; $p < 0.001$) (Figure 36).

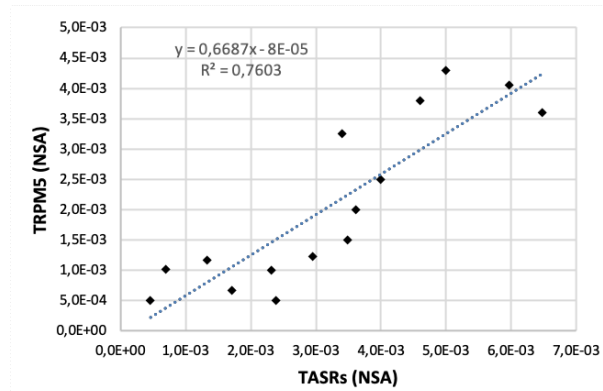


Figure 36: Correlation between TASRs and TRPM5 ($r = 0.87$; $p < 0.001$) was determined by using Spearman's correlation analysis.

2.4 PROTEIN EXPRESSION AND LOCALIZATION

In order to confirm data from gene analysis, we analyzed TAS2Rs protein expression by western blot analysis in human sperm before and after *in vitro* capacitation. The results confirm the low expression of TAS2R3 and revealed three distinct bands with different molecular weights (ranging from 35 to 50 kDa). Interestingly, immunoreactivity visualizing the receptor with the highest molecular weight (ca. 50 kDa) was only detectable in uncapacitated sperm, whereas capacitated sperm showed the expression of the two smaller proteins (Figure 37a). The results of the immunofluorescence localization, showed in Figure 37b, demonstrated a faint TAS2R3 derived staining at the equatorial segment of the sperm head and the midpiece segment of the tail, in both uncapacitated and capacitated sperm, suggesting that the distribution of this TAS2R subtype did not change upon sperm capacitation.

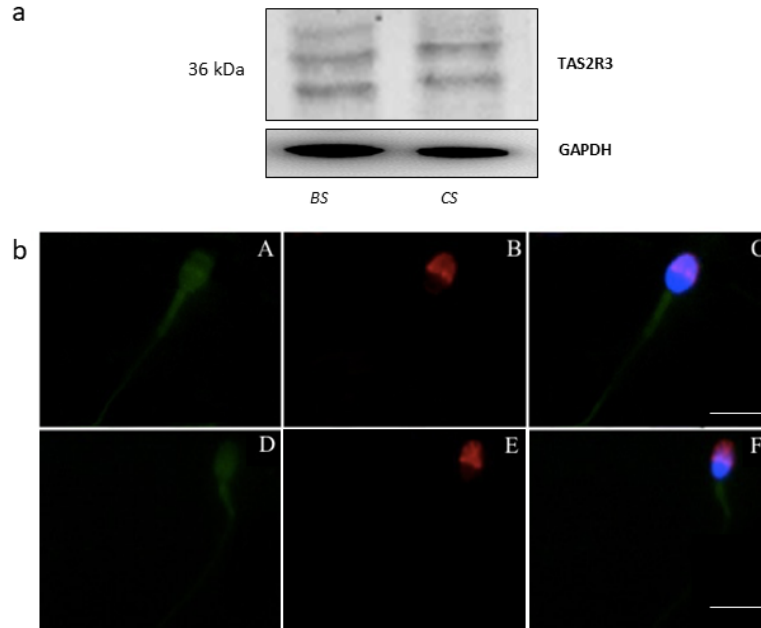


Figure 37: Expression of TAS2R3 in human ejaculated sperm. (a) Western blot of TAS2R3 in ejaculated sperm before (BS) and after *in vitro* capacitation (CS). Equal protein loading of the two sperm preparations was verified using the housekeeping GAPDH. (b) Representative micrographs (from three independent experiments) of immunofluorescence staining of TAS2R3 (green), the acrosomal lectin marker PSA (red) and the fluorescent DNA binding dye DAPI (6-diamino-2-phenylindole, blue) in ejaculated sperm before (A–C) and after *in vitro* capacitation (D–F). Micrographs in C and F are composed by an overlay of the three fluorescent channels (TAS2R3 green; PSA, red; DAPI, blue). Scale bar = 15 μ m.

As regard to TAS2R4, an immunoreactive band (36 kDa) was observable in capacitated sperm; in addition, two additional discrete bands with a higher molecular weight were detectable in uncapacitated sperm, which possibly reflects a different degree of receptor glycosylation. Remarkably, *in vitro* capacitation led to a change in the expression pattern of TAS2R4, accompanied by a complete disappearance of the immunoreactive band with the highest molecular mass (Figure 38a). Immunofluorescence analyses confirm TAS2R4 expression in human sperm and show that TAS2R4 was mainly localized in the equatorial segment of the head and in the midpiece and end piece of the tail (Figure 38b).

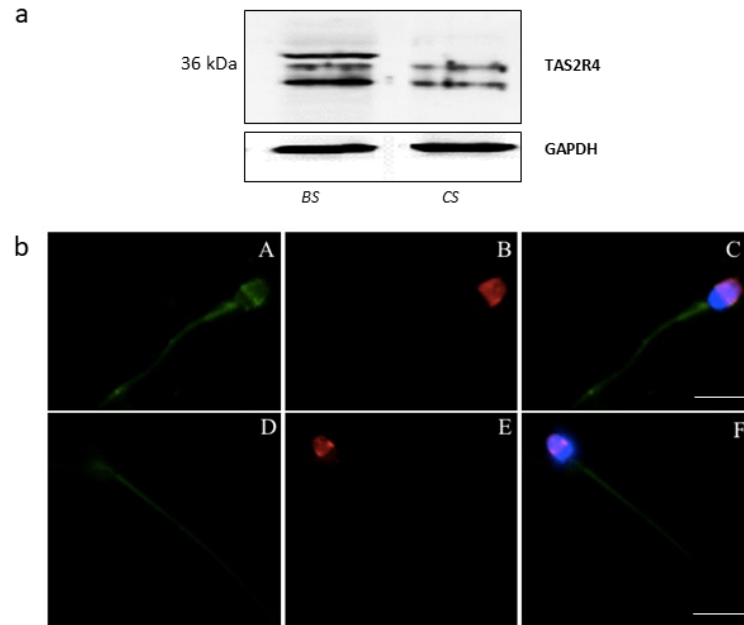


Figure 38: Expression of TAS2R4 in human ejaculated sperm. (a) Western blot of TAS2R4 in ejaculated sperm before (BS) and after in vitro capacitation (CS). Equal protein loading of the two sperm preparations was verified using the housekeeping GAPDH. (b) Representative micrographs (from three independent experiments) of immunofluorescence staining of TAS2R4 (green), the acrosomal lectin marker PSA (red) and the fluorescent DNA binding dye DAPI (6-diamino-2-phenylindole, blue) in ejaculated sperm before (A–C) and after in vitro capacitation (D–F). Micrographs in C and F are composed by an overlay of the three fluorescent channels (TAS2Rs green; PSA, red; DAPI, blue). Scale bar = 15 μ m.

The TAS2R14 (36 kDa) was detected in both basal and capacitated sperm; however, the additional immunopositive band with a higher molecular weight (45 kDa) was mainly present in uncapacitated sperm, whereas capacitated sperm only show a very faint 45 kDa derived staining (Figure 39a). Immunofluorescence analysis of TAS2R14 illustrates a pale TAS2R14 derived labeling in the area of the post acrosomal region and a weak but restricted staining of the mitochondria-reach midpiece region of the sperm tail of uncapacitated sperm (Figure 39b, A–C); in contrast, in capacitated sperm, a bright staining of the whole tail was evident, as well as a very faint staining in the acrosomal region and the post nuclear region (Figure 39b, D–F). These results uncover that TAS2R14, highly expressed in human spermatozoa, indeed shows a redistribution upon capacitation.

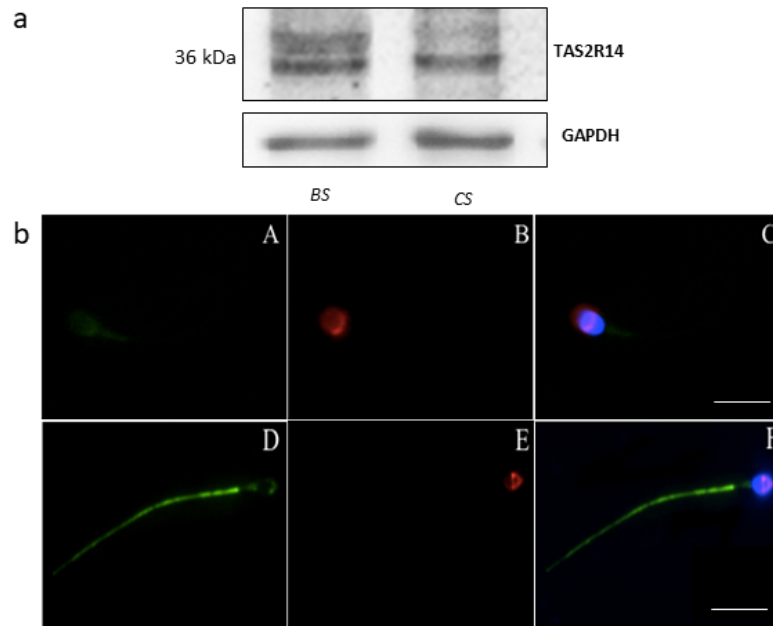


Figure 39: Expression of TAS2R14 in human ejaculated sperm. (a) Western blot of TAS2R14 in ejaculated sperm before (BS) and after in vitro capacitation (CS). Equal protein loading of the two sperm preparations was verified using the housekeeping GAPDH. (b) Representative micrographs (from three independent experiments) of immunofluorescence staining of TAS2R14 (green), the acrosomal lectin marker PSA (red) and the fluorescent DNA binding dye DAPI (6-diamino-2phenylindole, blue) in ejaculated sperm before (A–C) and after in vitro capacitation (D–F). Micrographs in C and F are composed by an overlay of the three fluorescent channels (TAS2Rs green; PSA, red; DAPI, blue). Scale bar = 15 μ m.

Regarding TAS2R19, the protein is expressed in both uncapacitated and capacitated sperm, as demonstrated by the presence of a 36 kDa immunopositive band (Figure 40a). The immunolocalization detected this protein in the basal region of the head and at the neck region; the capacitation process, as well as acrosomal reaction, seems not to affect its subcellular localization (Figure 40b).

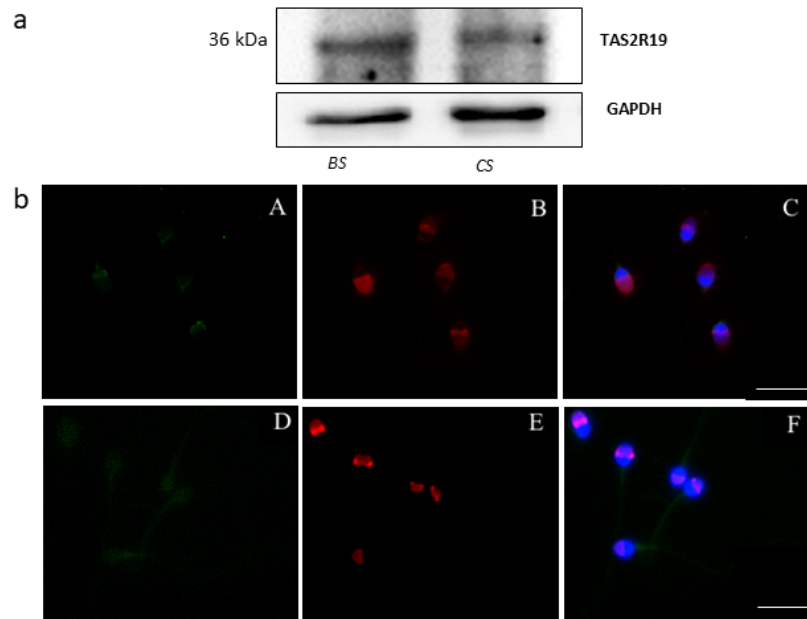


Figure 40: Expression of TAS2R19 in human ejaculated sperm. (a) Western blot of TAS2R19 in ejaculated sperm before (BS) and after in vitro capacitation (CS). Equal protein loading of the two sperm preparations was verified using the housekeeping GAPDH. (b) Representative micrographs (from three independent experiments) of immunofluorescence staining of TAS2R19 (green), the acrosomal lectin marker PSA (red) and the fluorescent DNA binding dye DAPI (6-diamino-2phenylindole, blue) in ejaculated sperm before (A–C) and after in vitro capacitation (D–F). Micrographs in C and F are composed by an overlay of the three fluorescent channels (TAS2Rs green; PSA, red; DAPI, blue). Scale bar = 15 μ m.

Figure 41a shows an evident band corresponding to the predicted molecular weight of TAS2R43 (34 kDa), which was present in both uncapacitated and capacitated sperm. TAS2R43 immunolocalization in uncapacitated spermatozoa was characterized by a positive labelling of the pericentriolar region and a staining along the whole sperm tail. After the capacitation process, TAS2R43 staining appears more diffuse in the entire head and in the midpiece region of the flagellum, while it disappears from the principal piece of the tail (Figure 41b), suggesting that capacitation seems also to affect subcellular localization of this bitter taste receptor subtype.

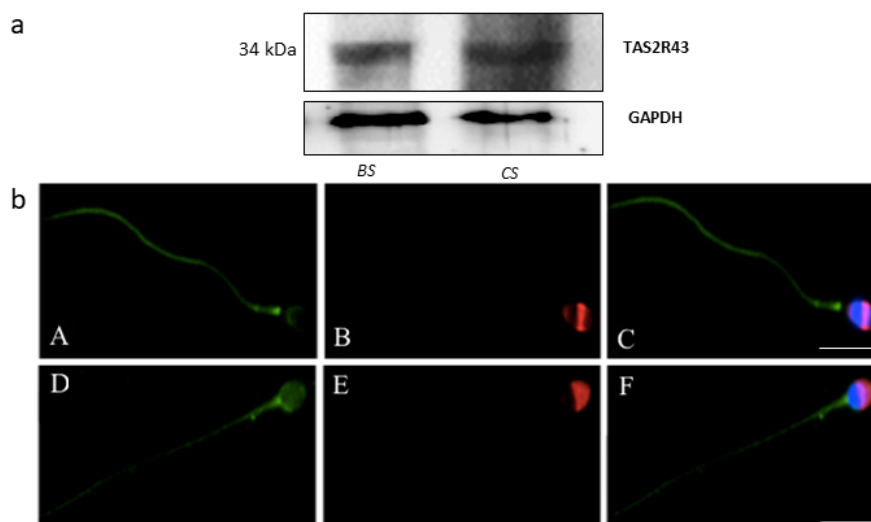


Figure 41: Expression of TAS2R43 in human ejaculated sperm. (a) Western blot of TAS2R43 in ejaculated sperm before (BS) and after *in vitro* capacitation (CS). Equal protein loading of the two sperm preparations was verified using the housekeeping GAPDH. (b) Representative micrographs (from three independent experiments) of immunofluorescence staining of TAS2R19 (green), the acrosomal lectin marker PSA (red) and the fluorescent DNA binding dye DAPI (6-diamino-2-phenylindole, blue) in ejaculated sperm before (A–C) and after *in vitro* capacitation (D–F). Micrographs in C and F are composed by an overlay of the three fluorescent channels (TAS2Rs green; PSA, red; DAPI, blue). Scale bar = 15 μ m.

Western blot analysis of protein extracts prepared from human sperm before and after *in vitro* capacitation showed that both G α subunits are expressed in uncapacitated as well as in *in vitro* capacitated sperm (Figure 42 and 43). However, as regard α -gustducin, we can observe two more bands (50 kDa and 65 kDa, respectively) in addition to the predicted theoretical band (36 kDa), both in uncapacitated and capacitated sperm (Figure 42a). Figure 38b (A–C) shows a representative image of α -gustducin staining in uncapacitated sperm, characterized by an acrosomal signal, associated with a positive labelling of the sperm's pericentriolar region and the tail. On the contrary, after the capacitation process, the staining is in the region of the post nuclear cup and along the entire tail was found to increase. This observation led to the suggestion that the process of secondary maturation of sperm seems to induce a subcellular translocation of α -gustducin to another sub-compartment of the cell (Figure 42b, D-F).

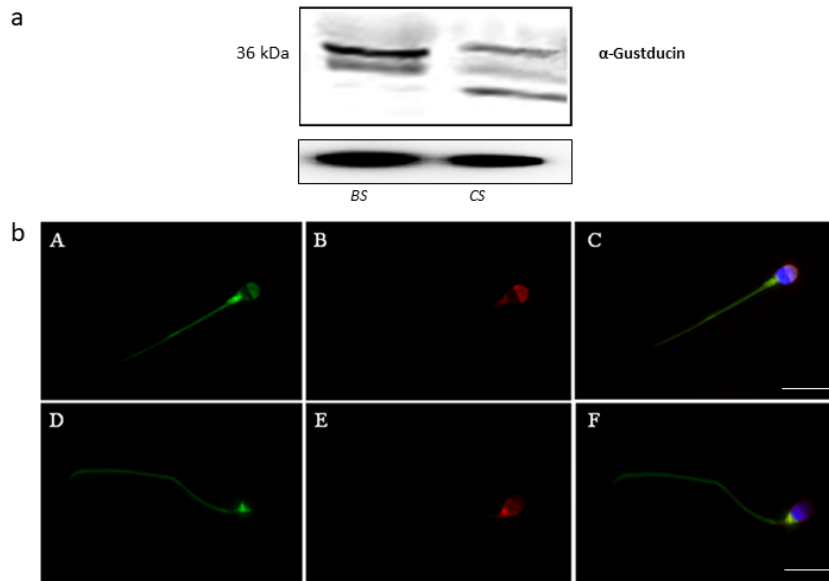


Figure 42: Expression of α -gustducin in human ejaculated sperm. (a) Western blot of α -gustducin and α -transducin in ejaculated sperm before (BS) and after in vitro capacitation (CS). GAPDH was immunodetected to control equal loading per lane for the two examined sperm suspensions. (b) Representative images of immunofluorescence staining (from three independent experiments) of α -gustducin and α -transducin (green), PSA (red), and DAPI (blue) in ejaculated sperm before (A–C) and after in vitro capacitation (D–F). Scale bar = 15 μ m.

Regarding α -transducin in uncapacitated sperm, an additional band of 40 kDa was observable beside the predicted band with a molecular mass of about 50 kDa. In addition, in capacitated sperm, an extra α -transducin-reactive band at a higher molecular mass (75 kDa) was detectable (Figure 43a). The bright fluorescence signals were visible in the equatorial region of the head, in the post nuclear region, and in the whole tail. In addition, it was also observable that capacitation induces a reorganization of α -transducin: whereas uncapacitated sperm showed a pronounced staining of the equatorial segment and a labeling along the entire tail (Figure 43b, A–C), fluorescence signals in capacitated sperm were much more concentrated in the region of the post nuclear region (Figure 43b, D–F). Comparing the protein expression results of α -transducin, seems that this protein was more expressed than α -gustducin, thus confirming the results obtained by ddPCR.

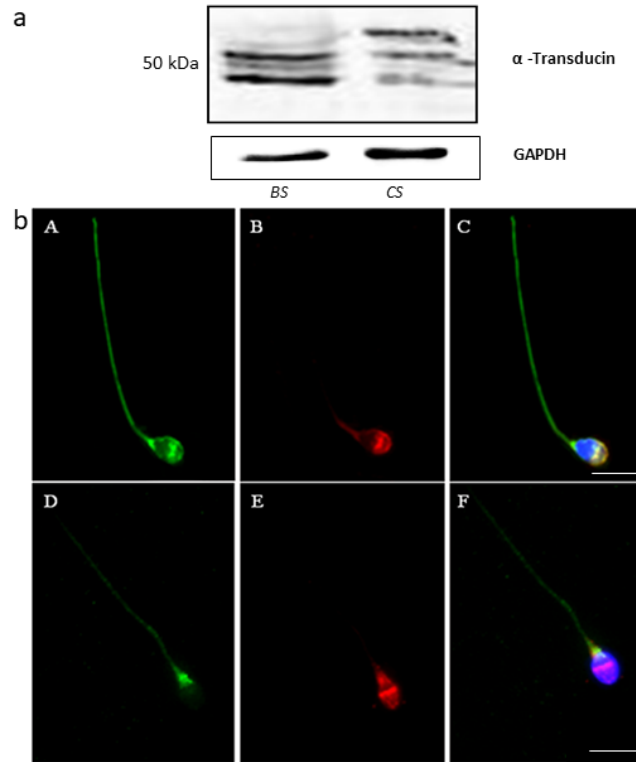


Figure 43: Expression of α -transducin in human ejaculated sperm. (a) Western blot of α -transducin in ejaculated sperm before (BS) and after in vitro capacitation (CS). GAPDH was immunodetected to control equal loading per lane for the two examined sperm suspensions. (b) Representative images of immunofluorescence staining (from three independent experiments) of α -transducin (green), PSA (red), and DAPI (blue) in ejaculated sperm before (A–C) and after in vitro capacitation (D–F). Scale bar = 15 μ m.

3 Discussion

The expression of taste receptor genes has been reported in non-taste tissues, thus suggesting that the role of these G-protein coupled receptors in the oral cavity does not represent the totality of their signaling capability (Rozengurt, 2006; Fehr et al, 2007; Deshpande et al, 2010; Shin et al, 2010; Elliott et al, 2011; Tizzano et al, 2011; Meyer et al, 2012). Indeed, it has become increasingly evident that the role of bitter taste perception may not be solely linked to dietary habits, such as to prevent the ingestion of toxic secondary metabolites (Martin et al, 2019). In this regard, the presence of these receptors in the male reproductive system (Meyer et al, 2012; Li, 2013; Gentiluomo et al, 2017; Governini et al, 2020) gives cues to investigate their possible role in human reproduction.

To the best of our knowledge, data regarding TASRs expression in the female reproductive system is lacking or conflicting (Zheng et al, 2017). This thesis provides evidence for the first time about the expression of TAS2Rs in GCs and CCs, the somatic cells surrounding the oocyte, considered to be fundamental for oocyte development and fertilization process. We demonstrated that selected TAS2Rs are expressed at higher levels in GCs than in CCs, confirming that these cells, despite the same origin, are able to acquire a highly specialized profile. Noteworthy, this thesis work highlighted the *TAS2R14* gene as the most expressed in both GCs and CCs. This result lets hypothesize a key role of this receptor in the follicular cells physiology and, consequently, in reproduction. A recent study demonstrated that, in the brain, TAS2R14 is specifically activated by resveratrol (Duarte et al, 2020), a natural polyphenol, with an antidiabetic, antioxidant and anti-inflammatory actions (Oyenihi et al, 2016; Xia et al, 2017; Malaguarnera, 2019). At the ovarian level, resveratrol supplementation has been reported to increase the total number of oocytes, by decreasing the production of reactive oxygen species (ROS) (Liu et al, 2013). Moreover, resveratrol seems to decrease the number of atretic follicles and to inhibit the apoptosis in rats (Kong et al, 2011). Interestingly, it has been reported that NOS may induce apoptosis in human ovarian cancer cells not solely through its documented alteration of microtubule assembly dynamics (Zhou et al, 2002) but also through the activation of TAS2R14 (Martin et al, 2019). In this context, our data, highlighting *TAS2R14* as the most expressed *TAS2Rs* gene in GCs and CCs, suggest a possible mechanism by which resveratrol may exert potential beneficial actions on reproductive functions and ovary.

Considering these observations, our analysis of the signal transduction cascade components in the somatic cells of the ovarian follicle is very interesting. Our results highlighted slightly higher expression of *GNAT1*, *GNAT3*, *PDE4A* and *PLCB2* genes in GCs; the same behavior was observed

for *MYC*, *STAT5B*, *PPARG* and *GABPA*, confirming the trend showed for *TAS2Rs*. Our observations agree with several studies demonstrating that the transcriptome of GCs and CCs is distinctive for each cell population, giving a possible explanation to the different expression pattern observed (Burnik Papler et al, 2015; Andrei et al, 2019).

Interesting insights come from the analysis of α -transducin and α -gustducin, the most important G-proteins coupled to bitter taste receptors. The western blot analysis of these proteins, obligate mediators of all signal transduction elicited by *TAS2Rs* receptors, showed the presence of different isoforms. The nature of these isoforms, which have never been described in the literature, was not defined at the time: often they are due to alternative splicing or to post-translational modification, but numerous isoforms are also due to the presence of SNPs (Shim et al, 2015).

In light of these observation, our data pave the way for understanding the biological functions exerted by these receptors in the female reproductive tract. Future studies are required to shed light on the molecular mechanisms triggered by these receptors in the follicular microenvironment. This knowledge could be useful to improve the *in vitro* fertilization techniques currently in use, as well as potential therapeutic approaches concerning infertility field.

This thesis work also shed light into the role of *TAS2Rs* receptors in the biology of male gametes. For the first time, we provided evidence for the expression of members of the bitter *TAS2Rs* family in ejaculated human sperm cells as well as in testicular tissue. In addition, expression of single components of the taste signal transduction cascade, such as the α -subtypes gustducin and transducin and the effector enzymes PDE4A, PLC β 2, and TRPM5, was observed in testicular tissue and ejaculated spermatozoa.

During their journey through the female genital tract, sperm cells are exposed to different concentration of possible external ligands for taste receptors, including hormones, single amino acids, carbohydrates, changes in pH and bicarbonate, but also toxins. Therefore, it may be hypothesized that taste receptors and the coupled signal transduction cascade might be functionally operative in the perception of different biochemical stimuli, thereby driving sperm maturation, motility, chemotaxis, and probably also final fertilization (Meyer et al, 2012; Li, 2013; Xu et al, 2013; Spinaci et al, 2014, Luddi et al, 2019).

One observation confirming this hypothesis comes from genetic studies; in this regard, polymorphic variants in taste receptors are often functional, and several gene polymorphisms have been proposed as modulators of spermatogenetic process efficiency, leading in some cases to impaired sperm production (Aston et al, 2010; Plaseski et al, 2012; Siasi & Aleyasin, 2016). Recently, our research group definitively demonstrated the role of the genetic variability of taste receptors in human male infertility (Governini et al, 2020).

Another important result of this thesis work is the demonstration that each sperm cell expresses, at a different level, a distinct subset of taste receptor subtypes. This datum is in agreement with previous studies, carried out in taste buds, showing that not all gustatory cells express all members of the TAS2Rs family in order to discriminate different bitter compounds (Behrens et al, 2007). Even if we do not know which TAS2Rs receptor subtypes are selectively expressed or inactivated in each sperm cells, it should be interesting to identify the mechanisms by which the expression of particular human bitter taste receptors in sperm may be finely tuned to possibly detect a limited subset of bitter stimuli (Governini et al, 2020).

Interestingly, we also demonstrated that the *in vitro* capacitation induces a significant redistribution of TAS2Rs. For example, TAS2R43 was found to be concentrated in the midpiece of the flagellum of capacitated sperm, while it was present in the entire flagellum and in the pericentriolar region of uncapacitated sperm. The sequestering of distinct proteins and lipids to a specific subcellular region within sperm is a strategy often adopted during sperm capacitation within the female genital tract. Indeed, it is known that a lateral redistribution of seminolipids (Goto-Inoue et al, 2009) as well as a subcellular reorganization of proteins involved in acrosome reaction and in oocyte's binding occur during sperm capacitation (Ackermann et al, 2008; Boerke et al, 2008). This redistribution may affect several important physiological processes, such as acrosomal reaction, zona pellucida penetration, as well as hyperactivated sperm motility (Gadella, 2008; Zitranski et al, 2010).

Moreover, this work of thesis also demonstrates the expression of α -gustducin and α -transducin in ejaculated human sperm cells (Fehr et al, 2007), together with the bitter taste transduction cascade. The expression of the α -gustducin and α -transducin has already been reported in boar testicular tissue and ejaculated spermatozoa (Spinaci et al, 2014); therefore, we confirm a role for this G-proteins also in human male gametes. Since capacitation renders sperm competent to fertilize an egg, we also investigated the expression of both G-proteins α -subtypes in uncapacitated and capacitated human sperm. We demonstrated a maturation-dependent subcellular redistribution of the two G-proteins; this phenomenon of translocation may be relevant for several physiologically significant processes, such as acrosomal reaction, zona pellucida penetration, as well as hyperactivated sperm motility (Gadella et al, 2008; Zitranski et al, 2010). In addition, as already reported for granulosa and cumulus cells, different G-protein isoforms may be detected in capacitated spermatozoa compared with uncapacitated sperm. These results might reflect post-translational modifications, proteolytic cleavage, phosphorylation, or nucleotide exchange (GDP to GTP), as has been described for transducin in the retina (Calvert et al, 2000). Although the exact functional relevance of a possible post-translational modification of gustducin and transducin or

an interaction with regulatory proteins is still unclear, it may be hypothesized that this alteration could reflect a different activation stage of the two G-protein subtypes in uncapacitated sperm versus capacitated spermatozoa or might be important for the detected capacitation-dependent redistribution.

In this work of thesis, we also demonstrated for the first time the expression of TRPM5, the common downstream element for sweet, umami and bitter taste transduction (Kusumakshi et al, 2015), in human testis tissue as well as in sperm. TRPM5 seems to have a more restricted expression profile, if compared with other members of the huge family of TRP channel proteins (Guinamard et al, 2011) and, on the contrary from the other members, it is not permeable for calcium, but allow sodium entry into the cell. However, calcium represents the key regulator of their activity since these channel proteins are activated by a rise in intracellular calcium (Prawitt et al, 2003). Calcium plays an important role in sperm physiology being involved in the activation of chemotaxis, hyperactivated motility, and acrosome reaction (Lishko et al, 2018; Brown et al, 2019). Interestingly, the sperm-specific calcium channel CatSper (Lishko et al, 2018) seems to be not regulated by bitter taste receptors. To this regard, the existence of other mechanisms triggering increased in calcium levels in sperm cells is also demonstrated by the fact that species not expressing CatSper also exhibit calcium influx (Lishko et al, 2012). In this context, TAS2R4, that in human sperm exhibits a high expression level, is reported to regulates the levels of cytosolic calcium by inactivating a member of the Rho family small GTPases that, in turn, may regulate actin cytoskeleton reorganization (Sidhu et al, 2017). Considering the key role of the actin cytoskeleton on the acrosome remodeling, and its persistence in the subacrosomal space of mature mammalian sperm, including humans (Breitbart et al, 2005), an important role of TAS2R4 in male acrosome ontogeny and physiology may be hypothesized. Furthermore, we also highlight for the first time, a significant correlation between TAS2Rs and TRPM5 expression in human sperm, suggesting a functional link between these molecules in controlling male gamete physiology. Since it is known that bitter compounds, such as caffeine, are able to induce sperm hyperactivation (Colàs et al, 2010), it may be possible that bitter receptors can control sperm motility by a TAS2R-induced TRPM5 stimulation, which can induce the depolarization of sperm membrane. However, it cannot be excluded that TAS2Rs in sperm may have a more defensive and protective function, where they serve as warning sensors against the toxic compounds (Antinucci et al, 2017).

Our results of TAS2Rs expression in human testis and sperm may be the first step on the way to better understand the molecular mechanisms underlying the communication between environmental activators or toxicants and male germ cells, as well as male gametes.

Future studies are required to shed light on the mechanism through which these molecules are linked to human fertility. Indeed, the identification of the mechanisms triggered by these receptors in the reproductive processes, could improve the *in vitro* fertilization techniques currently in use, as well as it may have a potential therapeutic approach to the treatment of human infertility.

References

- Ackermann F, Zitanski N, Heydecke D, Wilhelm B, Gudermann T, Boekhoff I, 2008. The Multi-PDZ domain protein MUPP1 as a lipid raft-associated scaffolding protein controlling the acrosome reaction in mammalian spermatozoa. *J. Cell. Physiol* 214:757–768.
- Ahmed EA, Barten-van Rijbroek AD, Kal HB, Sadri-Ardekani H, Mizrak SC, van Pelt AM, de Rooij DG, 2009. Proliferative activity in vitro and DNA repair indicate that adult mouse and human Sertoli cells are not terminally differentiated, quiescent cells. *Biol. Reprod* 80(6):1084–91.
- Albertini DF, Combelles CM, Benecchi E, Carabatsos MJ, 2001. Cellular basis for paracrine regulation of ovarian follicle development. *Reproduction* 121:647–653.
- Andrei D, Nagy RA, van Montfoort A, Tietge U, Terpstra M, Kok K, van den Berg A, Hoek A, Kluiver J, Donker R, 2019. Differential miRNA Expression Profiles in Cumulus and Mural Granulosa Cells from Human Pre-ovulatory Follicles. *Microna* 8(1):61–67.
- Antinucci M, Risso D, 2017. A Matter of Taste: Lineage-Specific Loss of Function of Taste Receptor Genes in Vertebrates. *Front MolBiosci* 4:81.
- Asano M, Furukawa K, Kido M, Matsumoto S, Umesaki Y, 1997. Growth retardation and early death of beta-1, 4-galactosyltransferase knockout mice with augmented proliferation and abnormal differentiation of epithelial cells. *Embo J* 16: 1850–1857.
- Assidi M, Montag M, Van der Ven K, Sirard MA, 2011. Biomarkers of human oocyte developmental competence expressed in cumulus cells before ICSI: a preliminary study. *Journal of Assisted Reproduction and Genetics* 28(2):173–88.
- Aston KI, Krausz C, Laface I, Ruiz-Castané E, Carrell DT, 2010. Evaluation of 172 candidate polymorphisms for association with oligozoospermia or azoospermia in a large cohort of men of European descent. *Hum Reprod* 25(6):1383–97.
- Austin CR, 1951. Observations on the penetration of the sperm in the mammalian egg. *Aust. J Sci. Res. B.* 4: 581–596.
- Bachmanov AA, Beauchamp GK, 2007. Taste receptor genes. *Annu Rev Nutr* 27: 389–414.

Balhorn R, 1982. A model for the structure of chromatin in mammalian sperm. *J Cell Biol* 93:298–305.

Baum JS, Gorge JP, McCall K, 2005. Programmed cell death in the germline. *Sem Cell Devel Biology* 16:245-259.

Behrens M, Foerster S, Staehler F, Raguse J-D, Meyerhof W, 2007. Gustatory expression pattern of the human TAS2R bitter receptor gene family reveals a heterogenous population of bitter responsive taste receptor cells. *J. Neurosci. Off. J. Soc. Neurosci* 27:12630–12640.

Behrens M, Meyerhof W, 2010. Oral and extraoral bitter taste receptors. *Results Probl. Cell Differ* 52:87–99

Biggers J, Whittingam D, Donahue R, 1967. The pattern of energy metabolism in the mouse oocyte and zygote. *Proceedings of the National Academy of Sciences of the United States of America* 58:560-567.

Boerke A, Tsai PS, Garcia-Gil N, Brewis IA, Gadella BM, 2008. Capacitation-dependent reorganization of microdomains in the apical sperm head plasma membrane: Functional relationship with zona binding and the zona-induced acrosome reaction. *Theriogenology* 70:1188–1196.

Boland NI, Humpherson PG, Leese HJ, Gosden RG, 1994. The effect of glucose metabolism on murine follicle development and steroidogenesis in vitro. *Hum Reprod* 9:617–623.

Bradford MM, 1976. A rapid and sensitive method for the quantitation of microgram quantities of protein utilizing the principle of protein-dye binding. *Analyt. Biochem.* 72:248-325.

Breitbart H, Cohen G, Rubinstein S, 2005. Role of actin cytoskeleton in mammalian sperm capacitation and the acrosome reaction. *Reproduction* 129(3):263-8.

Brown SG, Publicover SJ, Barratt CLR, Martins da Silva SJ, 2019. Human sperm ion channel (dys) function: Implications for fertilization. *Hum Reprod Update* 25:758–776.

Burnik Papler T, Vrtacnik Bokal E, Maver A, Kopitar AN, Lovrečić L, 2015. Transcriptomic Analysis and Meta-Analysis of Human Granulosa and Cumulus Cells. *PLoS One* 10(8):0136473.

Calvert PD, Krasnoperova NV, Lyubarsky AL, Isayama T, Nicolás M, Kosaras B, Wong G, Gannon KS, Margolskee RF, Sidman RL, 2000. Phototransduction in transgenic mice after targeted deletion of the rod transducin alpha -subunit. *Proc Natl Acad Sci* 97:13913–13918.

Calvert PD, Krasnoperova NV, Lyubarsky AL, Isayama T, Nicolás M, Kosaras B, Wong G, Gannon KS, Margolskee RF, Sidman RL, Pugh EN Jr, Makino CL, Lem J, 2000. Phototransduction in transgenic mice after targeted deletion of the rod transducin alpha -subunit. *Proc Natl Acad Sci U S A* 97(25):13913-8.

Casarini L, Lispi M, Longobardi S, Milosa F, La Marca A, Tagliasacchi D, Pignatti E, Simoni M, 2012. LH and hCG action on the same receptor results in quantitatively and qualitatively different intracellular signalling. *PLoS One* 7(10):46682.

Casarini L, Reiter E, Simoni M, 2016. β -arrestins regulate gonadotropin receptor-mediated cell proliferation and apoptosis by controlling different FSHR or LHCGR intracellular signaling in the hGL5 cell line. *Mol Cell Endocrinol.* 437:11-21.

Champroux A, Torres-Carreira J, Gharagozloo P, Drevet JR, Kocer A, 2016. Mammalian sperm nuclear organization: resiliencies and vulnerabilities. *Basic Clin Androl* 21; 26:17.

Chang MC, 1951. Fertilizing capacity of spermatozoa deposited into the fallopian tubes. *Nature* 168:697-698.

Chen Y, Cann MJ, Litvin TN, Iourgenko V, Sinclair ML, Levin LR, Buck J, 2000. Soluble adenylyl cyclase as an evolutionarily conserved bicarbonate sensor. *Science* 289(5479):625–628.

Clark GF, Dell A, 2006. Molecular models for murine sperm-egg binding. *J Biol Chem* 281(20):13853–13856.

Colás C, Cebrián-Pérez JA, Muiño-Blanco T, 2010. Caffeine induces ram sperm hyperactivation independent of cAMP-dependent protein kinase. *Int J Androl* 33:187–197.

Colás C, Cebrián-Pérez JA, Muiño-Blanco T, 2010. Caffeine induces ram sperm hyperactivation independent of cAMP-dependent protein kinase. *Int J Androl.* 33(1):187-97.

Cross NL, 1998. Role of cholesterol in sperm capacitation. *Biology of Reproduction* 59:7-11.

D and Liman ER, 2003. Intracellular Ca²⁺ and the phospholipid PIP₂ regulate the taste transduction ion channel TRPM5. *Proc Natl AcadSci U S A* 100(25):15160–15165.

De Blas GA, Darszon A, Ocampo AY, Serrano C, Castellano LE, 2009. TRPM8, a versatile channel in human sperm. *PLoS One* 4:60–95.

De Jonge CJ, Barratt C, 2006. *The sperm cell: production, maturation, fertilization, regeneration*: Cambridge University Press.

De Jonge CJ, Barratt C, Gadella BM, Visconti A, 2006. Regulation of capacitation the Sperm Cell. Cambridge: Cambridge University Press p.134–69.

De Rooij DG. 1998. Stem cells in the testis. *International Journal of Experimental Pathology*, 79:67–80.

De Toni L, Garolla A, Menegazzo M, Magagna S, Di Nisio A, Šabović I, Rocca MS, Scattolini V, Filippi A, Foresta C, 2016. Heat Sensing Receptor TRPV1 Is a Mediator of Thermotaxis in Human Spermatozoa. *PLoS One* 11(12), e0167622.

Dehkordi O, Rose JE, Fatemi M, Allard JS, Balan KV, Young JK, Fatima S, Millis RM, Jayam-Trouth A, 2012. Neuronal expression of bitter taste receptors and downstream signaling molecules in the rat brainstem. *Brain Research* 1475:1–10.

Duarte AC, Rosado T, Costa AR, Santos J, Gallardo E, Quintela T, Ishikawa H, Schwerk C, Schroten H, Gonçalves I, Santos CRA, 2020. The bitter taste receptor TAS2R14 regulates resveratrol transport across the human blood-cerebrospinal fluid barrier. *Biochem Pharmacol* 177:113953.

Elliott RA, Kapoor S, Tincello DG, 2011. Expression and distribution of the sweet taste receptor isoforms T1R2 and T1R3 in human and rat bladders. *J Urol* 186:2455–2462.

Eppig JJ, Chesnel F, Hirao Y, O'Brien MJ, Pendola FL, Watanabe S, Wigglesworth K, 1997. Oocyte control of granulosa cell development: how and why. *Human Reproduction Update* 12:127–32.

Ezzati M and Zosmer A, 2007. Reproductive ageing in women. *Journal of Pathology* 211:219–231.

Fauser BC, Van Heusden AM, 1997. Manipulation of human ovarian function: physiological concepts and clinical consequences. *Endocrine Reviews* 18:71-106.

Fehr J, Meyer D, Widmayer P, Borth HC, Ackermann F, Wilhelm B, Gudermann T, Boekhoff I, 2007. Expression of the G-protein alpha-subunit gustducin in mammalian spermatozoa. *J Comp Physiol A Neuroethol Sens Neural Behav Physiol* 193:21–34.

Feki NC, Therond P, Couturier M, Limea G, Legrand A, Jouannet P and Auger J, 2004. Human sperm lipid content is modified after migration into cervical mucus. *Molecular Human Reproduction* 10:137-142.

Finger TE and Kinnamon SC, 2011. Taste isn't just for taste buds anymore. *F1000 Biol Rep* 3, 20.

Florman HM, Jungnickel MK, Sutton KA, 2010. Shedding light on sperm fertility. *Cell* 140: 310–312.

Freund JR, Lee RJ, 2018. Taste receptors in the upper airway. *World J Otorhinolaryngol Head Neck Surg* 4(1):67-76.

Fukuda N, Yomogida K, Okabe M, Touhara K, 2004. Functional characterization of a mouse testicular olfactory receptor and its role in chemosensing and in regulation of sperm motility. *J Cell Sci* 117:5835-45.

Furat Rençber S, Kurnaz Ozbek S, Eraldemir C, Sezer Z, Kum T, Ceylan S, Guzel E, 2018. Effect of resveratrol and metformin on ovarian reserve and ultrastructure in PCOS: an experimental study. *J Ovarian Res.* 29;11(1):55.

Gadella B, 2008. Sperm membrane physiology and relevance for fertilization. *Anim Reprod Sci* 107(3-4):229-36.

Ge L, Sui HS, Lan GC, Liu N, Wang JZ, Tan JH, 2008. Coculture with cumulus cells improves maturation of mouse oocytes denuded of the cumulus oophorus: observations of nuclear and cytoplasmic events. *Fertil Steril* 90:2376–88.

Gentiluomo M, Crifasi L, Luddi A, Locci D, Barale R, Piomboni P, Campa D, 2017. Taste receptor polymorphisms and male infertility. *Hum Reprod Oxf Engl* 32:2324–2331.

Gilchrist RB, Lane M, Thompson JG, 2008. Oocyte-secreted factors: regulators of cumulus cell function and oocyte quality. *Human Reproduction Update* 14(2):159-77

Gosden R and Lee B, 2010. Portrait of an oocyte: our obscure origin. *J Clin Invest* 120(4):973–983.

Goto-Inoue N, Hayasaka T, Zaima N, Setou M, 2009. The specific localization of seminolipid molecular species on mouse testis during testicular maturation revealed by imaging mass spectrometry. *Glycobiology* 19:950–957.

Governini L, Semplici B, Pavone V, Crifasi L, Marrocco C, De Leo V, Arlt E, Gudermann T, Boekhoff I, Luddi A, Piomboni P, 2020. Expression of Taste Receptor 2 Subtypes in Human Testis and Sperm. *J Clin Med* 9(1).

Guinamard R, Sallé L, Simard C, 2011. The Non-selective Monovalent Cationic Channels TRPM4 and TRPMIn. In *Transient Receptor Potential Channels*; Islam, M.d.S., Ed.; Springer: Dordrecht, The Netherlands pp. 147–171.

Harris SE, Gopichandran N, Picton HM, Leese HJ, Orsi NM, 2005. Nutrient concentrations in murine follicular fluid and the female reproductive tract. *Theriogen* 64:992–1006.

Hennet ML, Combelles CM, 2012. The antral follicle: a microenvironment for oocyte differentiation. *International Journal of Developmental Biology* 56(10-12):819-31.

Hofmann T, Chubanov V, Gudermann T, Montell C, 2003. TRPM5 is a voltage-modulated and Ca⁽²⁺⁾ activated monovalent selective cation channel. *CurrBiol* 13(13):1153–1158.

Hoon MA, Adler E, Lindemeier J, Battey JF, Ryba N.P, Zuker CS, 1999. Putative mammalian taste receptors: a class of taste-specific GPCRs with distinct topographic selectivity. *Cell* 96:541–551.

Huang A, Stone LM, Pereira E, Yang R, Kinnamon JC, Dvoryanchikov G, Chaudhari N, Finger TE, Kinnamon SC, Roper SD, 2011. Knocking out P2X receptors reduces transmitter secretion in taste buds. *J Neurosci* 31(38):13654–13661.

Huang L, Shanker YG, Dubauskaite J, Zheng JZ, Yan W, Rosenzweig S, Spielman AI, Max M, Margolskee RF, 1999. Ggamma13 colocalizes with gustducin in taste receptor cells and mediates IP3 responses to bitter denatonium. *Nat Neurosci* 2(12):1055-62.

Huang YJ, Maruyama Y, Dvoryanchikov G, Pereira E, Chaudhari N, Roper SD, 2007. The role of pannexin 1 hemichannels in ATP release and cell-cell communication in mouse taste buds. *Proc Natl AcadSci U S A* 104(15):6436–6441.

Hussein TS, Thompson JG, Gilchrist RB, 2006. Oocyte-secreted factors enhance oocyte developmental competence. *Developmental Biology* 296(2):514-21.

Hyttel F, Fair T, Callesen H, Greve T, 1997. Oocyte growth, capacitation and final maturation. *Theriogenology* 47:23-32.

Ickowicz D, Finkelstein M, and Breitbart H, 2012. Mechanism of sperm capacitation and the acrosome reaction: role of protein kinases. *Asian J Androl* 14(6):816–821.

Johnson MH, Everitt BJ, 2007. *Essential reproduction* (6th ed.). Malden, Mass: Blackwell Pub.

Jozwik M, Jozwik M, Teng C, Battaglia FC, 2006. Amino acid, ammonia and urea concentrations in human pre-ovulatory ovarian follicular fluid. *Hum. Reprod* 21:2776–2782.

Kinnamon SC, 2012. Taste receptor signalling - from tongues to lungs. *ActaPhysiol (Oxf)* 204(2):158-68.

Kong XX, Fu YC, Xu JJ, Zhuang XL, Chen ZG, Luo LL, 2011. Resveratrol, an effective regulator of ovarian development and oocyte apoptosis. *J Endocrinol Invest* 34(11):374-81.

Kusumakshi S, Voigt A, Hübner S, Hermans-Borgmeyer I, Ortalli A, Pyrski M, Dörr J, Zufall F, Flockerzi V, Meyerhof W, 2015. A Binary Genetic Approach to Characterize TRPM5 Cells in Mice. *Chem. Senses* 40:413–425.

Latham KE, Bautista FD, Hirao Y, O'Brien MJ, Eppig JJ, 1999. Comparison of protein synthesis patterns in mouse cumulus cells and mural granulosa cells: effects of follicle-stimulating hormone. and insulin on granulosa cell differentiation in vitro. *Biology of Reproduction* 61:482-92.

Leese HJ, Astley NR, Lambert D, 1981. Glucose and fructose utilization by rat spermatozoa within the uterine lumen. *J Reprod. Fertil* 61:435–437.

Li F, 2013. Taste perception: from the tongue to the testis. *Mol Hum Reprod* 19(6):349–360.

Li F, Zhou M, 2012. Depletion of bitter taste transduction leads to massive spermatid loss in transgenic mice. *Mol Hum Reprod* 18(6):289-97.

Lishko PV, Kirichok Y, Ren D, Navarro B, Chung J-J, Clapham DE, 2012. The Control of Male Fertility by Spermatozoan Ion Channels. *Ann Rev Physiol* 74:453–475.

Lishko PV, Mannowetz N, 2018. CatSper: A Unique Calcium Channel of the Sperm Flagellum. *Curr Opin Physiol* 2:109–113.

Liu D, Liman ER, 2003. Intracellular Ca²⁺ and the phospholipid PIP₂ regulate the taste transduction ion channel TRPM5. *Proc Natl Acad Sci U S A.* 9;100(25):15160-5.

Liu M, Yin Y, Ye X, Zeng M, Zhao Q, Keefe DL, Liu L, 2013. Resveratrol protects against age-associated infertility in mice. *Hum Reprod* 28(3):707-17.

Luddi A, Governini L, Wilmskötter D, Gudermann T, Boekhoff I, Piomboni P, 2019. Taste Receptors: New Players in Sperm Biology. *Int J Mol Sci* 20(4).

Maekawa M, Kamimura K, Nagano T, 1996. Peritubular myoid cells in the testis: their structure and function. *Archives of Histology and Cytology* 59(1):1–13.

Malaguarnera L, 2019. Influence of Resveratrol on the Immune Response. *Nutrients* 11(5):946.

Margolskee RF, 2002. Molecular mechanisms of bitter and sweet taste transduction. *J Biol Chem* 277(1):1–4.

Martin LTP, Nachtigal MW, Selman T, Nguyen E, Salsman J, Delleire G, Dupré DJ, 2019. Bitter taste receptors are expressed in human epithelial ovarian and prostate cancers cells and noscapine stimulation impacts cell survival. *Mol Cell Biochem.* 454(1-2):203-214.

Max M, Shanker YG, Huang L, Rong M, Liu Z, Campagne F, Weinstein H, Damak S, Margolskee RF, 2001. *Tas1r3*, encoding a new candidate taste receptor, is allelic to the sweet responsiveness locus *Sac*. *Nat Genet* 28(1):58-63.

McGee EA and Hsueh AJ, 2000. Initial and cyclic recruitment of ovarian follicles. *Endocr Rev* 21(2):200–214.

McLaughlin SK, McKinnon PJ, Margolskee RF, 1992. *Gustducin* is a taste-cell-specific G protein closely related to the transducins. *Nature* 357(6379):563-9.

Meyer D, Voigt A, Widmayer P, Borth H, Huebner S, Breit A, Marschall S, de Angelis MH, Boehm U, Meyerhof W, Gudermann T, Boekhoff I, 2012. Expression of *Tas1* taste receptors in mammalian spermatozoa: functional role of *Tas1r1* in regulating basal Ca^{2+} and cAMP concentrations in spermatozoa. *PLoS One* 7(2):32354.

Meyerhof W, Born S, Brockhoff A, Behrens M, 2011. Molecular biology of mammalian bitter taste receptors. A review. *Flavour and Fragrance Journal* 26(4):260–268.

Miki K and Clapham DE, 2013. Rheotaxis guides mammalian sperm. *CurrBiol* 23(6):443–452.

Montmayeur JP and Matsunami H, 2002. Receptors for bitter and sweet taste. *Curr Opin Neurobiol* 12(4):366–371.

Nelson G, Chandrashekar J, Hoon MA, Feng L, Zhao G, Ryba NJ, Zuker CS, 2002. An amino-acid taste receptor. *Nature* 416:199–202.

Nelson G, Hoon MA, Chandrashekar J, Zhang Y, Ryba NJ, Zuker CS, 2001. Mammalian sweet taste receptors. *Cell* 106:381–390.

Nixon B, Lu Q, Wassler MJ, Foote CI, Ensslin MA, 2001. Galactosyltransferase function during mammalian fertilization. *Cell Tiss Org* 168: 46–57.

O'Donnell L, Robertson KM, Jones ME, Simpson ER, 2001. Estrogen and spermatogenesis. *Endocr Rev* 22(3):289-318.

Oktem O and Oktay K, 2008. The ovary: anatomy and function throughout human life. *Annals of the New York Academy of Sciences* 1127:1-9.

Oyenihi OR, Oyenihi AB, Adeyanju AA, Oguntibeju OO, 2016. Antidiabetic Effects of Resveratrol: The Way Forward in Its Clinical Utility. *J Diabetes* 2016:9737483.

Plaseski T, Noveski P, Popeska Z, Efremov GD, Plaseska-Karanfilska D, 2012. Association study of single-nucleotide polymorphisms in FASLG, JMJDIA, LOC203413, TEX15, BRDT, OR2W3, INSR, and TAS2R38 genes with male infertility. *J Androl* 33(4):675-83.

Prawitt D, Monteilh-Zoller MK, Brixel L, Spangenberg C, Zabel B, Fleig A, Penner R, 2003. TRPM5 is a transient Ca^{2+} -activated cation channel responding to rapid changes in $[\text{Ca}^{2+}]$. *Proc Natl AcadSci* 100:15166–15171.

Rainey WH, Sawetawan C, Shay JW, Michael MD, Mathis JM, Kutteh W, Byrd W, Carr BR, 1994. Transformation of human granulosa cells with the E6 and E7 regions of human papillomavirus. *J ClinEndocrinolMetab* 78(3):705-10.

Ramaswamy S and Weinbauer GF, 2014. Endocrine control of spermatogenesis: Role of FSH and LH/ testosterone. *Spermatogenesis* 4(2), e996025.

Rato L, Alves MG, Socorro S, Duarte AI, Cavaco JE, Oliveira PF, 2012. Metabolic regulation is important for spermatogenesis. *Nature Reviews Urology* 9(6):330–338.

Ren D, Navarro B, Perez, G, Jackson AC, Hsu S, Shi Q, Tilly JL, Clapham DE, 2001. A sperm ion channel required for sperm motility and male fertility. *Nature* 413(6856):603–609.

Ren X, Zhou L, Terwilliger R, Newton SS, de Araujo IE, 2009. Sweet taste signaling functions as a hypothalamic glucose sensor. *Front IntegrNeurosci* 19;3:12.

Revelli A, Delle Piane L, Casano S, Molinari E, Massobrio M, Rinaudo P, 2009. Follicular fluid content and oocyte quality: from single biochemical markers to metabolomics. *ReprodBiolEndocrinol* 7:40.

Rossler P, Kroner C, Freitag J, Noe J, Breer H, 1998. Identification of a phospholipase C beta subtype in rat taste cells. *Eur J Cell Biol* 77(3):253–261.

Rozengurt E, 2006. Taste receptors in the gastrointestinal tract. Bitter taste receptors and α -gustducin in the mammalian gut. *J Physiol* 1786:171–177.

Sainz E, Korley JN, Battey JF, Sullivan SL, 2001. Identification of a novel member of the T1R family of putative taste receptors. *J Neurochem* 77:896–903.

Scott K, 2004. The sweet and the bitter of mammalian taste. *Curr Opin Neurobiol* 14(4):423–427.

Siasi E, Aleyasin A, 2016. Four Single Nucleotide Polymorphisms in INSR, SLC6A14, TAS2R38, and OR2W3 Genes in Association with Idiopathic Infertility in Persian Men. *J Reprod Med* 61(3-4):145-52.

Sidhu C, Jaggupilli A, Chelikani P, Bhullar RP, 2017. Regulation of Rac1 GTPase activity by quinine through G-protein and bitter taste receptor T2R4. *Mol. Cell Biochem* 426:129–136.

Simon A, Goodenough D, Li E, Paul D, 1997. Female infertility in mice lacking connexin 37. *Nature* 385:525–529.

Simon BR, Learman BS, Parlee SD, Scheller EL, Mori H, Cawthorn WP, Ning X, Krishnan V, Ma YL, Tyrberg B, MacDougald OA, 2014. Sweet taste receptor deficient mice have decreased adiposity and increased bone mass. *PLoS One* 22;9(1):86454.

Spinaci M, Bucci D, Mazzoni M, Giaretta E, Bernardini C, Vallorani C, Tamanini C, Clavanzani P, Galeati G, 2014. Expression of α -gustducin and α -transducin, G proteins coupled with taste receptors, in boar sperm. *Theriogenology* 82:144–151.

Strünker T, Goodwin N, Brenker C, Kashikar ND, Weyand I, Seifert R, Kaupp UB, 2011. The CatSper channel mediates progesterone-induced Ca^{2+} influx in human sperm. *Nature* 471:382.

Suarez SS and Pacey AA, 2006. Sperm transport in the female reproductive tract. *Hum Reprod Update* 12(1):23–37.

Sugiyama H and Chandler DE, 2014. Sperm guidance to the egg finds calcium at the helm. *Protoplasma* 251(3):461–475.

Taniguchi K, 2004. Expression of the Sweet Receptor Protein, T1R3, in the Human Liver and Pancreas. *J Vet Med Sci* 66:1311–1314.

Taruno A, Matsumoto I, Ma Z, Marambaud P, Foskett JK, 2013. How do taste cells lacking synapses mediate neurotransmission? CALHM1, a voltage-gated ATP channel. *Bioessays* 35(12):1111–1118.

Verde I, Vandecasteele G., Lezoualc'h F., Fischmeister R, 1999. Characterization of the cyclic nucleotide phosphodiesterase subtypes involved in the regulation of the Ltype Ca²⁺ current in rat ventricular myocytes. *Br J Pharmacol* 127:65-74.

Voigt A, Hubner S, Lossow K, Hermans-Borgmeyer I, Boehm U, Meyerhof W, 2012. Genetic labeling of Tas1r1 and Tas2r131 taste receptor cells in mice. *Chem Senses* 37(9):897–911.

Ward WS, Coffey DS, 1991. DNA packaging and organization in mammalian spermatozoa: comparison with somatic cells. *Biology of Reproduction* 44(4):569–74.

WHO Laboratory Manual for the Examination and Processing of Human Semen, 5th ed; World Health Organization (Ed.) World Health Organization: Geneva, Switzerland, 2010; ISBN 978-92-4-154778-9.

Wu C, Du YW, Huang L, Ben-ShoshanGaleczki Y, Dagan-Wiener A, Naim M, Niv MY, Wang P, 2017. Biomimetic Sensors for the Senses: Towards Better Understanding of Taste and Odor Sensation. *Sensors (Basel)* 17(12):2881.

Xia N, Daiber A, Förstermann U, Li H, 2017. Antioxidant effects of resveratrol in the cardiovascular system. *Br J Pharmacol* 174(12):1633-1646.

Xu J, Cao J, Iguchi N, Riethmacher D, Huang L, 2013. Functional characterization of bitter-taste receptors expressed in mammalian testis. *Mol. Hum. Reprod* 19:17–28.

Yanagimachi R, 2005. Male gamete contributions to the embryo. *Ann N Y AcadSci* 1061:203-7.

Zanetti N, Mayorga LS, 2009. Acrosomal swelling and membrane docking are required for hybrid vesicle formation during the human sperm acrosome reaction. *Biology of Reproduction* 8:396-405.

Zhang Y, Hoon MA, Chandrashekar J, Mueller KL, Cook B Wu D, Zuker CS, Ryba NJ, 2003. Coding of sweet, bitter, and umami tastes: different receptor cells sharing similar signaling pathways. *Cell* 112:293–301.

Zheng K, Lu P, Delpapa E, Bellve K, Deng R, Condon JC, Fogarty K, Lifshitz LM, Simas TAM, Shi F, ZhuGe R, 2017. Bitter taste receptors as targets for tocolytics in preterm labor therapy. *FASEB J.* 31(9):4037-4052.

Zhou J, Gupta K, Yao J, Ye K, Panda D, Giannakakou P, Joshi HC, 2002. Paclitaxel-resistant human ovarian cancer cells undergo c-Jun NH2-terminal kinase-mediated apoptosis in response to noscapine. *J Biol Chem.* 18;277(42):39777-85.

Zitranski N, Borth H, Ackermann F, Meyer D, Vieweg L, Breit A, Gudermann T, Boekhoff I, 2010. The "acrosomal synapse": Subcellular organization by lipid rafts and scaffolding proteins exhibits high similarities in neurons and mammalian spermatozoa. *CommunIntegrBiol* 3(6):513-21.